APPLICATION OF WAVELET TRANSFORM TO CRACK DETECTION IN ULTRASONIC NDE: AN FEM STUDY

by
Vijay Shankar Babu. Ch

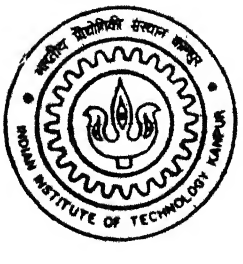

DEPARTMENT OF MECHANICAL ENGINEERING
INDIAN INSTITUTE OF TECHNOLOGY KANPUR
March, 2000

APPLICATION OF WAVELET TRANSFORM TO CRACK DETECTION IN ULTRASONIC NDE: AN FEM STUDY

A Thesis Submitted

In Partial Fulfillment of the Requirements

For the Degree of

MASTER OF TECHNOLOGY

by

Vijay Shankar Babu. Ch

to the

DEPARTMENT OF MECHANICAL ENGINEERING

INDIAN INSTITUTE OF TECHNOLOGY KANPUR

March, 2000

Dedicated to

My Parents

CERTIFICATE

This is to certify that the present work titled ***Application of Wavelet Transform to crack detection in Ultrasonic NDE: an FEM study*** by Ch. Vijay Shankar Babu has been carried out under my supervision and has not been submitted elsewhere for the award of a degree.

Dr. N.N.KISHORE
Professor,
Mechanical Engg. Deptt.,
I I T Kanpur,
INDIA.

Acknowledgements

I would like to express my deep sense of gratitude to my guide Dr. N. N. Kishore for his invaluable guidance throughout my M.Tech programme. It is because of his constant encouragement, motivation and suggestions, I could accomplish good results in my thesis work. His vast experience and immense knowledge in the field of FEM and Wave Propagation were always found to be coming to my help whenever I faced any difficulty. I am always grateful to him for sparing his precious time and providing me valuable suggestions at each and every stage of my M.Tech programme.

I would like to pay sincere regards to Mr. S.K. Rathore, Mr. Atul Agarwal, sasi bhushan and santosh kulkarni for giving motivation and encouragement during my thesis work.

I am very much thankful to my friends pmurali, swaroop, pav, cbnsmurthy, bprasad, csudheer who helped me a lot technically. When ever there is unhappyness on my face, they cheered me, which made this thesis in front of you.

I am debted to my friends narasimha, suresh (chem.), jayaram, satyapavan, bheema, chandra sekhar who worked for me during documentation in the late night also.

Special thanks goes to my Friend Sudheer for sparing his time for his help throughout the documentation work inspite of being heavily loaded. I am thankful to him for making all the figures in this book. Whenever I am tired he is there to encourage me to get back and work again. Without him I may not even dream to complete this work with in this span of time.

I cannot forget the alu-pyaj parathas and veg-rolls of jogi's canteen which gave me energy to do this work. And I thank one and all who are involved in this thesis work directly or indirectly. I am thankful to all of my classmates and friends for giving me a good company providing a friendly atmosphere and making my stay at IIT Kanpur a sweet memory.

Ch. Vijay Shankar Babu.

ABSTRACT

For thick structures and components subjected to large loads, it is very important to have a Non destructive method, which detects the cracks. This detection has to be done by analyzing the data obtained from the ultrasonic testing. In the present problem a methodology using wavelet transform approach has been developed to detect the cracks as well as sizing them. Wavelet transforms are particularly suited to extracting the small features embedded in the signal. Sending and receiving ultrasonic signal is simulated using finite element method. The elastic wave propagation data is obtained for several source and receiver locations. These signals are analyzed using wavelet transforms, which decomposes the data into different levels. The wavelet coefficients of different levels of all the signals are plotted as images to detect the cracks. Cracks are identified by the moving nature of the wavelet coefficients of a certain level in time-domain. These are observed in first few wavelet levels only. From level 2 or 3, arrival times of the crack reflections are evaluated and crack size is determined. Using Daubechies db2 wavelet, good results are obtained, which agree with actual crack size and location.

CONTENTS

List of Figures

List of Tables

List of Symbols

τ_{ij}	stress tensor
ρ	mass density
f_i	body force
C_{ijkl}	elastic constants
λ, μ	Lames constants
C_L	Longitudinal velocity
C_T	Transverse velocity
υ	Poisson ratio
E	Youngs modulus
γ	wave number
C_R	Rayleigh velocity
$[D]$	material property matrix
$[M]$	mass matrix
$[C]$	consistent damping matrix
$[K]$	stiffness matrix
$\{F\}$	load vector
$[N]$	displacement interpolation matrix
$\{a_n\}$	acceleration vector
$\{v_n\}$	velocity vector
$\{d_n\}$	displacement vector
δt, Δt	time-step
x, y	Cartesian co-ordinates
ξ, η	Natural co-ordinates
$f(t)$	signal
$\phi(t)$	Scaling function or transformation kernal
ω	frequency
τ, t	time

$w(t-\tau)$	window function
$\psi(t)$	mother wavelet
a	Scaling parameter
b	translation parameter
N_j	shape function
$L_2(\Re)$	square integrable function space
V_n	square integrable function subspace of $L_2(\Re)$
$\overline{h}_0(n)$	low-pass digital filter
$\overline{h}_1(n)$	high-pass digital filter
$\alpha_i(m)$	Scaling coefficients
$\beta_i(m)$	Wavelet coefficients

Chapter 1

INTRODUCTION

1.1 Introduction

Inspection of thick structure is very much important as the cracks developed will propagate quickly and thus disaster may occur with in a short period. The rich propagation properties of ultrasonic waves have been found to be very effective in detecting and characterizing the defects in a wide range of structural materials.

With the advent of high strength materials and their use in extreme conditions, ultrasonic NDE is becoming an important technique to evaluate the soundness of the structures. In this method ultrasonic energy generated by piezo electric transducer is directed towards the flaw through a compression or shear mode. The flaw scatters a part of the incident energy, in general, both in shear and compression modes. The receiving transducer collects these scattered waves. As the wave reflected by the flaw depends on the flaw size the displacement amplitude received by the transducer is directly related to the crack dimensions.

The ultrasonic signal received contains various reflections superimposed and it is hard to predict whether the reflection is from flaw or not. The data thus obtained from the simulated ultrasonic NDE contains various reflections. Some of them are mode converted, which have different frequency other than the applied frequency. Because of the superimposition, it is very hard to detect the crack reflections. To study these superimposed and different frequency reflections in both time and frequency domain wavelet analysis has evolved in the present day NDE.

Wavelet transform is one of the recent techniques used to analyze these type of signals. The WT is defined as a mathematical function, which divides the signal into different frequencies/scales/levels in terms of basis functions obtained by compression/dilation and translation of mother wavelet. Main advantage of WT is, it does not suffer from time bandwidth resolution trade off. This new technique with the

ability to use different sized windows at different frequencies tends to model the signal in an efficient way. The wavelet, which is used for the analysis of these signals, should be similar to the applied pulse for better crack detection.

The wavelet transform (WT) technique is a recent method to process the transient signals. There has been a large interest in this field at present and many papers have been published on wavelet technique, related to different fields including NDE.

In particular these wavelet transforms are extremely useful for noise suppression, peak detection, and for the joint time frequency representation of ultrasonic signals.

1.2 Literature Survey

Developments in the high speed computing machines and their storage facility made simulation of non-destructive testing possible. Also in recent years, many mathematical models, which can represent non-destructive techniques, were developed.

Understanding the interaction of elastic wave with flaws is an essential feature in sizing the defect [1]. Many analytical and numerical methods have been developed to detect the defects. Temple [2] and Bond [3] had reviewed the relative advantages of various numerical methods to solve wave equation and it is concluded that finite element method is superior because of its versatility to model arbitrary shape flaws, and its ability to incorporate anisotropic and inhomogenous material nature.

One of the latest technique is modelling of wave equation using finite element method for scattered ultrasonic waves [5]. A two dimensional finite element method with absorbing boundary conditions has been used to investigate the scattering of ultrasonic waves in infinite isotropic media with wavelet technique. The finite element code developed by Jaleel [4] is further modified by Kishore, Sridhar and Iyengar [5]. Absorbing boundary conditions on the side boundaries were included to simulate the infinite plate. Newmark method for time marching is replaced by unconditionally stable second order accurate θ method developed by Hoff and Pohl [6].

The energy received by the receiver has been used for various purposes in literature. Ultrasonic data may be in some situations is very difficult to analyze, due to poor sound to noise ratio (SNR) or due to complex multiple scattering phenomena,

Moubarik, Vadder and Benoist [7] have used the results using wavelet technique to decrease the noise by thresholding the coefficients. Abbate and Koay [8] used wavelet transform for ultrasonic signals to detect the peaks and to extract the frequency dispersion of the Lamb wave velocity. They were successful in estimating group velocities of first three modes of a plate wave induced by laser generation. Abbate, Frankel and Das [9] applied wavelet transform technique to obtain the dispersion relation of surface acoustic wave group velocity. The Ultrasonic waves are induced by the laser generation on a steel substrate with chromium coating to obtain the dispersion relation.

Nevel, Defacio and Neal [10] presented a flaw signature estimation approach. This estimation utilizes the Wiener filter along with wavelet based procedure to achieve deconvolution and reduction of acoustic noise by chopping. Abbate, Frankel and Das [11] presented wavelet technique for flaw detection. Plot of time-frequency is used to study and characterize different components of an ultrasonic signal in order to obtain its dispersive behavior. Roy, Sallard and Moubarik [12] investigated new filtering application based on some particular properties of the wavelet transform. They have extracted a disturbing echo of high amplitude from an experimental ultrasonic signal to point out other echoes of lower amplitude that may contain information about the micro defects.

Choa, Udpa and Udpa [13] presented an automated pattern classification system for the interpretation of ultrasonic NDE signals using wavelet transform and neural networks to obtain good localization and classification of the signals. Han, Cheng, Wang and Berthelot [14] performed the mode analysis of transient ultrasonic Lamb waveforms excited by pulsed laser in a composite plate employing the wavelet analysis. Group velocity of each mode is calculated using the time frequency plot.

1.3 Present Work

In the present work, the wavelet technique is used to detect the reflections coming from a crack with the help of A-scan data obtained at different receiver locations. The data to be decomposed is obtained by a finite element simulation of the domain modelled with a crack. Using the simulation, the required A-scans at the receiver locations are recorded.

To model a very large plate, the investigation is carried out by modelling a finite length plate with the incorporation of absorbing boundary condition on the side boundaries. Finite element code written by Jaleel [4] and further modified by Kishore, Sridhar, and Iyengar [5] is used for simulation, after replacing Newmark method with θ method for time marching and incorporating absorbing boundary conditions on the side boundaries.

In the wavelet analysis, the signal is decomposed using the *discrete wavelet transform* technique into different scales or levels. Decomposed levels represent different frequency levels and as the level is increasing, frequency decreases. The crack reflections are quantified by decomposing A-scan data obtained at different receiver locations into a finite number of wavelet levels. Same level of all the decomposed signals is grouped into each row of a 2-D matrix. Finally, the wavelet coefficients are examined how they are moving along the time axis. The moving coefficients correspond to the crack located in the domain. This method gives the arrival times of the wave reflections from crack. And from these times, location of the crack in the domain is identified.

In Chapter 2, basics of the elastic wave theory are presented. Important wave modes that are involved in the propagation are discussed.

Chapter 3 deals with the finite element formulation of the elastic wave propagation. Absorbing boundary condition, θ-method for time marching, stability requirements and implementation of the finite element code are discussed.

Chapter 4 presents the wavelet theory and the signal analysis techniques are discussed. Types of wavelet transforms, multi resolution analysis are given.

Chapter 5 gives different applications of the wavelet transforms to non-destructive evaluation. In this, wavelet applications to noise removal, and its applications to the present problem of crack detection are discussed.

Chapter 6 presents the results obtained by following the methodology given in the previous Chapters.

Chapter 7 gives the conclusions and suggestions for the future work.

Chapter 2

BASICS OF ELASTIC WAVE PROPAGATION

This Chapter briefly describes the linear theory of elastic wave propagation in homogeneous isotropic media. Different types of waves that propagate in the half space are discussed.

2.1 Theory

The linear theory of elasto dynamics is described by the following equations defined for a body of volume V enclosed by surfaces $S = S_1 + S_2$. Where S_1 and S_2 are the surfaces on which displacements or tractions are specified respectively.

Dynamic equation in solid mechanics is given by

$$\tau_{ij,j} + f_i = \rho \frac{\partial^2 u_i}{\partial t^2}, \quad i,j=1,2,3. \tag{2.1}$$

where τ_{ij} is the stress tensor, u_i is the displacement, f_i is the body force vector per unit volume and ρ is the mass density of the material.

Using the constitutive equations, the Navier-Cauchey equation of motion for anisotropic inhomogeneous elastic solids is given by

$$\frac{\partial}{\partial x_j}[C_{ijkl}\frac{\partial u_l}{\partial x_k}] + f_i = \rho \frac{\partial^2 u_i}{\partial t^2} \quad , \quad i=1,2,3 \tag{2.2}$$

where C_{ijkl} are the Elastic constants.

The governing equations in terms of displacements is obtained as

$$(\lambda + 2\mu)\nabla\nabla.\vec{u} - \mu\nabla\times\nabla\times\vec{u} + \vec{f} = \rho\frac{\partial^2\vec{u}}{\partial t^2} \tag{2.3}$$

where λ and μ are the *Lames constants.*

The equation can be further simplified by assuming displacement field, $\vec{u}$, as combination of scalar and vector potential ϕ and $\vec{H}$ respectively. such that,

$$\vec{u} = \nabla\phi + \nabla\times\vec{H}, \tag{2.4}$$

where $\nabla.\vec{H} = 0$

$\nabla.\vec{H}=0$ provides the necessary additional condition to uniquely determine the three components of $\vec{u}$ from the four components of ϕ and $\vec{H}$.

Further the body force can be represented as

$$\vec{f} = \nabla f + \nabla \times \vec{B}, \tag{2.5}$$

where $\nabla.\vec{B} = 0$

Thus the scalar and vector elastic wave equations are given by

$$(\lambda + 2\mu)\nabla\nabla.\vec{u} - \mu\nabla \times \nabla \times \vec{u} + \rho\vec{f} = \rho\frac{\partial^2\vec{u}}{\partial t^2} \tag{2.6}$$

and

$$\mu\nabla \times \nabla\vec{H} + \rho\vec{B} = \rho\frac{\partial^2\vec{H}}{\partial t^2} \tag{2.7}$$

The scalar potential ϕ is associated with the dilatational part of the disturbance and the vector potential $\vec{H}$ with the rotational part.

2.2 Dilatational and Rotational Waves

The governing equation of motion in the absence of body forces is given by

$$(\lambda + \mu)\nabla\nabla\vec{u} + \mu\nabla^2\vec{u} = \rho\frac{\partial^2\vec{u}}{\partial t^2} \tag{2.8}$$

By performing vector operation or divergence, the equation transforms to

$$(\lambda + 2\mu)\nabla^2\Delta = \rho\frac{\partial^2\Delta}{\partial t^2} \quad \text{, where } \Delta = \nabla.\vec{u} \tag{2.9}$$

This vector wave equation can further expressed as

$$\nabla^2\Delta = \frac{1}{C_L{}^2}\frac{\partial^2\Delta}{\partial t^2} \tag{2.10}$$

Where $C_L = \left(\frac{\lambda + 2\mu}{\rho}\right)^{1/2} = \left\{\frac{E(1-\upsilon)}{\rho(1+\upsilon)(1-2\upsilon)}\right\}^{1/2}$

Thus C_L gives longitudinal velocity, E is Youngs modulus, and υ is poisson ratio.

Thus it can be seen that a change in volume or dilatational disturbance, will propagate at the velocity C_L.

By performing the curl operation, the equation transforms to $\mu\nabla^2\vec{\omega} = \rho\frac{\partial^2\vec{\omega}}{\partial t^2}$

This form of vector wave equation can be expressed as

$$\nabla^2 \vec{\omega} = \frac{1}{C_T^2} \frac{\partial^2 \vec{\omega}}{\partial t^2} \qquad (2.11)$$

where $C_T = \left(\frac{\mu}{\rho}\right)^{1/2}$, which represents Transverse velocity.

Thus the rotational waves propagate with a velocity C_T.

So, elastic wave propagates in elastic solid with two different speeds C_L and C_T. Volumetric waves involving no rotation propagate at C_L while rotational waves involving no volume change propagate at C_T.

The ratio of two waves can be expressed as

$$k = \frac{C_L}{C_T} = \left(\frac{\lambda + 2\mu}{\mu}\right)^{1/2} = \left(\frac{2 - 2\upsilon}{1 - 2\upsilon}\right)^{1/2} \qquad (2.12)$$

Since $0 \le \upsilon \le 0.5$, C_L is $> C_T$

Dilatational waves are called irrotation, primary *(P)* or longitudinal *(L)* waves and rotational waves are called secondary *(S)* or Transverse *(T)* waves.

2.3 Plane waves

Considering simple harmonic plane wave propagating in isotropic media, say along x-direction, the deformation can be given by

$$u = Ae^{i\gamma(x-ct)}, \quad v = Be^{i\gamma(x-ct)}, \quad w = Ce^{i\gamma(x-ct)} \qquad (2.13)$$

where γ is the wave number and A, B, C are the amplitudes.

Substituting these in the governing equation, following equations are obtained

$$\begin{aligned} \{(\lambda + 2\mu) - \rho c^2\}A = 0 \\ (\mu - \rho c^2)B = 0 \\ (\mu - \rho c^2)C = 0 \end{aligned} \qquad (2.14)$$

If $c=C_L$, which satisfies first of the above equations, then $B=C=0$ is required. where as, if $c=C_T$, which satisfies the last two of the above equations, then $A=0$ is required.

In the first case where $A \neq 0$, the motion is purely longitudinal while in last case, with $A=0$, the motion is purely transverse. Also in the last case, the transverse components B and C are independent of one and another. It can be shown that the

stresses along the wave are normal to the wave front for longitudinal wave and that only shear stresses are acting along the wave front for transverse wave. And it can also be shown that $\nabla \times \vec{u} = 0$ for the former and $\nabla . \vec{u} = 0$ for the later.

2.4 Mode conversion

When an elastic wave encounters a boundary between two media, energy is reflected and transmitted (refracted) from and across the boundary. If the boundary is a free surface, pure reflections will occur. What distinguishes the elastic wave boundary interaction from other related fields is the phenomenon of mode conversion. This describes the behavior by which, an incident wave either compression or shear, is converted into both types on reflection.

2.4.1 Rayleigh Surface wave

In an unbounded elastic media only two types of waves can be propagated. However, when there is a boundary as in a half space problem, a third type of wave may exist. These waves will have effects confined closely to the surface and called Rayleigh surface waves. Their effect decreases rapidly with depth and their velocity of propagation is smaller than body waves.

By investigating the propagation in a half space the frequency equation for surface wave may be obtained. An approximate expression for Rayleigh wave velocity (C_R), which is slightly less than shear wave velocity is given as

$$\frac{C_R}{C_T} = \left(\frac{0.87 + 1.12\upsilon}{1+\upsilon} \right) \qquad (2.15)$$

The particle motion can be shown to be elliptical in nature and retrograde with respect to the direction of propagation. (i.e. it is counter clockwise for a wave traveling to the right). The amplitude decreases exponentially away from the surface. Rayleigh waves are two-dimensional waves, hence energy associated with these waves will not disperse as rapidly as that of three-dimensional waves of dilatation and rotation.

2.4.2 Header wave

Due to the velocity differences in C_L and C_T another type of wave come into existence. This wave is tangential to transverse wave and connected to longitudinal

wave at surface. This type of wave is called as *Header wave.* This wave has a velocity in between C_L, C_T and depends on the propagation angle.

2.5 Closure

In this chapter the basics of the elastic wave propagation are presented. The different waves that propagate in the elastic medium are discussed. This theory is used to calculate the arrival times of different waves theoritically, which are presented in results and discussion Chapter. In the next Chapter the implementation of this wave theory, by finite element method is presented.

Chapter 3

FEM FORMULATION

This Chapter deals with the finite element formulation. The spatial and temporal discretization problem of governing partial differential equations for wave propagation analysis is discussed.

3.1 Introduction

For a general homogeneous, linear, isotropic perfectly elastic solid, the equation of motion in the absence of body forces can be represented by the equation [17],

$$(\lambda + 2\mu)\nabla\nabla.\vec{u} - \mu\nabla\times\nabla\times\vec{u} = \rho\frac{\partial^2\vec{u}}{\partial t^2} \qquad (3.1)$$

where $\vec{u}$ is the displacement vector, ρ is the material density, λ and μ are Lame's constants of the medium and t is the time.

The finite element solution involves the discretization of domain into a number of elements, approximating displacement values of the interior elements in terms of its nodal values through the shape functions of the chosen element. Then nodal values are determined by the minimization of the residue using Galerkin method [18]. This procedure reduces the Eq. *3.1* to the following system of ordinary second-order linear differential equations

$$[M]\left\{\frac{\partial^2 U}{\partial t^2}\right\} + [K]\{U\} = \{F\} \qquad (3.2)$$

where, $[K]$ is the stiffness matrix determined by the elastic properties of the medium and $[M]$ is the mass matrix determined by the density distribution of the medium and $\{F\}$ is the applied load vector

Both stiffness and mass matrices are large, sparse, symmetric and positive-definite and can be stored efficiently by skyline storage technique.

To investigate the scattering from the inhomogeneity/flaw in an infinite plate, it is necessary to model a very large plate so that no reflection will come back in the duration of the study. Or the investigation can be carried out by modelling a finite length plate

with the incorporation of absorbing boundary condition on the side boundaries. Lysmer and Kuhlemeyer [20] have formulated a system of viscous dampers at the boundary, which damp out most of the reflections. It is worthy to note that these formulations are independent of incident frequency and angle. In the present work, unwanted reflections from side walls have been overcome by providing damping on the side boundaries of the domain.

The approximate boundary condition, which must be applied to simulate the effect of damping for a two-dimensional problem is given by:

$$\{\sigma\} = [D] \left\{\frac{\partial u}{\partial t}\right\} \tag{3.1}$$

where,

$$[D] = \rho \begin{bmatrix} aC_L & 0 \\ 0 & bC_T \end{bmatrix} \text{ and} \tag{3.2}$$

C_L, C_T are the velocities of Longitudinal and Transverse waves respectively and

a, b are dimensionless constants and

$\left\{\frac{\partial u}{\partial t}\right\}$ is the particle velocity vector on the boundary

Very good absorption characteristics can be achieved with $a=b=1.0$ [18]. In the literature this boundary has been termed as a *standard viscous boundary.* The consistent damping matrix in terms of shape functions may be written as,

$$[C] = \int_S [N]^T [D][N] ds \tag{3.3}$$

where $[N]$ - is displacement interpolation matrix and

$[D]$ - is material property matrix

The damping matrix is also sparse, symmetric and positive-definite. Chow [21] compared the solutions obtained by employing consistent and lumped standard viscous dampers. In the present work consistent formulation has been employed. The finite element equations including the damping term in the semi-discretization form is given by,

$$[M]\left\{\frac{\partial^2 u}{\partial t^2}\right\}+[C]\left\{\frac{\partial u}{\partial t}\right\}+[K]\{U\}=\{F\} \qquad (3.6)$$

where $[M]=\Sigma[M]^e$, $[K]=\Sigma[K]^e$, $[F]=\Sigma[F]^e$, $[C]=\Sigma[C]^e$ and

$[M]^e=\int_{V^e}\rho[N]^T[[N]dv$, $\quad [K]^e=\int_{V^e}[B]^T[D][B]\,dv$

The velocity and acceleration terms have to be approximated in finite difference form in order to get a fully discretized formulation. For high-frequency ultrasonic waves, it is desirable to have algorithmic damping and good accuracy. Hoff and Pahl [5] presented an unconditionally stable and of second order accurate θ method with controlled damping. This algorithm has been used in this present work and is described briefly in the following paragraph.

Let $\{d_n\}$, $\{v_n\}$ and $\{a_n\}$ be the displacement, velocity and acceleration vectors at the n^{th} time step respectively, then the corresponding quantities at $(n+1)^{th}$ step with step size δt can be obtained as

$$\{a_{n+1}\}=\{a_n\}+\{\delta a\} \qquad (3.7)$$

$$\{V_{n+1}\}=\{V_n\}+\delta t*\{a_n\}+(1.5-\theta)*\delta t*\{\delta a\} \qquad (3.8)$$

$$\{d_{n+1}\}=\{d_n\}+\delta t*\{v_n\}+0.5*(\delta t)^2*\{a_n\}+\frac{1}{4\theta_1^{\,2}}*(\delta t)^2(\delta a) \qquad (3.9)$$

$$[M_m]\{\delta a\}=\left\{\overline{F}_{n+1}\right\}-[M]\{a_n\}-[C]\{v_{n+1}\}-[K]\left\{\overline{d}_{n+1}\right\} \qquad (3.10)$$

where,

$[M_m]=[M]+(1.5-\theta_1)*\delta t[C]+\frac{1}{4\theta_1^{\,2}}*(\delta t)^2*[K]$ and

$\left\{\overline{F}_{n+1}\right\}=\{F_n\}+\theta_0*(F_{n+1}-F_n)$ and

$\left\{\overline{V}_{n+1}\right\}=\left\{V_n\right\}+\theta_1*\{a_n\}$ and

$$\left\{\bar{d}_{n+1}\right\} = \{d_n\} + \theta_1 * \delta t\{V_n\} + 0.5 * (\delta t)^2 * \{a_n\}$$

with $0.95 \leq \theta_1 \leq 1.0$ and $\theta_o = 1.0$

For each iteration, the above algebraic equations are solved using Cholesky decomposition.

3.2 Spatial discretization

Since, for wave propagation lower order elements and uniform meshes are recommended, bilinear quadrilateral isoparametric elements have been chosen for spatial discretization. The four node quadrilateral element and its transformation into natural co-ordinates is shown in Fig 3.1. In the natural co-ordinates it is a square centered at the origin having the vertices at

$$\{A'(\xi_1, \eta_1) = (1,1), B'(\xi_2,\eta_2) = (-1,1), C'(\xi_3,\eta_3) = (-1,-1), D'(\xi_4,\eta_4) = (1,-1)\} \quad (3.11)$$

where $A'B'C'D'$ is the transformed element into natural co-ordinate system

ξ, η are the natural co-ordinates.

Shape functions in natural co-ordinate system are given by

$$N_j(\xi,\eta) = (1+\xi_j\xi)(1+\eta_j\eta)/4 \quad (3.12)$$

3.3 Error and Stability requirements

Numerical solution of wave equation introduces several errors due to discretization. To minimize these errors, spatial and temporal grids must be chosen carefully. The accuracy of modelling strongly depends on the number of nodes per wavelength and hence on the frequency of the transducer used. As high frequency is used, the restriction on the spatial discretization is very crucial. Seron et al [22] pointed out the numerical discretization errors associated with the spatial discretization of the domain. According to him using at least 10 nodes per minimum wavelength (i.e. Rayleigh) in the case of isotropic materials can minimize the error. Time step should be such that the wave travels less than the spatial step size in one step size. The following criterion is used for the selection of time step

$$\delta t = \frac{h}{(C_L^{\,2} + C_T^{\,2})^{\frac{1}{2}}} \qquad (3.13)$$

where, h is the minimum spatial resolution.

This criterion is required to produce all the artifacts of the propagation. The criterion is essentially that energy should not propagate right across one mesh volume in one single time step [23].

3.4 Implementation

The two dimensional plane strain finite element (FE) code obtained from Jaleel [4] and further modified by Kishore, Sridhar and Iyengar [5] to use θ -algorithm for time integration, is used to model the pulse-echo ultrasonic wave propagation. Domain modelled for FE simulation of wave propagation is shown in Fig 3.2

Finite element input is obtained from a preprocessor mesh generation code, which mainly contains co-ordinates and connectivity numbers. This is checked before feeding the data to main code.

The output from the finite element code consists of nodal displacements at successive discrete time instants. The x, y displacement components at the receiver location is used for signal analysis by wavelet technique. The basics of wavelets and its NDE applications are discussed in the following chapters.

3.5 Closure

In this chapter finite element formulation of the problem is presented. Absorbing boundary condition, which is included in the FE code is given and θ -algorithm used for the time integration scheme is explained. Some of the discretization requirements on spatial and temporal grids are discussed. Finally the implementation of finite element part in the present problem given. In the coming chapters this method is implemented and simulated data is analyzed.

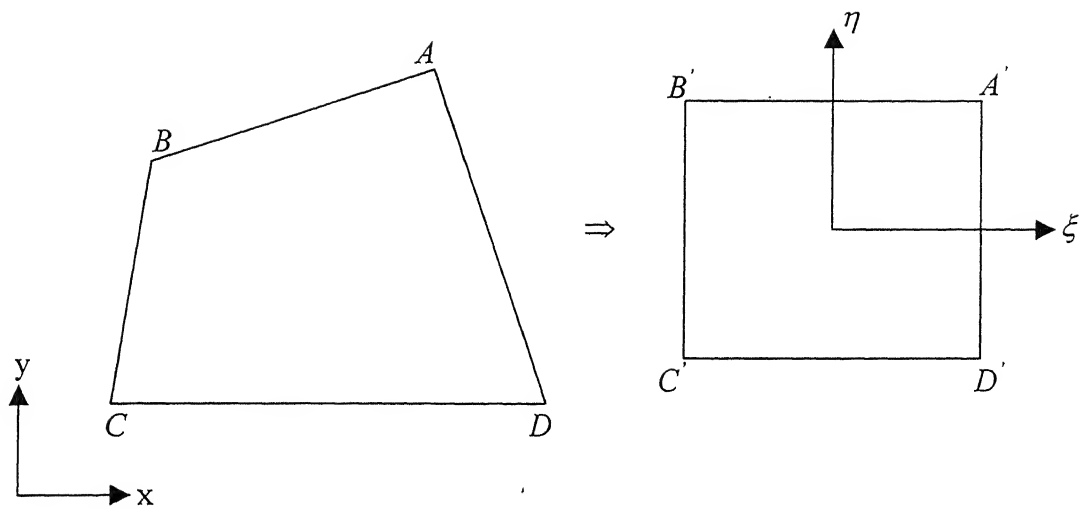

Fig 3.1 Four node quadrilateral element ABCD and its transformation into natural co-ordinate system

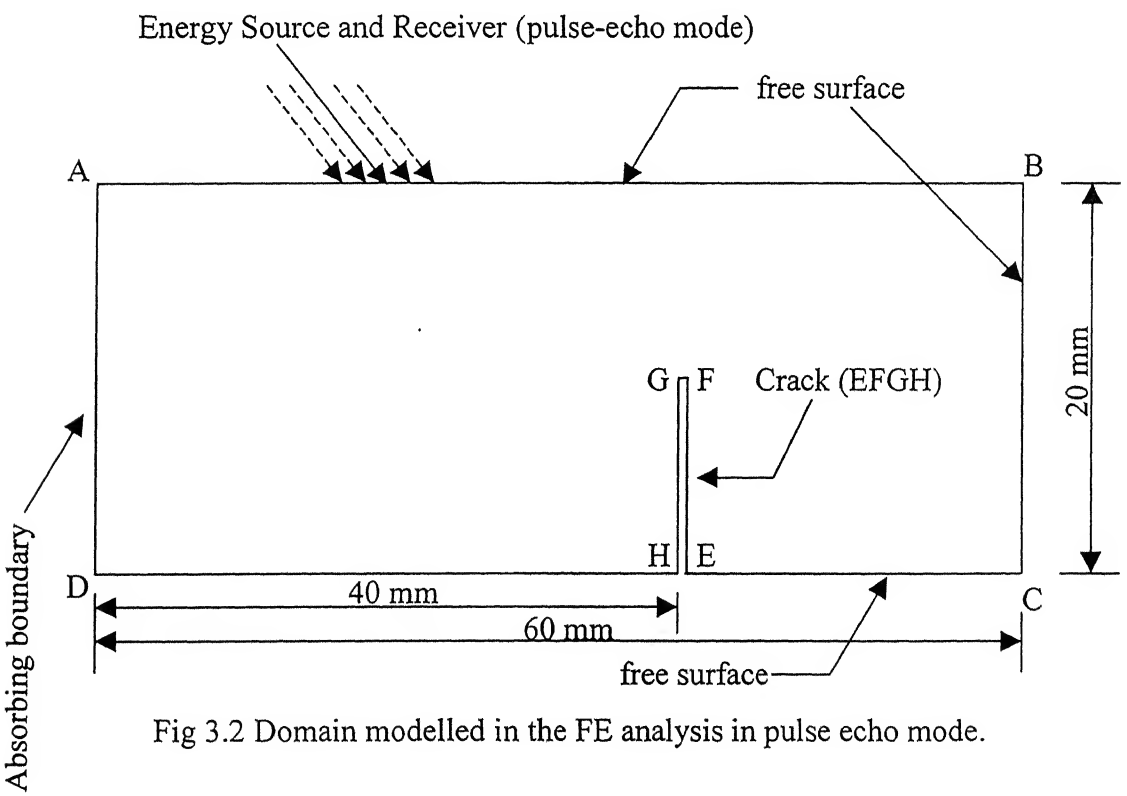

Fig 3.2 Domain modelled in the FE analysis in pulse echo mode.

Chapter 4

Wavelet Transform Theory and Analysis

4.1 Introduction

Wavelets are the mathematical functions that split the data into different frequency bands, matching the signal with a resolution matched to its scale. Basically wavelet transform of a function *f(t)* is the correlation between the signal and a set of basic wavelets generated from the mother wavelet. It has the advantage over traditional Fourier methods in analyzing a signal when it contains sharp spikes and discontinuities .The most important advantage is time-frequency localization of the signal, by which it can be known when the required frequency had occurred in the signal. Wavelet analysis has wide applications in earthquake prediction, signal processing, image compression, turbulence, radars, non-destructive evaluation (NDE) etc. In the following sections, the basic operations needed for wavelet transform are presented [24].

4.2 Basic Signal Analysis techniques

Generally, in the signal space of continuous time energy functions, a scalar product of $f(t)$ and $\phi(t)$, is defined as

$$< f(t), \phi(t) >= \int_{-\infty}^{\infty} f(t)\, \phi(t)\, dt, \quad f(t) \in L_2(\Re) \tag{4.1}$$

where $L_2(\Re)$ is the square integrable function space.

Using this scalar product, signals $f(t) \in L_2(\Re)$ are mapped from the original domain into the transform domain, to obtain and make use of further information about them. The function $\phi(t)$ is called the *transformation kernal.*

4.2.1 Fourier Transform (FT)

If $\phi(t) = e^{-j\omega t}$ in the Eq. 4.1 then it is called as *Fourier Transform* given by

$$FT\{f(t), \omega\} = < f(t), e^{-j\omega t} > \tag{4.2}$$

where ω is the frequency

The Fourier transform of a signal *f(t)* depends on the parameter ω. So, time dependency of the signal is lost in the transformed domain. It cannot be seen when exactly the spectral components of the signal appear, and this is unsatisfactory for analyzing non-stationary signals.

4.2.2 Short-Time Fourier Transform (STFT)

Short-Time Fourier Transform is a modification of the Fourier transform. In this, the exponential function of the Fourier transform $e^{-j\omega t}$ is weighed additionally with a window function $w(t-\tau)$. This transform is expressed as

$$STFT\{f(t),\omega,\tau\} =< f(t), w(t-\tau).e^{-j\omega t} > \qquad (4.3)$$

This offers a remedy to non-stationary signals by ensuring that, only a section of *f(t)* is ever observed. If Gaussian error function e^{-t^2} is used as window, it is called as *Gabor transform*. Time resolution of STFT is given by the time width of the window function. As the product of time and bandwidth is constant, division of time-bandwidth product into time duration and bandwidth is the same for all values of ω and τ. This implies that STFT has a constant resolution.

4.2.3 Wavelet Transform (WT)

In many applications it is desirable to divide the time-bandwidth product differently at different frequencies and/or at different time. This is attained through *wavelet transform*, given by

$$WT\{f(t),a,b\} =< f(t), \frac{1}{\sqrt{a}}\psi\left(\frac{t-a}{b}\right) > \qquad (4.4)$$

where $\psi(t)$ is a mother wavelet, b is a time shift parameter and a is a scaling parameter. Different types of mother wavelets are given in Figs. 4.1 to 4.2.

Parameter a is scaling of the time variable t. Thus a is a trade-off parameter between resolution in time and in frequency offering a flexible window. This flexibility is

not present in STFT. The difference between STFT and wavelet transform is shown in Fig.4.3. And the difference between wavelet bases and Gabor bases is shown in Fig. 4.4.

4.3 Theory of Wavelet Transform

4.3.1 Introduction

Idea behind wavelets is to process the data at different scales. Unlike in STFT, the size of the window can be changed using wavelets and by changing the size of window, small features can be observed in small window and vice versa. Usefulness of wavelets is to separate the small and large features in the signal, which cannot be done with the traditional Fourier methods.

In wavelet analysis a basis function called analyzing or mother wavelet is used. Temporal analysis is performed with a contracted high frequency version of mother wavelet and frequency analysis is performed with a dilated low frequency version. The signal is represented as a wavelet expansion using shifted and scaled versions of the mother wavelet along with coefficients. Scaling a wavelet means stretching the original mother wavelet, and shifting a wavelet means delaying its start. By choosing a best wavelet, which resembles the signal data, the required information can be obtained from the original signal easily.

Wavelet analysis can be performed in two ways

1. Using continuously translated and dilated versions of mother wavelet (CWT).
2. Using discretely translated and dilated versions of mother wavelet. This should have a compact support in order to split the data. So that if the signal is reconstructed, then the original signal is back (DWT).

4.3.2 Continuous Wavelet Transform (CWT)

The continuous wavelet transform (CWT) is defined as the sum over all time of the signal multiplied by scaled and shifted versions of the wavelet function ψ.

Continuos wavelet transform is given by

$$C(a,b) = \int_{-\infty}^{\infty} f(t)\psi^{*}_{a,b}(t)\ dt \qquad (4.5)$$

where * denotes the complex-conjugate.

$$\psi_{a,b} = a^{-1/2}\psi\left(\frac{t-a}{b}\right)$$

$a \in R^{+}$-{0}, $b \in R$

$C(a,b)$ are the coefficients of the wavelet transform, $f(t)$ - is the signal being analyzed. as the parameters a, b are continuous it is called CWT.

The word continuous in CWT means, that the transform operates the wavelets on the signal at each and every scale from that of signal upto some maximum level. CWT is also continuous in terms of shifting. During the computation, the analyzing wavelet is shifted smoothly over the full domain of the analyzed signal/function. As a, b are continuously varying, the wavelet transform is highly redundant and associated inverse transform is not unique. If the operating scales a' s are continuous, which real numbers then the type of transform is CWT. If the operating scales are varying by a multiple of 2 then it is called as DWT.

Analysis using CWT is time taking and redundant. These disadvantages of the CWT have been overcome by discrete wavelet transform.

4.3.3 Discrete Wavelet Transform (DWT)

4.3.3.1 Multi Resolution Analysis (MRA)

Practically discrete wavelet transform is manageable through multi resolution. The concept of multi resolution is based on three fundamental assumptions.

- There exists a set of nested signal subspaces V_i's of the *signal space* $L_2(\Re)$, with various resolutions. Such that

$$V_{-\infty} \ldots\ V_{-2} \subset V_{-1} \subset V_0 \subset V_1 \subset V_2 \ldots \subset V_{\infty} = L_2(\Re) \qquad (4.6)$$

  Where V_i is the square integrable function subspace, having a particular resolution for it.

Each space has different basis vectors, which provide a different time resolution. The time resolution becomes finer in the space V_i for increasing index i.

- For a scaling function $\phi(t)$, let the functions $\phi_k(t)$ are defined as

$$\phi_k(t) = \phi(t-k), \quad k \in Z, \tag{4.7}$$

where Z is the positive real number set.
These $\phi_k(t)$'s are known as the translates of the scaling function. These scaling function $\phi(t)$ and translates $\phi_k(t)$ constitutes an orthonormal basis of the space V_0 .which means the space is spanned by all the translated versions of the scaling function

$$V_0 = \text{span}_k\{\phi_k(t)\}$$

where

$$\langle \phi_k , \phi_l \rangle = \delta_{kl}, \quad k,l \in Z \tag{4.8}$$

- Moving inside the set of nested subspaces from one level to the next is such that, they are described by the two scale property

$$f(t) \in V_i \Leftrightarrow f(2t) \in V_{i+1} \tag{4.9}$$

V_i's constructed such that, using the two-scale property and the property of the scaling function to generate an orthonormal basis in V_0, the orthonormal basis systems for all the spaces V_i is written as

$$\phi_{i,k}(t) = 2^{i/2}\phi(2^i t - k), \quad i, k \in Z. \tag{4.10}$$

where i is the scaling parameter and k is the shifting parameter.
The vectors $\phi_{i,k}(t)$ represent an orthonormal basis of the space V_i. So,

$$\langle \phi_{i,k}, \phi_{i,l} \rangle = \delta_{kl}, \quad i,k,l \in Z \tag{4.11}$$

Scaled and Shifted versions of scaling function $\phi(t)$ are shown in Fig. 4.5.
The preceding factor $2^{i/2}$ in Eq. *4.10* ensures that the norm $||\phi_{i,k}(t)||$ is always unity independent of the indices i and k. This means

$$\| \phi_{i,k}(t) \| = \int_{-\infty}^{\infty} \phi_{i,k}^2(t)\, dt = 1$$

Since $\phi(t) \in V_0$, $V_0 \subset V_1$ and the functions $2^{1/2}\phi(2t-n)$, $n \in Z$ spans the space V_1. $\phi(t)$ can be represented as a linear combinations of the functions $\phi(2t-n)$ with coefficients $\bar{h}_0(n)$, $n \in Z$ as

$$\phi(t) = \sum_n \bar{h}_0(n)\phi(2t-n) \qquad (4.12)$$

where $\bar{h}_0(n)$ is the low-pass digital finite impulse response (FIR) filter coefficients.

Using the introduced bases, a signal $f(t) \in V_i$ can be represented as

$$f(t) = \sum_m \alpha_i(m).\phi_{i,m}(t) \qquad (4.13)$$

With the expansion coefficients

$$\alpha_i(m) = < f(t).\phi_{i,m}(t) > \qquad (4.14)$$

where $\alpha_i(m)$ are the scaling coefficients of the signal.

Further, since $f(t)$ is also an element of the space V_{i+1}, it can be expanded as

$$f(t) = \sum_n \alpha_{i+1}(n).\phi_{i+1,m}(t) \qquad (4.15)$$

The function $\phi(2^{i+1}t)$ is compressed by a factor two along the time axis compared with the function $\phi(2^i t)$. Hence a signal in the space V_{i+1} has double the resolution in time of a signal in the space V_i.

4.3.3.2 Dyadic Wavelets

For every subspace $V_i \subset V_{i+1}$, an orthogonal complement W_i can be defined to represent the subspace V_{i+1} as a direct sum of both as

$$V_{i+1} = V_i \oplus W_i, \quad \text{where } i \in Z \qquad (4.16)$$

The complementary space W_i, is spanned by an orthonormal base

$$\psi_{i,k}(t) = 2^{i/2}\psi(2^i t - k), \; i,k \in Z \qquad (4.17)$$

to become

$$W_i = \text{span}_k\{\psi_{i,k}(t)\},$$

Where $\psi_{i,k}(t)$ are the basis wavelets constructed from a the selected *mother wavelet*

Hence for signal $f(t) \in W_i$ can be written as

$$f(t) = \sum_m \beta_i(m).\psi_{i,m}(t) \qquad (4.18)$$

where $\beta_i(m) = \langle f(t), \psi_{i,m}(t) \rangle$ are the wavelet coefficients

Since $W_i \subset V_{i+1}$, the signals $f(t) \in W_i$ can be expanded in terms of the scaling functions of the next higher space. It is expressed as

$$\psi(t) = \sum_n \bar{h}_1(n)\phi(2t-n) \qquad (4.19)$$

where $\bar{h}_1(n)$ are the high pass digital FIR filter coefficients

The space V_i can be decomposed into direct sum as in Eq. 4.16 as $V_i = V_{i-1} \oplus W_{i-1}$ and similarly V_{i-1} can be represented. The decomposition of the signal space $L_2(\Re)$ according to Eq. 4.6 can be rewritten as

$$L_2(\Re) = V_j \oplus W_j \oplus W_{j+1} \oplus \ldots \oplus W_{-1} \oplus W_0 \oplus W_1 \oplus \ldots\ldots \qquad (4.20)$$

The index j is arbitrary and denotes the depth of decomposition.

From Eq. *4.20*, the signals $f(t) \in L_2(\Re)$ can be decomposed in a unique manner into a sum of subband signals expanded in terms of scaling functions, and several subband signals expanded in terms of dyadic wavelets.

DWT:

Calculating wavelet coefficients at every possible stage takes much computational time and space. Choosing only a subset of scales and positions based on powers of two, so called dyadic scales and positions, the analysis will be efficient with a little loss in accuracy. Performing this type of analysis is called discrete wavelet transform (DWT). Here the signals are projected into a finite number of subspaces. In DWT the signals must be a proper subspace of $L_2(\Re)$. That means the signal should belong to one of the subspaces $V_{-\infty} \ldots V_{\infty}$. If the signal

$$f(t) \in V_0 \subset L_2(\Re).$$

The decomposition with the help of MRA and Dyadic wavelets is analogously given as

$$V_0 = V_j \oplus W_j \oplus W_{j+1} \oplus W_{j+2} \oplus \ldots \oplus W_0. \qquad (4.21)$$

If the expansion coefficients $\alpha_0(m)$ of a signal $f(t) \in V_0$ are known, then the wavelet series expansion is a matter of calculating the expansion coefficients $\alpha_i(m)$ and $\beta_i(m)$ from $\alpha_0(m)$. This discrete computation can be represented as

$$f(t) = \sum_j \sum_k c(j,k)\, \psi_{a,b}(t) \qquad (4.22)$$

where $c(j,k)$ are the wavelet coefficients.

4.3.3.3 Decomposition

In DWT the expansion coefficients are calculated by projecting the signal from the space V_{i+1} into the subspaces V_i and W_i, and this projection is carried down with the help of two-channel analysis filter bank.

With the signal in hand, it can be represented as

$$f(t) = \sum_n \alpha_{i+1}(n).\phi_{i+1,m}(t) \in V_{i+1} \qquad (4.23)$$

whose coefficients $\alpha_{i+1}(n)$ must be known (the signal discrete points are taken as the initial coefficients). Since $V_{i+1} = V_i \oplus W_i$, the signal can be expressed uniquely as the sum of its projections into the subspaces, whereby the projections are expanded in terms of the respective bases as

$$f(t) = \sum_m \alpha_i(m).\phi_{i,m}(t) + \sum_m \beta_i(m).\psi_{i,m}(t) \qquad (4.24)$$

The projections are in practice carried out by calculating the unknown coefficients $\alpha_i(m)$ and $\beta_i(m)$ from the known coefficients $\alpha_{i+1}(n)$. The basis vectors $\phi_{i,m}(t)$ of the space V_i can be expressed in terms of the basis vectors $\phi_{i+1,m}(t)$ of the space V_{i+1} from the previous sections.

Thus it can be written as

$$\begin{aligned} \phi_{i,m}(t) &= 2^{i/2}\phi(2^i t - m) \\ &= 2^{i/2}\sum_v \bar{h}_0(v).\phi(2^{i+1}t - 2m - v) \end{aligned} \qquad (4.25)$$

and making the substitution as $2m+v=n$ and $h_0(k) = 2^{-1/2}\bar{h}_0(k)$, $k \in Z$. $\phi_{i,m}$ is obtained as

$$\phi_{i,m}(t) = \sum_n h_0(n-2m).2^{(i+1)/2}.\phi(2^{(i+1)}t - n)$$

$$= \sum_n h_0(n-2m).\phi_{i+1,n}(t) \qquad (4.26)$$

In a similar manner, the basis vectors $\psi_{i,m}(t)$ can be represented with respect to the wavelet space W_i as

$$\psi_{i,m}(t) = \sum_n h_1(n-2m).\phi_{i+1,n}(t) \qquad (4.27)$$

So, expansion coefficients $\alpha_i(m)$ and $\beta_i(m)$ in Eq. *4.24* can be written as scalar products from Eq. *4.14* and Eq. *4.26*. Then

$$\alpha_i(m) = < f(t), \phi_{i,m}(t) >$$

$$= h_0(-n)\ \alpha_{i+1}(n)\,|_{n=2m} \qquad (4.28)$$

and $$\beta_i(m) = h_1(-n)\ \alpha_{i+1}(n)|_{n=2m} \qquad (4.29)$$

α_i*'s* correspond to scaling coefficients and β_i*'s* correspond to wavelet coefficients. This decomposition process is summarized as shown in Fig. 4.6.

Thus the calculation of the coefficients for the decomposition of a signal is achieved by an analysis filter bank with impulse responses $h_0(-n)$ and $h_1(-n)$ and $f(t) \in V_{i+1}$ has twice as fine a resolution as its projection into the subspaces. Correspondingly, the expansion coefficients $\alpha_i(m)$ and $\beta_i(m)$ arise with half the sampling rate of the coefficients $\alpha_{i+1}(n)$.

Here $h_0(-n)$ is a low-pass filter and $h_1(-n)$ is the associated complementary high-pass filter. If more two channel filter banks are repeatedly connected to low-pass output of the two channel filter bank, then the decomposition will be as given in the Eq. *4.21* and the structure formed is a dyadic tree structure as shown in Fig. 4.7. The coefficients series β_{-1} to β_{-4} are of the wavelets. These can be thought of as discrete-time band pass signals and α*'s* can be thought of as low-pass.

4.3.4 Properties of the Scaling function

A few necessary conditions for scaling function $\phi(t)$ to be used in DWT are given. The scaling function is an averaging function so that the orthogonal projection of a function onto the scaling function basis is an averaged approximation. Scaling function has low-pass characteristics and therefore it transmits constant signals. Its Fourier transform is therefore nonzero, and it can be shown that integrating a scaling function gives *one*.

$$\int_{-\infty}^{\infty} \phi(t)\, dt = 1 \qquad (4.30)$$

The orthonormality of the bases in the subspaces V_i is directly related to the orthonormality of the impulse response of analysis filter bank and its translates. This is verified by convolving the two scaling functions of the same scale and it is obtained as

$$< \phi_{i,k}, \phi_{i,l} >= \delta_{kl}\,,\ i,k,l \in z \qquad (4.31)$$

The sum of the coefficients of $h_0(n)$ of the DWT analysis filter bank is given as

$$\sum_n h_0(n) = \sqrt{2} \qquad (4.32a)$$

The squared coefficients of the DWT analysis filter bank $h_0(n)$ produce the value *one*, when summed up. Which means $\sum_n h_0^2(n)=1$. (4.32b)

4.3.5 Properties of Wavelets

Some general properties related to wavelets are discussed in this section. The orthogonal projection of the signal on to the wavelet basis is the difference between two approximations at two adjacent resolution levels. The wavelets should satisfy the regularity condition, so that the wavelet coefficients decrease quickly with decrease of scale. The wavelet transform is local in both time and frequency.

An important characteristic of the wavelet arises from the Fourier transform, at $\omega=0$. This is called as admissible condition given by

$$\int_{-\infty}^{\infty} \psi(t)\, dt = 0 \qquad (4.33)$$

Since the subspace W_i and W_j are orthogonal to each other, wavelets from different spaces are also orthogonal. All together orthonormality can be expressed as

$$< \psi_{i,k}(t), \psi_{j,k}(t) >= \delta_{ij}\delta_{kl}, \qquad where\ i,j,k,l \in Z \tag{4.34}$$

and for particular case where $i=j$ and $k=l$, $||\psi_{i,k}(t)|| = 1$ is obtained.

It is also obtained that sum of the high-pass filter coefficients is *zero* and the sum of its squared coefficients is *one*. These conditions are represented as

$$\sum_n h_1(n)=0 \text{ and } \sum_n h_1^2(n)=1 \tag{4.35}$$

Finally the required property of the wavelets and scaling functions is that in particular

$$\int_{-\infty}^{\infty} \phi(t).\psi(t)\,dt = 0 \tag{4.36}$$

4.4 Closure

In this chapter the basic theory related to wavelet analysis is presented. Initially basic signal analysis techniques are discussed. Some of the important mother wavelets are presented in the form of pictures and the difference between the two types of wavelet transforms is explained. Multi resolution analysis is presented which is used for discrete wavelet transform. Finally decomposition procedure with DWT and MRA is given through dyadic wavelets and the properties of the wavelets are discussed. In the next chapters the applications of wavelets and results obtained after implementation are presented.

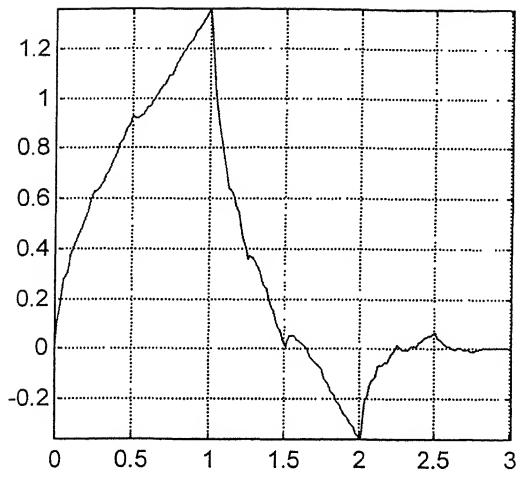

db2 Scaling

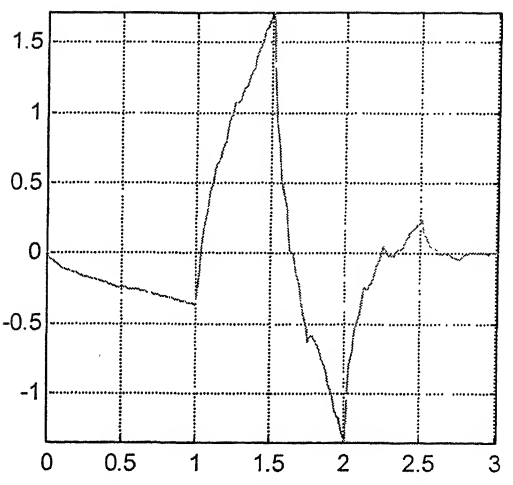

db2 Wavelet

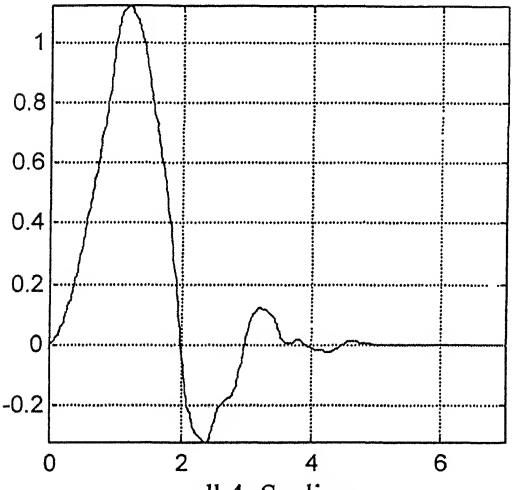

db4 Scaling

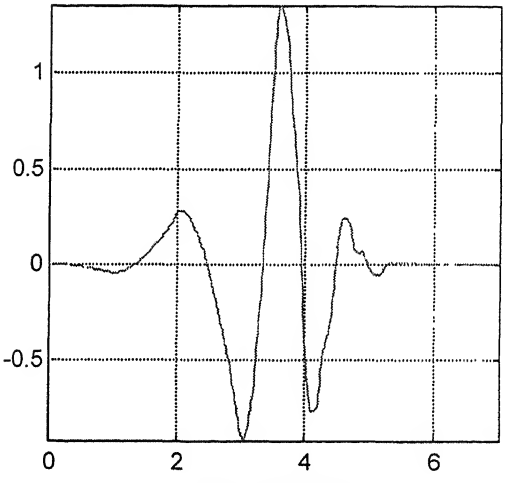

db4 Wavelet

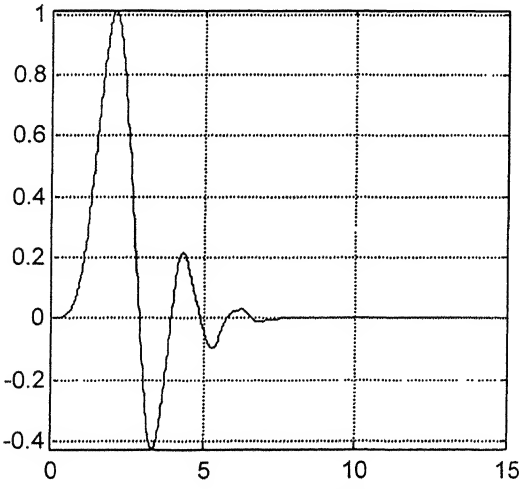

db8 Scaling

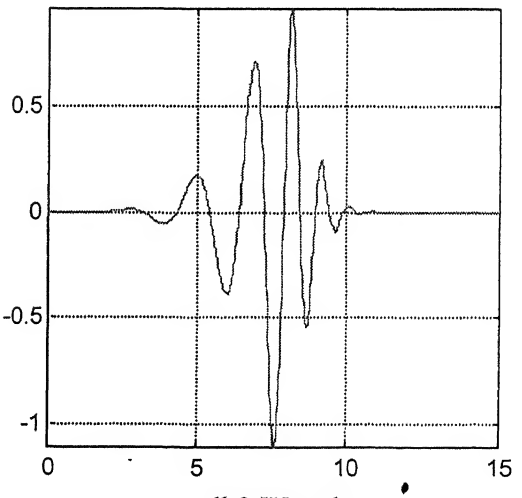

db8 Wavelet

Fig. 4.1 Daubechies Wavelets

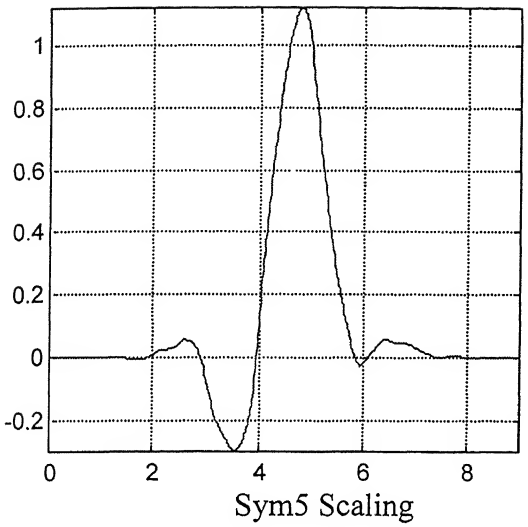

Sym5 Scaling

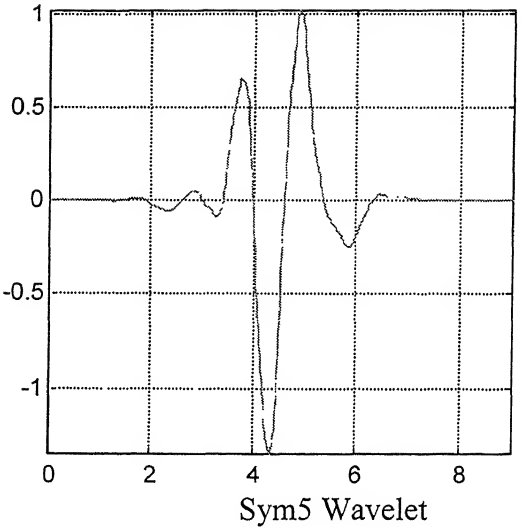

Sym5 Wavelet

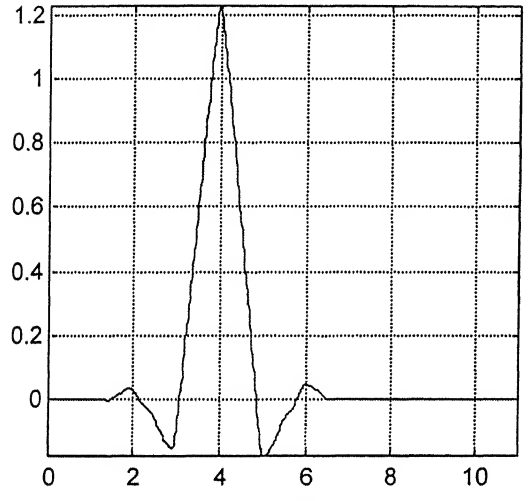

Coif2 Scaling

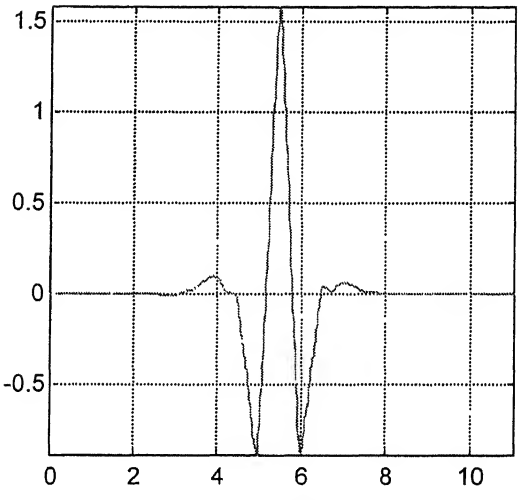

Coif2 Wavelet

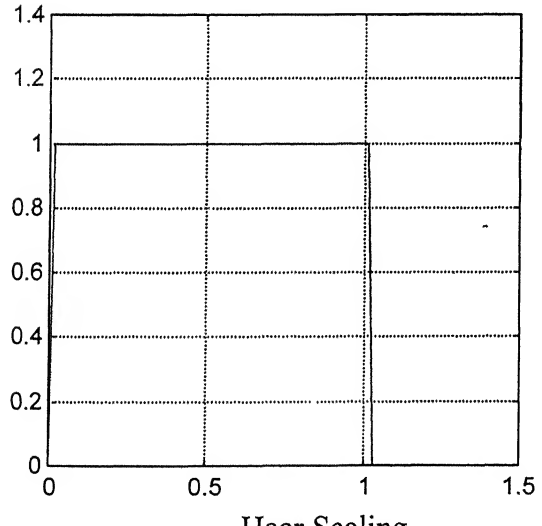

Haar Scaling

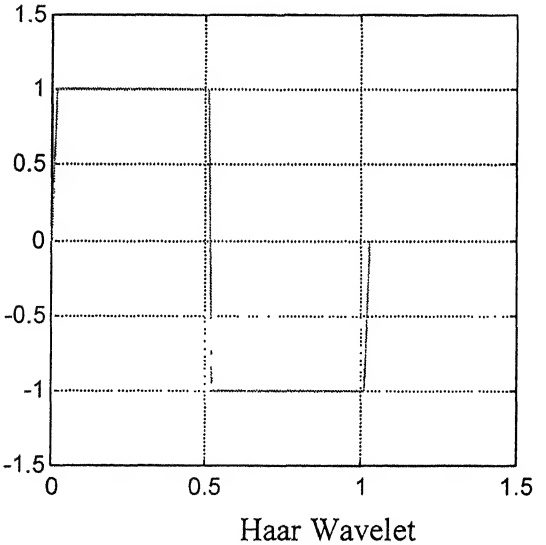

Haar Wavelet

Fig 4.2 Sym5, coif2, Haar Scaling and wavelets

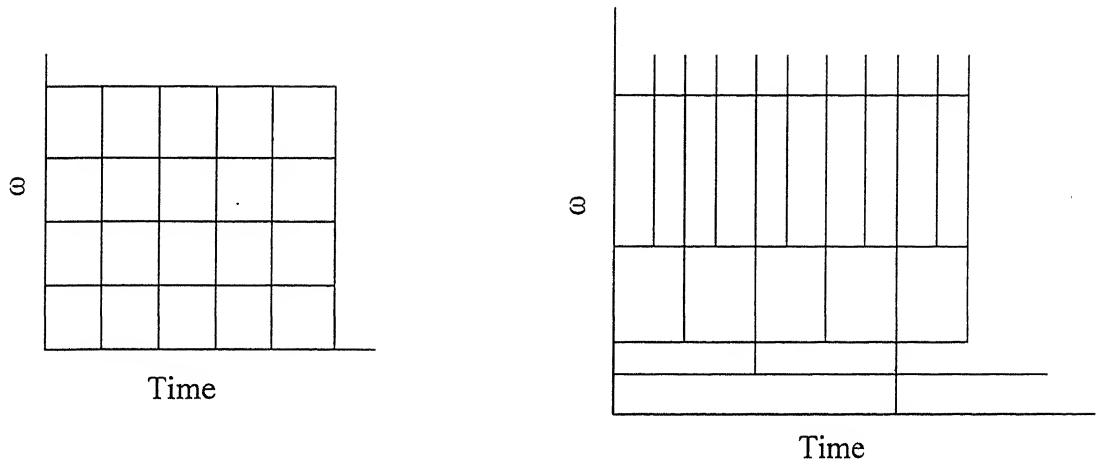

Fig. 4.3 Short-Time Fourier Transform (Time,ω), Wavelet Transform (Time,ω)

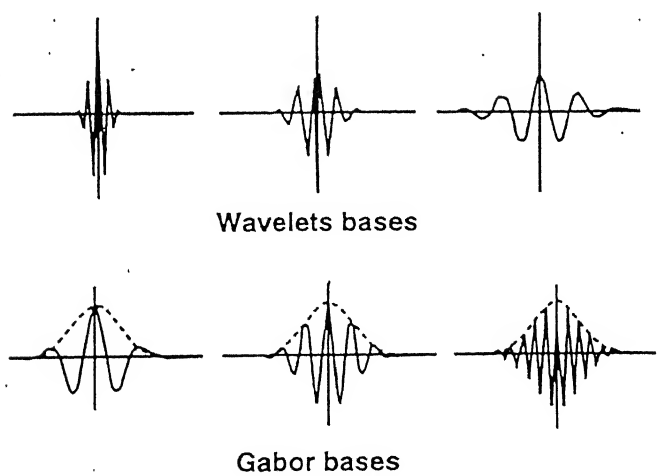

Fig. 4.4 Comparison between Wavelet bases and Gabor bases

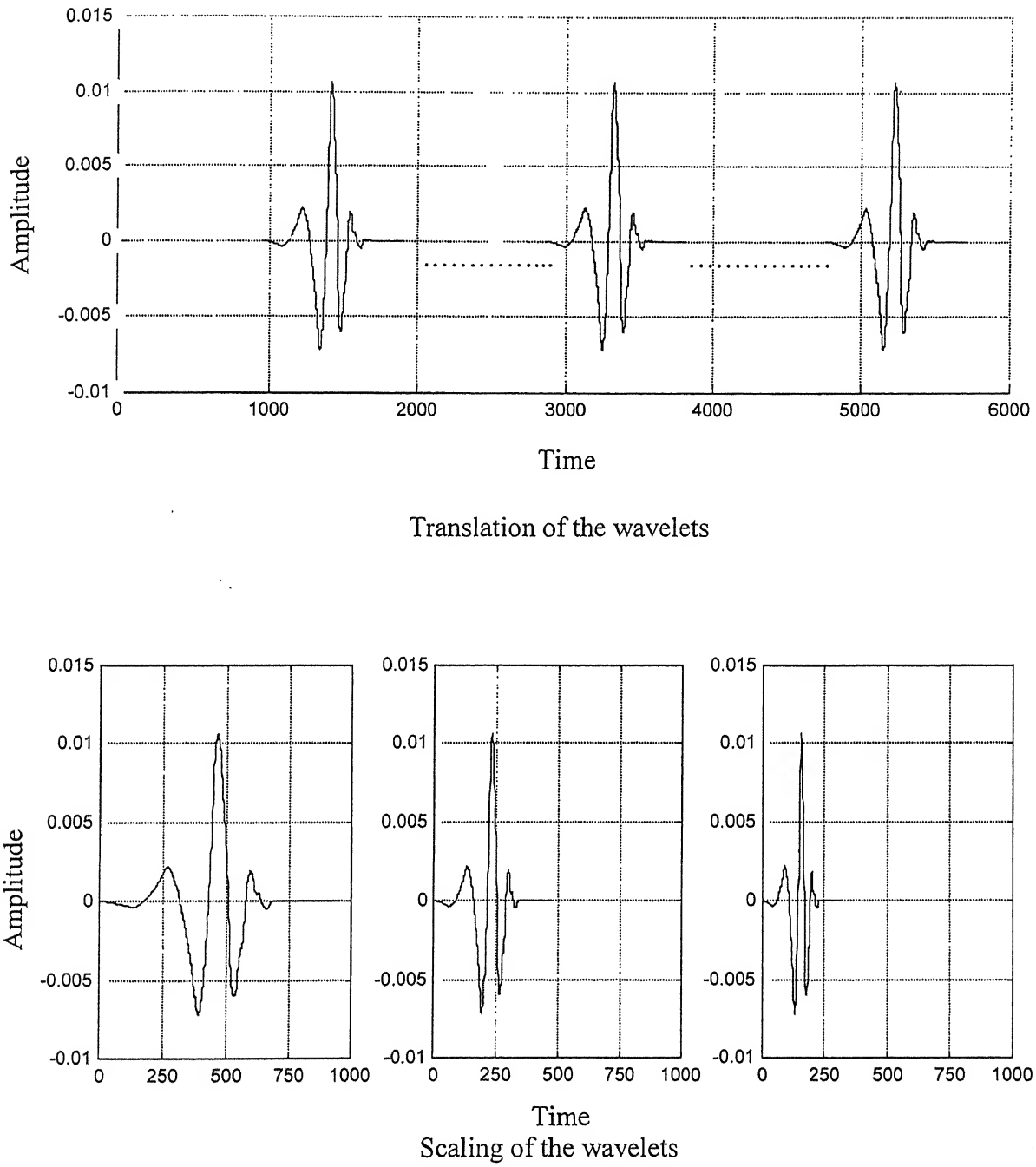

Fig.4.5 Translation and Scaling of the wavelets

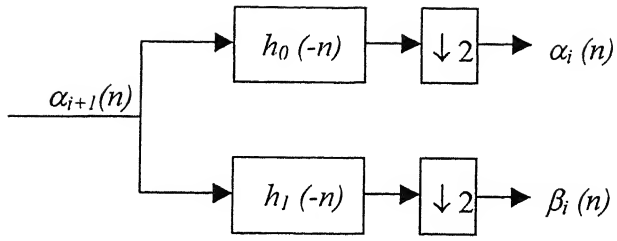

Fig.4.6 Two-channel Analysis filter bank for calculating Wavelet coefficients

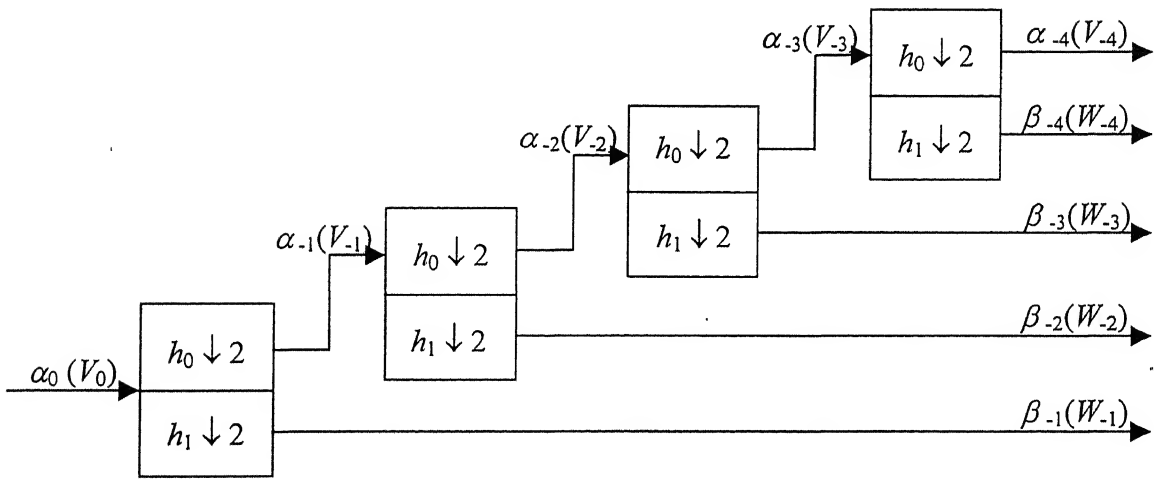

Fig.4.7 The discrete wavelet transform using a dyadic tree structure

Chapter 5

Application of wavelet Transform to Ultrasonic NDE

In Ultrasonic NDE, wavelet technique is being applied to experimentally obtained signals for various purposes. This chapter describes the various wavelet applications to ultrasonic non-destructive testing (NDT) and its implementation to the detection of a crack existing at the back surface.

5.1.1 Flaw detection with Noise Removal in frequency domain

If a signal contains the noise and flaw signals superimposed, then in the time domain flaw signal and noise occupy the same time window. And unless the flaw size is significantly greater than the grain size, time domain smoothing or low pass filtering in frequency cannot substantially reduce the noise without reducing the flaw component also.

Wavelet transforms are applied to both the real and imaginary parts of the estimated scattering amplitude ($\hat{A}(\omega)$ is the frequency domain data of the time domain signal $A(t)$) that was calculated using sub-optimal wiener filter. This weiner filter is used to transform the time domain data into frequency domain data as the Fourier transform does. As signal is a finite discretely sampled one, this places restriction on number of frequency scales (j-scales) that wavelet transform can decompose into. The signal to be extracted lives in a few of the j-scales, while noise will be found in all the j-scales with varying degrees. A pruning scheme is applied to select a few coefficients, where the desired signal is thought to live and remaining coefficients are made zero. Threshold level for small coefficients is determined by a percentage of the largest coefficient. After completing the threshold process, inverse transform is performed to get the noise free scattering amplitudes. A Coiflet [14,15] wavelet gives the lowest error norms consistently for the real part of $\hat{A}(\omega)$ (transformed domain of signal $A(t)$ into frequency domain by wiener filter), while a db10 wavelet of the daubechies family gives the lowest error norms [9] for the imaginary part of $\hat{A}(\omega)$.

5.1.2 Extracting a disturbing echo

Some times high amplitude echoes, which are disturbing the signal may come into picture. Then to pinpoint the echoes of lower amplitude, which may contain information, the extraction of higher amplitude echoes is necessary. Sometimes higher amplitudes are obtained due to the overlap of the echoes. To process this data, wavelet is the tool that divides the data, based on frequency.

In most of the experimental data, the above problem occurs due to the surface effects. Consider a signal obtained from the A-scan. Normally it contains intense echoes from the surface while the weaker one's come from the defects. This signal is decomposed using CWT and produces a time frequency plot. After decomposing a threshold value is determined which extracts the disturbing echo, and this threshold is applied for the B-scan to detect the defects. Research is in progress to better select the wavelet coefficients related to disturbing echo and thus reduce their effect.

5.1.3 Detecting the Disbond

The disbond in composites can be evaluated by the adhesion quality and this is done by ultrasonic pulse-echo method. The experimental A-scan data gives the signal containing multiple reflections. In them some reflections correspond to Longitudinal Wave and other corresponds to reflections from longitudinal to transverse mode conversion. It is reported that longitudinal mode reflected echoes do not vary with adhesion quality, while mode converted echoes are more sensitive to adhesion conditions. Therefore, mode converted echoes may be used to evaluate the adhesion quality which inturn tells about the disbonding of fibers and matrix in composites.

5.1.4 Elastic Property estimation

As the ultrasonic wave contains different frequencies, by the commonly used Fourier methods, frequencies only can be detected loosing the time domain information. So it is not possible to calculate the velocities of the waves propagating in the medium. For these dispersed ultrasonic waves, wavelet transform is very much useful. Time-frequency representation of signals made wavelet technique useful in this field of dispersion. The

magnitude of the analytic wavelet transform is directly related to the rate of energy arrival. Thus it is an optimal estimator for the measurement of group delay or velocity in the analysis of ultrasonic dispersed signals.

The time of arrival of the acoustic energy is utilized to determine the group velocity as a function of frequency of the wave. Thus the variation of Elastic properties with depth is characterized.

There are many mother wavelets that can be used for the purpose of dispersion analysis. But among all the available wavelets, an optimal mother wavelet used is the Morlet wavelet [8]. Analyzing with this type of wavelet produces wavelet components, which has a Gaussian bandwidth about a center frequency and this is useful in calculating the group velocities. When the A-scan data is decomposed using wavelet transform, each wavelet component is characterized by an associated group of waves that have a particular propagation velocity. The center frequency of a wavelet component determines the group velocity. And group delay time is obtained from the peak point of the envelope curve of the received signal waveform.

5.1.5 Anisotropic behavior of Composites

This is based on the effectiveness of the time–frequency (T-F) plot of wavelet transform. The use of T-F plot is to know how many wave modes are present in the transient Lamb waveform. Each mode has same velocity, because of this all modes are received at the same time duration. So, it is difficult to distinguish the modes by seeing the transient signals. To distinguish each mode separately, T-F plot is utilized through continuous wavelet transform. Number of modes present in the waveform, is known by the number of separate bright regions formed in the T-F plot.

The group delay at the different frequencies is measured from T-F plot for each mode and thus the group velocity is calculated as quotient of the propagating distance divided by the time delay.

The advantage of wavelet transform is, while trying to analyze wave modes with no idea of frequency region, they can be found from the T-F plot.

5.2 Neural Network classification of Ultrasonic Signal through wavelet decomposition

Major area of research in Ultrasonic NDE is the analysis of reflected waveforms representing the interaction between the ultrasonic wave and inhomogeneties in the material under inspection.

The signals, which are being reflected from various inhomogeneties is processed by the wavelet transform and relevant features are extracted that carry the discriminatory information. An automated pattern classification system using neural networks is described [12], which uses the extracted data from the wavelet decomposition for the estimation of size, shape and location of the defects. This defect classification based on neural networks and wavelet transforms is based on pattern recognition methods. These methods are being increasingly used for signal interpretation. Overall strategy for defect classification is given as

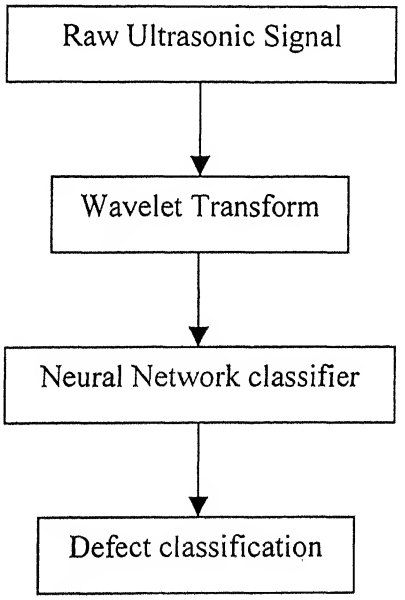

5.3 Implementation of the Wavelet Technique to present problem

In the present problem wave propagation is simulated with the help of finite Element code obtained from Jaleel [4] which is further modified by Kishore et al [5]. In this code the Newmark method for time marching is replaced by θ method to improve accuracy of

accuracy of simulation. The data for wavelet processing is obtained in the form of A-Scans at different receiver locations. The wave propagation simulation is carried till all the waves from the crack reach the receiver location. The total duration is divided into 512 time steps and wavelet analysis is performed.

Wavelet analysis is performed using the wavelet toolbox present in MATLAB 5.2 available in computer center, IIT, Kanpur. Various functions are available in the toolbox and some of the functions include n-scale decomposition, reconstruction, thresholding, compression, denoising etc. DWT is coded in MATLAB uses subband coding, Multi Resolution analysis of Mallat [26].

The receiver signal contains three main wave components corresponding to backwall reflections, sidewall reflections along with reflections from crack surface, crack root and scattered waves from crack tip. The backwall reflections are very strong compared to any other reflection. Present aim is to use the wavelet transform technique to separate each and every component from the raw signal.

Using db2 wavelet the signals obtained at different source locations (Fig 6.1) are decomposed into 6 wavelet levels by discrete wavelet transform. This is achieved by using MATLAB function. The relevant functions are given in Appendix A. The wavelet levels obtained are visualized in two ways. One way is, to visualize all wavelet levels of one location signal in Time-Scale plane at a time. Another way is to take same level coefficients of all the different location signals and then visualize the image plot. These plots are used for the crack detection analysis.

In the present work db2 wavelet is used as the mother wavelet. Reason for using db2 wavelet is that it is closer to the sine load pulse applied at the source. gives the arrival times of the reflections with slight error. If higher level wavelets are used for the analysis, then the error increases as the level of used wavelet increases. Also higher wavelets has more peaks compared to db2. This can be observed in the Fig 5.1, in which, comparison is made between db2 and db5. So, if the wavelet used contain less peaks then the coefficients are obtained as and when the reflection is received. So, it is justified to use db2 for the present analysis to get the better results.

To observe the small reflections from the crack, it is necessary to suppress the large coefficients. MATLAB provides a function, which is useful to see a range of coefficients. This function is utilized to observe the crack reflections.

At first the signals at different source locations are decomposed into 6 wavelet levels by db2 wavelet. They are plotted using the pseudo color gray scale image plot. These are shown in Figs. 6.12 to 6.17. For better visualization, these are plotted for the range 40-65 after converting the decomposition into image, which have a minimum value 1 and a maximum value 128. Plots obtained in this way are further used for crack detection.

In level 1 very high frequency components are decomposed. These high frequency components are not required by the analysis as such components are not present in the data. So this level is discarded from the analysis. The required frequencies lie in the levels 2, and 3 mainly. So they are analyzed for the crack. Each wavelet level of the signals is taken into one plot and then it is studied for good visualization.

It is observed that the crack reflections are moving along the time axis as the distance between crack and source is increasing. Where as for backwall they are stand still in time. This is observed in both levels 2 and 3.

The sidewall reflections are weak, as most of the energy incident upon side wall is absorbed and they are clearly observed. Reflections coming from the crack are clearly visible and some of the artifacts are identified in level 2 and 3. Crack tip reflection is the one, which is seen as first moving reflection. So, first a conclusion is drawn that there is a crack and then remaining coefficients are observed closely to identify the root reflection. Root reflection is slightly stronger than the tip reflection. In this way root and tip wavelet coefficients are identified.

For carrying out the analysis with wavelet transform, MATLAB 5.2 is used. This provides the necessary functions to perform the wavelet transform of a signal. In Appendix A all the available functions for wavelet analysis, and the functions which are used for the preset analysis are presented. MATLAB Graphics is also very much useful to visualize the data.

5.4 Closure

In this chapter different applications of the wavelet technique, related to NDE are discussed. Different ways of ultrasonic signal processing with wavelets is explained briefly related to noise removal from the raw signal, extraction of unwanted reflections, disbond detection, dispersion analysis and anisotropic nature of the composites. Lastly, wavelet implementation to present problem is discussed. In the next Chapter the wavelet transform is implemented on the simulated wave propagation and the obtained results are discussed in detail.

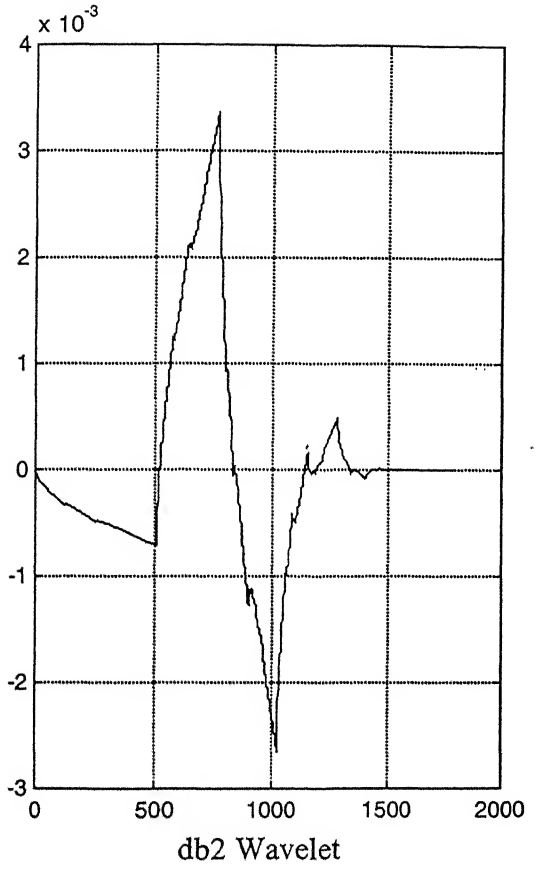

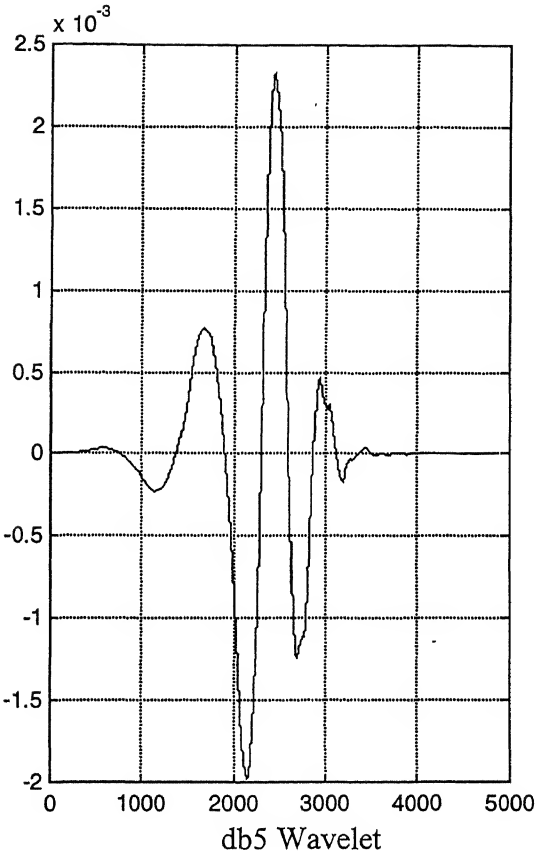

Fig. 5.1 Comparison of number of peaks in db2 and db5 wavelets

Chapter 6

Results and Discussion

6.1 Introduction

This Chapter presents the application of wavelet technique to analyze ultrasonic signals and detect a crack. The wave propagation due to a load pulse is simulated by FEM and displacement signal in a pulse-echo mode is decomposed into different wavelet scales, which are represented as image plots. It uses gray scale to represent each wavelet coefficient. As gray scale image is used to plot the coefficients, the required reflection coefficients can be identified easily by examining the Time-Scale (T-S) plot. From this plot the arrival times of the wave reflections from the crack are found, if they are present in the signal. These reflections are found by examining the plot.

6.2 Details of the Problem

6.2.1 Geometry

For the present analysis, a thick plate with the crack on the back surface as shown in Fig. 6.1 is considered. The geometry of the domain and crack is shown in the figure.

- domain size : 20 mm x 60 mm
- Crack length : 10 mm
- Crack width : 0.25 mm

6.2.2 Material

Steel is used as the plate material with the following properties.

- Youngs modulus, E : 210 GPa
- Density, ρ : 7700 kg/m^3
- Poisson ratio, ν : 0.33
- Longitudinal wave speed, C_L: 6356 m/s
- Shear wave speed, C_T: 3202 m/s
- Raleigh wave speed C_R: 2984 m/s

6.2.3 Details of Input pulse

To simulate the application of an ultrasonic pulse by a finite angle width transducer (i.e peizo electric transducer), the load is applied over a few nodes as shown in Fig. 6.2. Different types of input pulses such as mexican hat, daubechies4, cosine have been tried as input for better detection (Fig. 6.3). But among all the pulses, sine pulse is easier to apply and found to give good results.

Further, the load pulse is applied at successive nodes with appropriate delay to simulate the angle probe sending energy in a certain direction (45°). The analysis has been repeated for source locations `a`, `b`, `c`, `d`, `e` and `f` as shown in Fig. 6.1. Pulse is applied for a duration of 0.32μs (9 time steps).

details of the sine pulse :

- Force magnitude : 100 KN
- Applied frequency : 3.125 MHz
- Pulse duration : 0.32 μs

The simulation is done for a total period of 20.44 μs (512 time steps) so as to receive reflections from crack.

6.3 FEM simulation

6.3.1 Mesh details

Simulation is performed in plane strain case using the code developed by Jaleel [4] and modified by Kishore, Sridhar and Iyengar [5].

It is suggested to use lower order elements with uniform meshing for dynamic analysis. Accordingly, quadrilateral element is chosen to discretize the domain.

- Analysis method : plain strain
- Element used : iso-parametric 4-noded quadrilateral
- Nodal degrees of freedom : 2 (translation along x and y)
- No of elements : 19200 (80 elements in x, 240 elements in y direction)
- No of nodes : 19521 (81 nodes in x direction, 241 nodes in y direction)
- Element Length, width : 0.25 mm

- Time step, Δt : 0.04 μs

6.3.2 Directionality and Surface Scanning

In ultrasonic NDT, angle probes are used, which send out wave energy at a certain required direction. This is achieved in FEM by transmitting the same load pulse on a few successive nodes with proper time lag.

In the present problem, the force is applied in a 45° direction from the source and directionality is achieved by giving time delays to the force at all 5 nodes (Fig. 6.2) to have a strong wave propagating towards the crack and get the stronger reflections. At first the load is applied on the node n-2, then by calculating proper time lag load pulse is applied on the node n-1, this continues till the node n+2. This is incorporated in the finite element code used for simulation. Time delay is calculated using the velocity of the ultrasonic wave, element length and the directional angle of energy required. The locations `a`, `b`, `c`, `d`, `e` and `f`, are chosen such that wave energy propagation spans the whole crack.

6.3.3 Crack modelling

Crack is modelled in FEM by line crack or finite width notch. Notch is used so that the strong waves are reflected from crack tip. It is modelled by assingning zero values to all the material properties. In the present analysis the crack is vertical and starting on the surface CD (Fig. 6.1) till half the thickness, and width of the notch is one element size. The crack dimensions are 0.25 mm x 10 mm.

- No of notch elements : 40 (in Y direction)

6.3.4 Boundary conditions

On the edges BC and CD, free boundary conditions are applied. On the edge AD absorbing boundary condition is applied, which is given in Chapter 3. By applying the absorbing condition on any boundary, most of the energy going to that boundary is absorbed at the boundary itself. On the edge AB free boundary condition is applied except at the points where the force is applied.

6.4 Wavelet Analysis

6.4.1 Different Artifacts in Receiver Signal

The ultrasonic signal collected by receiver probe (Pulse-echo mode) consists a number of reflections superimposed. Important waves reaching the receiver location are from the backwall (*B*), sidewall (S), crack surface (*C*), crack root (*r*) and crack tip (*t*) and the waves may be Longitudinal (*L*), Transverse (*T*), Rayleigh (*R*), or Header (*H*) waves. They may be direct, single surface reflections from *B, C, t* and *r*. Some salient paths, and modes are shown in Figs. 6.4 (a), (b), (c) for source location `c`. It can be seen that the backwall, crack surface and crack root reflections are strong, whereas crack tip scattered waves are very weak. Thus the main complexity of the problem is to detect, and classify the reflections. The various reflections that are possible to reach the different receiver/source locations (receiver is also at the same location in pulse-echo mode) are tabulated in Table 6.1. These values are calculated using the formulae given in Chapter 2.

The type of reflections, which are possible are direct backwall reflections, direct sidewall reflections, and direct crack tip, root reflections. Other than direct reflections diffused reflections from crack, and few more paths are possible which are shown in Fig. 6.4. Among all of the reflections, backwall reflections are most significant and remaining are comparitively weak. Figs. 6.5 to 6.10 show the receiver signals obtained for each of the source locations. Each figure shows three graphs related to u, v displacements (in x, y directions) and the resultant displacement in 45°-direction. In the figures the wave modes of the reflection components are also marked. The reflections, which are most significant are backwall reflections L_BL, L_BT, T_BT, and sidewall reflections if the source locations are near to edge AD (ref. to Fig. 6.1). L_tL, L_rL, T_rL are also significant but they have very small magnitude compared to backwall. The reflected wave L_CL_BT is also significant but this is superimposed with other reflections. Some of the header waves coming from the crack tip like H_tT, H_tL and from root H_rL, H_rT are small, which cannot be seen in the displacement plots due to overlap with other reflections. Some of these reflections which are not seen in original displacement plots are seen in the T-S plots obtained from wavelet transform given in the coming sections.

6.4.2 Quantification using Wavelet Technique

To study the small reflections in the time domain, wavelet technique is used. Wavelet transform divides the data by correlating the signal data with the required wavelet. As explained in Sec. 4.3.2, in CWT the signal is decomposed into various scales, which are real numbers. Where as in DWT, scales are to be selected by the user. CWT gives coefficients at each and every sampling point of the signal being analyzed. As the number of coefficients obtained is equal to signal sampling points, each scale contains many coefficients related to same reflection. This will create confusion in selecting the required wavelet coefficients, during crack detection analysis. This also has computational disadvantages like redundancy, and takes considerable time to process the signal. Orthogonality condition is not satisfied by scaled and translated versions of the mother wavelet used to decompose the signal. So, reconstruction is not the same every time, if different scales are chosen.

For the present problem orthogonality is required to identify the weak reflections and also a limited number of coefficients should be there to identify particular reflection. Another option is to design or select a wavelet, matching the wave reflection from the crack tip. In such a case, the decomposition is exact. As the later option of wavelet design or selection is not possible, CWT cannot be used in practice for these applications.

The wavelet analysis is performed with the help of MATLAB 5.2 toolbox for Wavelets. The various functions available and the functions used in the present work are presented in appendix A.

6.5 Results and Discussion

In the previous sections it was explained about the many possible reflections and the complexity of the problem. In this section the signal analysis by wavelet transform (WT) and crack detection is presented.

Firstly, the signal data contains the effect of input pulse till 80-iterations approximately. This input pulse is much stronger than the later reflected signals and hence the initial signal upto 60 iterations (2.4μsec) is deleted (made equal to the signal value at 61st step to have smooth data). In the resultant displacement at location `a` (ref.

to Fig. 6.5), the first reflection is expected at 79th time step by L_SL, but this is weakly visible in the plot as most of the reflection is being shadowed by sidewall AD (Fig. 6.1). R_SL reflection from the sidewall is the first reflection observed in the resultant plot as this is the powerful wave propagating on the surface. Similarly R_ST is visible, but this is superimposed with the L_BL reflection. Then the powerful reflection T_BT is seen, this is seen in each and every plot at the same time step. Then L_CL_BT reflection is seen which is significant compared to the other reflections. The ultrasonic signal for source location `b` (Fig. 6.6), almost same reflections are seen in the same order that are seen for signal at location `a`, but the reflections coming from sidewall and crack change their timings.

For the signal at location `c` shown in Fig. 6.7, the first reflection is the L_BL reflection, and it is seen in the plot with a large magnitude. Then L_tL from crack tip is weak and is not visible due to the domination of L_BL. After this, every reflection comes in the similar fashion as the previous locations which is discussed. This pattern of reflections appearing in the resultant of u and v displacements at 45° direction, continue to appear in signal from other source locations (Figs.6.8 to 6.10). In all these signals, the dominant backwall reflections can be observed clearly. But the reflections from crack are small and overlap with other reflections. For better identification of the reflections, signals are processed using wavelet technique.

Wavelet Analysis:

There are many mother wavelets, using which the signal can be decomposed. Out of many, Daubecheis db2 (Fig. 5.1) wavelet is found to give good results for the present probe. This particular wavelet is chosen for the analysis purpose because it has less number of moments or peaks as the input pulse is one sinusiodal cycle, which has one positive peak and one negative peak. If higher order wavelet is used for the analysis, then wavelet coefficients of the signal data are obtained at little bit later times than calculated times and this is shown in Fig. 6.11, which shows the wavelet decomposed levels obtained by db5 (Fig 5.1) wavelet.

The db2 wavelet has a scaling function or low-pass filter and a wavelet function or high-pass filter. For each scale to obtain the decomposition, signal is divided into low-

pass and high-pass coefficients from previous scale low-pass coefficients. This is depicted in Fig. 5.7.

For the first scale, DWT produces (N/2) + 1 scaling and wavelet coefficients where N is the number of sampling points. In the next scale half the number of previous scale coefficients are produced and like this n scales can be obtained where n= (log(N)/2)-1. The analyzing signal contains 512 sampling points, so the maximum wavelet levels that can be obtained are 8. In the present analysis, the signal is decomposed into 6 levels, each representing a different scale or frequency. Decomposition of the signals for the various source locations is shown in Figs. 6.12 to 6.17 as an image plot on time-scale (T-S) plane. Coefficients are represented in gray scale values between 1 and 128. It was observed that backwall reflections are strongest and rest of the coefficients lie between to 40 to 65 of the gray scale. Therefore, to bring out clearly these coefficients 40 to 65 range of gray scale is chosen on the T-S plane. Important features are observed in the first three levels and the remaining levels 4, 5, 6 do not yield any significant information as they have wider coefficients in time domain. These wider coefficients are not required for analysis, as the input pulse is given for 9 time steps only.

For the signal at source location `a`, shown in Fig. 6.12. It can be seen that level-1 and level-2 most of the reflections have small coefficient value compared to level-3. As these correspond to location `a` which is near to sidewall L_SL, R_SL is seen at first. R_SL can be seen clearly in level-3 as it is one of the significant reflection, and from this image its arrival time can be found. L_BL from backwall is one of the dominating reflections and its arrival time is seen correctly in level-3. L_tL from tip is not visible due to the domination of L_BT, which arrives at the same time range. The multi surface reflections L_CL_BT and T_BL_CL occur at the same time and these can be seen in levels 1, 2, 3.

Fig. 6.13 gives the image of decomposed signal for source location `b`. In this the first reflection coming is the side wall reflection L_SL and can be seen clearly in first two levels. At time step 312 the strong backwall reflection L_BL is seen in first three levels and clearly pointed in level-3. From level-3 arrival time of this reflection can be calculated. In between 200 and 250 time steps some reflections like R_ST, T_ST, L_rL, L_tL can be seen in all the level's 1, 2, 3. Then the strong T_BT is seen. This appears at same time step in every

signal obtained at different source locations. L_CL_BT can be seen in all the levels and specifically visible in level-3. Reflections reaching the receiver after L_CL_BT reflection are many and it is difficult to classify them.

Fig. 6.14 is the decomposition of signal at source location `c`. In this image the same reflections as previously discussed can be seen. Fig. 6.15, Fig. 6.16 and Fig. 6.17 are the decomposed signals at source locations `d`, `e` and `f`, which are nearer to crack. In these image plots the tip scattered wave L_tL is the first wave observed and this is clear in first two levels. Then backwall reflection L_BL is seen clearly in first three levels. For all the three locations, the header wave scattered by crack tip H_tT can be seen which is weak compared to L_BL. The strong T_tT is seen clearly in first three levels.

Wavelet coefficients of levels 1, 2, 3 are plotted as line graphs in the Figs. 6.18 to 6.23. Explanation for these figures are also given as explained above, for the image plots. Other than L_BL and T_BT the other dominant reflection that is seen is all the plots is the H_rT reflection.

Crack Detection :

The detection of the crack involves the determination of the crack location, size and orientation. Here the procedure is described, which involves the simultaneous studying of various image plots obtained from various locations. The image plots of a certain level for various source locations are compared. The images for levels 1, 2, 3 are shown in Fig. 6.24 to Fig. 6.26 respectively. Prelimanary examination of these images shows that some coefficients are similar in all the signals a, b, c, d, e and f, out of them some are moving in time-domain and some are static in time-domain. The moving coefficients along the time domain are the reflections obtained from the crack and the static coefficients are backwall reflections. Thus getting the signals at different source locations and comparing images of one wavelet level, the reflections coming from the crack and backwall can be recognized. Differentiating the crack and backwall reflections is done by the method discussed as above.

The first important reflection coming from the crack is the tip scattered wave L_tL. This is a weak reflection compared to backwall reflections and can be observed in level-1 and level-2 images. This reflection is moving in time from source locations `f` to `a`. Moving nature of the crack is due to the difference in the distance between source and crack. This reflection is identified by examining the first moving reflection. And it can be identified clearly, as there is no overlap of other reflections. Because the reflection is weak, it cannot be viewed clearly in level-3 as in this level backwall reflection L_BL is dominant.

Second specific reflection that is seen moving is the header wave scattered by tip, H_tL. This is slightly strong reflection than previous one, so it can be seen in level-3. Since some of the reflections are arriving at the receiver location at the same time for some source locations, this cannot be seen as clear as L_tL. This is identified as the second fastest reflection coming from crack tip and having higher time-domain value to appear in all the signals (Range) than previous one in the image. Range is calculated from the arrival times of the same reflection at source locations `a` and `f`.

Third specific reflection seen moving is the crack root reflection L_rL. This is seen in level-2 of the source locations except location `f` due to over lap of other reflection. The arrival time of the reflection can be calculated for each source location and this is used to find the size of crack along with the help of L_tL. It is identified by examining the moving reflection, which has less time-domain range than L_tL and this arrives next to H_tL.

Next reflection that is seen moving is H_tT. This is seen in level-1 and level-2. It cannot be visualized clearly due to overlap with other reflections. It can be identified by its time location, which should be less than H_tL and L_tL.

Next reflection seen moving is H_rL. This is seen in level-1 and level-2 which is of low gray scale. This is identified by its range, which is less than any reflections range in time-domain.

The multiple surface reflection L_CL_BT is the next moving reflection that is seen very clearly in levels 1 and 2. This is one of the strong reflection, that is why even though it is arriving lately it can be seen clearly.

Analysis with no crack domain :

To obtain more understanding of the application of wavelet technique, signal data without crack is obtained for source locations `a`, `c` and `e`. These signal data are subtracted from the data with crack and the analysis results are presented. At the specified three locations the simulated data with crack and without crack is obtained. After getting the decomposed signal coefficients, without crack coefficients are subtracted from the coefficients with crack and the image is plotted in Figs. 6.27 to 6.29. Now the moving nature of the crack can be seen very clearly without without the effect of the backwall reflections. The different reflections discussed in the previous section can be clearly seen here in level-3. Arrival times of the required reflection can also be determined easily and correctly. This method using no crack data is used to justify the results obtained directly from the raw A-scan data, which is analyzed with wavelet transform in the previous section.

Crack location, crack size and angular location :

For the detection of crack it is enough that one reflection time from crack tip and another reflection time from crack root at two different source locations is known, to find the crack location and size. To find the crack inclination, the distance to backwall is also required. As L_tL is the fastest and not effected by any of the other reflections, this is used to determine the time taken to go and come from the crack tip at two locations. Similarly using L_rL, time taken to go and come from crack root at two source locations are calculated.

As times are known for two different source locations for the wave to go and come from crack tip and root, and from the known wave speeds, distance between the source and crack tip, crack root are calculated. From these calculations the crack location, crack size and crack angular location are calculated as shown in Fig 6.30

Let,

bf = (arrival time of L_tL x Δt / 2) x (Longitudinal velocity)

df = (arrival time of L_tL x Δt / 2) x (Longitudinal velocity)

be = (arrival time of L_rL x Δt / 2) x (Longitudinal velocity)

de = (arrival time of L_rL x Δt / 2) x (Longitudinal velocity)

bwd = (arrival time of backwall L_BL x Δt / 2) x (Longitudinal velocity)

$$\theta_1 = \text{Cos}^{-1} [(df^2 + bd^2 - bf^2) / 2(df)(bd)]$$

$$\theta_2 = \text{Cos}^{-1} [(de^2 + bd^2 - be^2) / 2(de)(bd)]$$

$$\theta = \theta_1 - \theta_2$$

$$\alpha_1 = \text{Cos}^{-1} [(de^2 + ef^2 - df^2) / 2(de)(ef)]$$

$$\alpha_2 = \text{Sin}^{-1} [\ bwd / de\ ]$$

Finally Crack length = $[de^2 + df^2 - 2(de)(df)\ \text{Cos}\theta\ ]^{1/2}$

Crack inclination is $(\alpha_1 + \alpha_2)$

Case study:

Taking the two source locations as `b` and `d` (ref. to Fig. 6.1) calculations performed.

Arrival times taken from the image plot by seeing all the three levels are.

For location `b` arrival time of $L_tL = 213$ and arrival time of $L_rL = 255$

For location `d` arrival time of $L_tL = 142$ and arrival time of $L_rL = 203$

Arrival time of backwall $L_BL = 157$

By following the above given procedure crack length = 0.0121

% error in detecting the crack length = 21

Crack inclination = 89.5°

6.6 Closure

In this Chapter the results obtained based on the methodology discussed. It can be seen clearly that reflections coming from crack and backwall are distinguished by comparing same level of decomposed signals obtained for various source locations. Time required for the particular wave coming from crack is noted and it is used to find crack location, crack size, and crack angle. The results obtained are in good agreement with actual values.

Table 6.1 Time (steps) taken for various waves reaching the receiver. Time step $\Delta t = 0.04\mu s$

Name	Description	Source/receiver locations (pulse-echo method)					
		a	*b*	*c*	*d*	*e*	*f*
L_tL	*L to crack tip, reflected L to source*	249	212	176	142	111	88
L_rL	*L to crack root, reflected L to source*	284	252	222	197	176	162
L_BL	*L to back wall, reflected L to source*	157	157	157	157	157	157
L_tT	*L to crack tip, reflected T to source*	371	316	263	212	166	131
L_rT	*L to crack root, reflected T to source*	423	376	332	294	263	242
L_BT	*L to back wall, reflected T to source*	235	235	235	235	235	235
T_tT	*T to crack tip, reflected T to source*	494	420	349	282	221	175
T_rT	*T to crack root, reflected T to source*	563	500	442	390	349	322
T_BT	*T to back wall, reflected T to source*	312	312	312	312	312	312
H_tL	*H to crack tip, reflected L to source*	310	272	234	197	162	131
H_tT	*H to crack tip, reflected T to source*	432	376	321	267	217	174
H_rL	*H to crack root, reflected L to source*	353	323	296	274	257	242
H_rT	*H to crack root, reflected T to source*	493	447	406	371	343	322
L_SL	*L to side wall, reflected L to source*	79	118	157	197	236	275
L_ST	*L to side wall, reflected T to source*	117	176	235	294	352	411
T_ST	*T to side wall, reflected T to source*	156	234	312	390	468	547
R_SL	*R to side wall, reflected L to source*	123	185	246	308	369	431
R_ST	*R to side wall, reflected T to source*	162	243	324	405	486	567
L_CT_BT	*L to crack surface, reflected T to back wall, reflected T to source*	-	-	-	-	-	-

$T_C L_B L$	*T to crack surface, reflected L to back wall, reflected L to source*	*415*	*365*	-	-	-	-
$L_C L_B T$	*L to crack surface, reflected L to back wall, reflected T to source*	*387*	*352*	*318*	*286*	*260*	*242*
$T_C T_B L$	*T to crack surface, reflected T to back wall, reflected L to source*	-	-	-	-	-	-
$L_C T_B L$	*L to crack surface, reflected T to back wall, reflected L to source*	-	-	-	-	-	-
$T_C L_B T$	*T to crack surface, reflected L to back wall, reflected T to source*	-	-	-	-	-	-
$L_B T_C T$	*L to back wall, reflected T to crack surface, reflected T to source*	-	-	-	-	-	-
$T_B L_C L$	*T to back wall, reflected L to crack surface, reflected L to source*	*387*	*352*	*317*	*286*	*259*	*241*
$L_B L_C T$	*L to back wall, reflected L to crack surface, reflected T to source*	*414*	*364*	-	-	-	-
$T_B T_C L$	*T to back wall, reflected T to crack surface, reflected L to source*	-	-	-	-	-	-
$L_B T_C L$	*L to back wall, reflected T to crack surface, reflected L to source*	-	-	-	-	-	-
$T_B L_C T$	*T to back wall, reflected L to crack surface, reflected T to source*	-	-	-	-	-	-
$H_C L_B T$	*H to crack surface, reflected L to back wall, reflected T to source*	-	-	-	-	-	-
$H_C L_B L$	*H to crack surface, reflected L to back wall, reflected L to source*	*408*	*361*	-	-	-	-
$H_C T_B T$	*H to crack surface, reflected T to back wall, reflected T to source*	*564*	-	-	-	-	-
$H_C T_B L$	*H to crack surface, reflected T to back wall, reflected L to source*	-	-	-	-	-	-
$H_B L_C T$	*H to back wall, reflected L to crack surface, reflected T to source*	-	-	-	-	-	-
$H_B L_C L$	*H to back wall, reflected L to crack surface, reflected L to source*	-	-	*314*	*282*	*253*	*228*
$H_B T_C T$	*H to back wall, reflected T to crack surface, reflected T to source*	-	-	-	-	-	-
$H_B T_C L$	*H to back wall, reflected T to crack surface, reflected L to source*	-	-	-	-	-	-
$L_B T_t T_d$	*L to back wall, reflected T to crack surface, dispersed T to source*	*460*	*408*	*359*	*314*	*275*	*246*
$T_B L_t L_d$	*T to back wall, reflected L to crack surface, dispersed L to source*	*387*	*351*	*318*	*287*	*260*	*242*
$L_B L_t T_d$	*L to back wall, reflected L to crack surface, dispersed T to source*	*414*	*364*	*316*	*273*	*235*	*207*

$T_BT_tL_d$	*T to back wall, reflected T to crack surface, dispersed L to source*	*455*	*411*	*369*	*332*	*302*	*281*
$L_BT_tL_d$	*L to back wall, reflected T to crack surface, dispersed L to source*	*337*	*304*	*272*	*244*	*220*	*202*
$T_BL_tT_d$	*T to back wall, reflected L to crack surface, dispersed T to source*	*509*	*456*	*404*	*357*	*315*	*286*
$H_BL_tT_d$	*H to back wall, reflected L to crack surface, dispersed T to source*	*508*	*454*	*404*	*352*	*306*	*270*
$H_BL_tL_d$	*H to back wall, reflected L to crack surface, dispersed L to source*	*386*	*350*	*315*	*282*	*252*	*226*
$H_BT_tT_d$	*H to back wall, reflected T to crack surface, dispersed T to source*	*573*	*514*	*456*	*401*	*352*	*312*
$H_BT_tL_d$	*H to back wall, reflected T to crack surface, dispersed L to source*	*450*	*409*	*369*	*331*	*297*	*268*

where,

L – Longitudinal wave, T – Transverse wave, H – Header wave, R – Raleigh wave

- represents either wave is not reaching the receiver or do not exist at all

a, b, c, d, e and f are the source / receiver locations as shown in Fig. 6.1

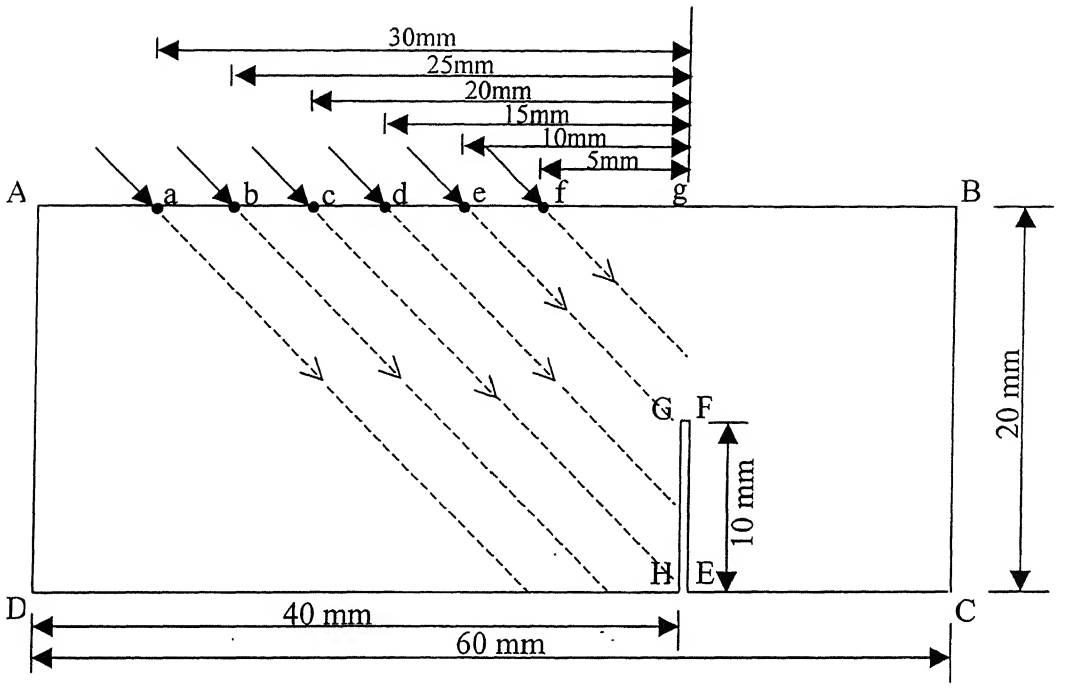

Fig 6.1 Domain modedelled with source locations and energy focussing direction

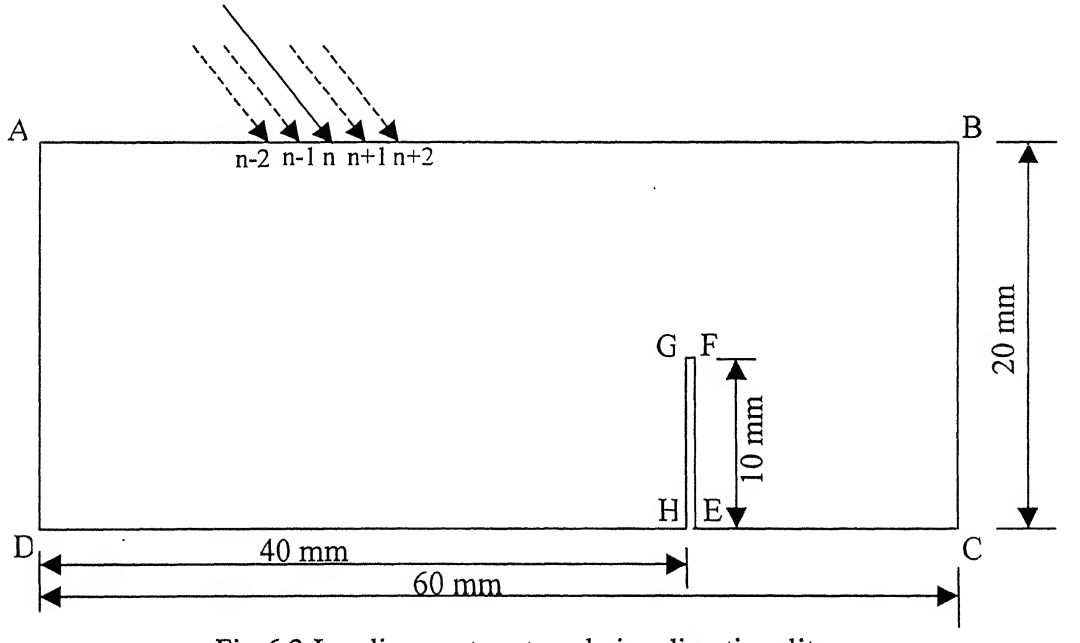

Fig 6.2 Loading system to acheive directionality

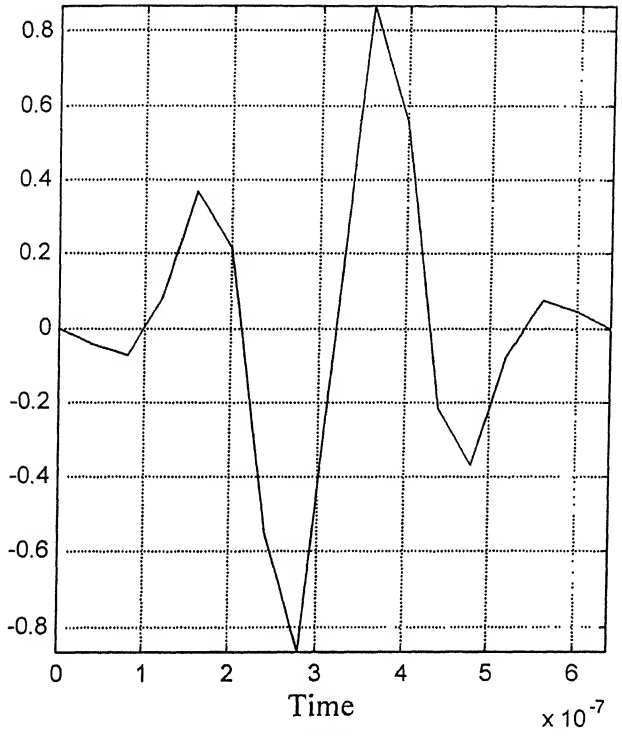

Approximate Daubechies4 pulse

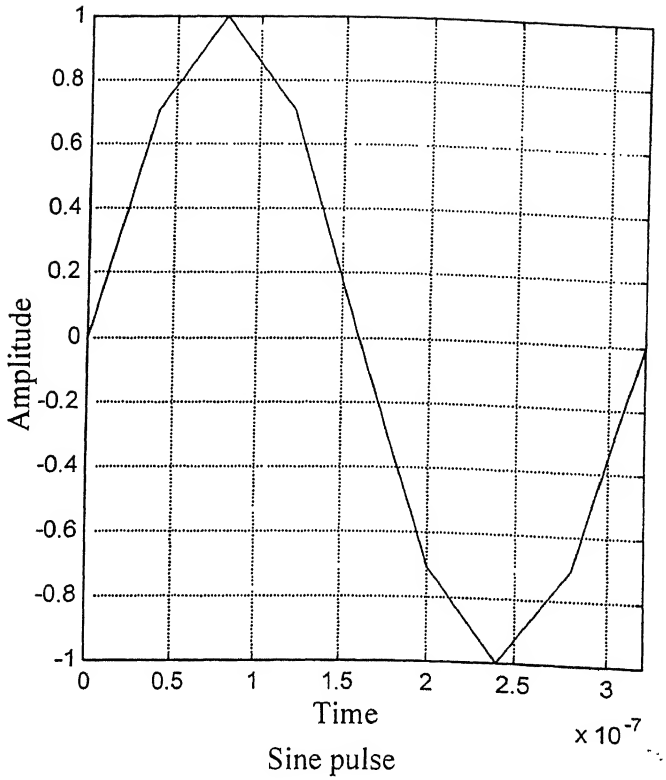

Sine pulse

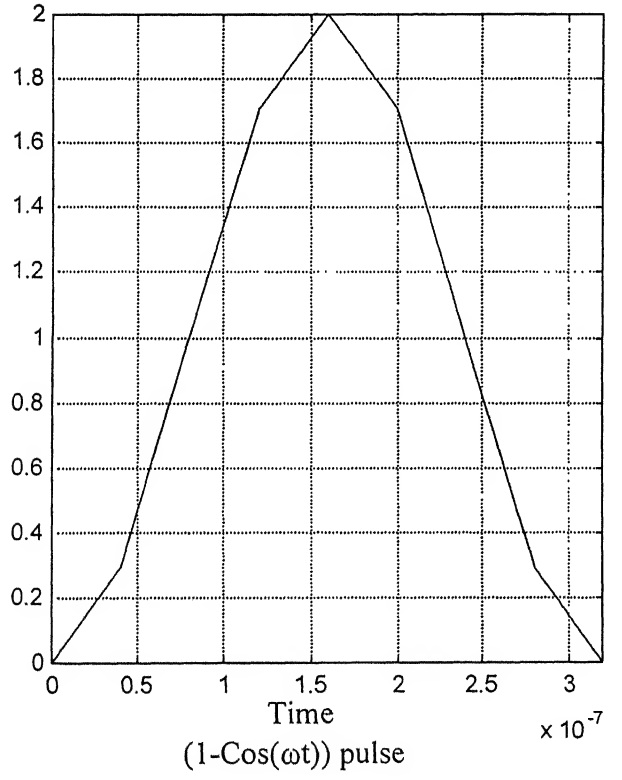

(1-Cos(ωt)) pulse

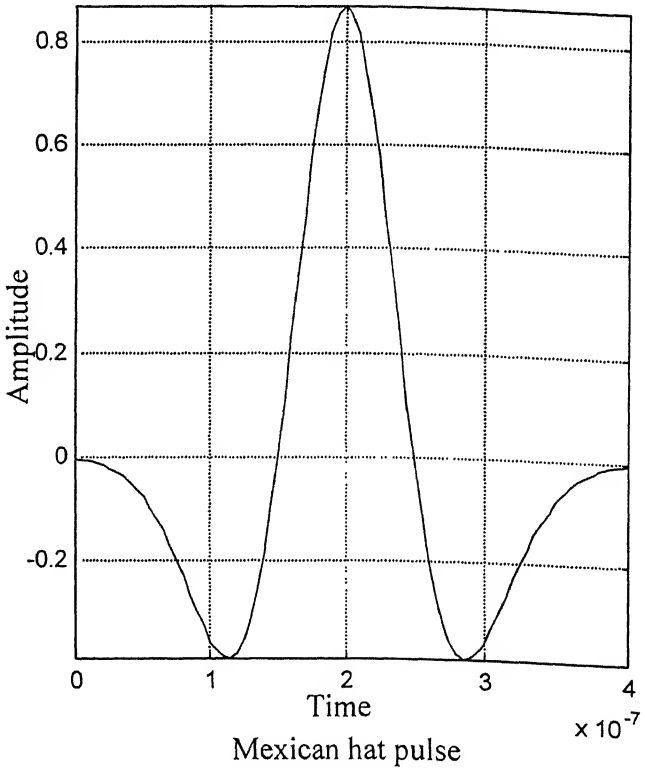

Mexican hat pulse

Fig. 6.3 Different input Pulses used for FE Simulation

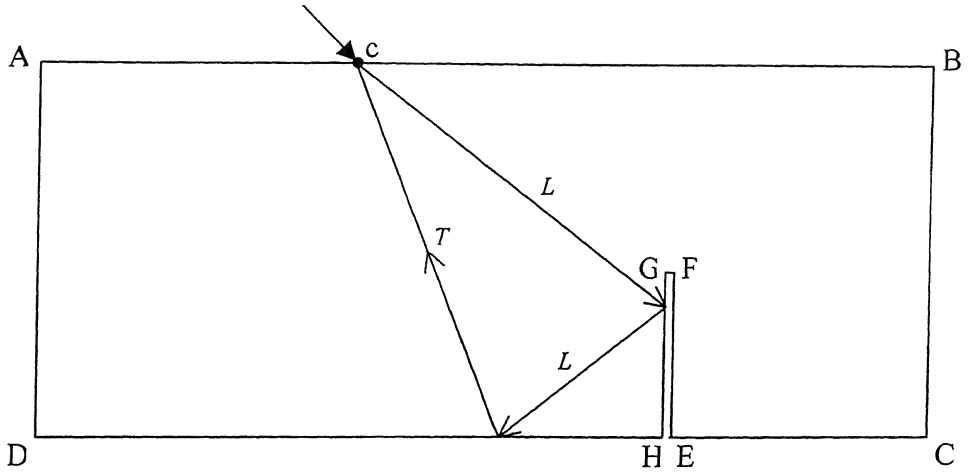

Fig 6.4 (a) $L_C L_B T$ reflection at location c

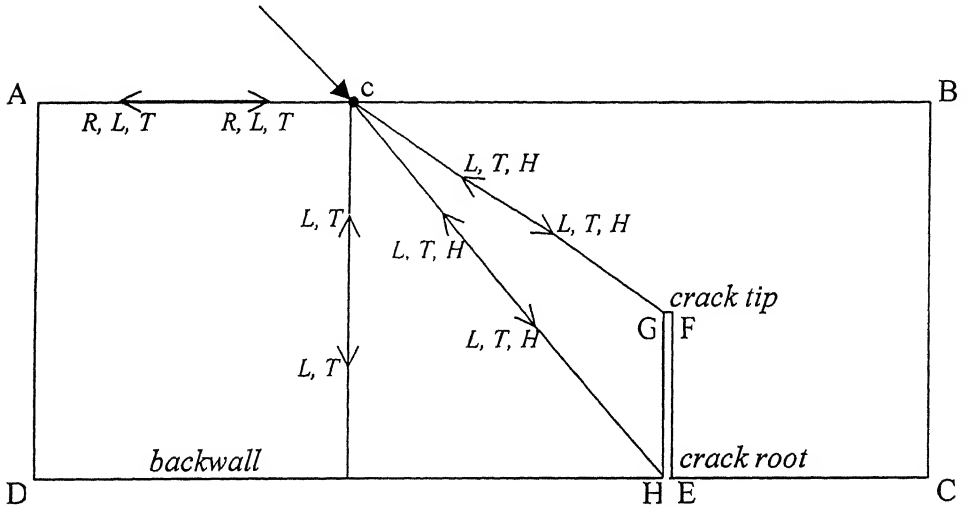

Fig 6.4 (b) This figure depicts all the direct and mode converted reflections from source to crack tip, crack root, backwall, sidewall and back to source at location c

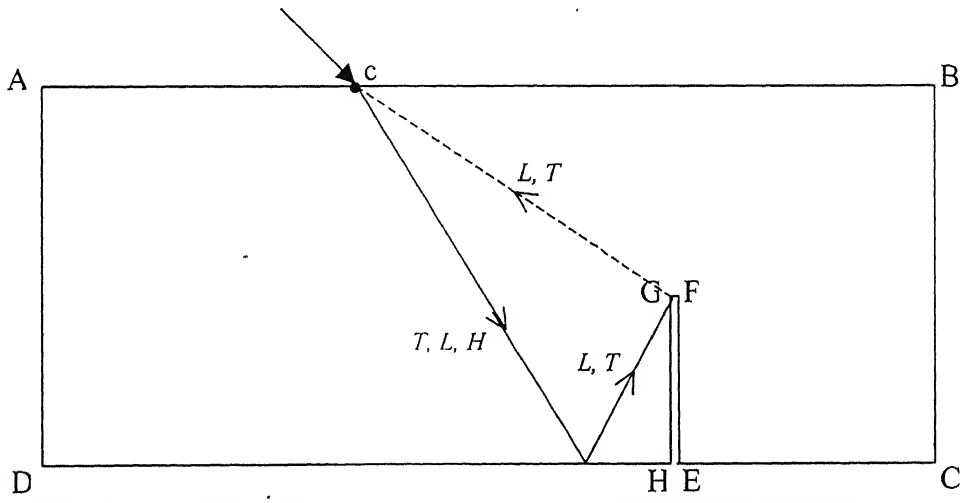

Fig 6.4 (c) This shows the dispersion at crack tip by reflected wave coming from backwall to tip when source at location c

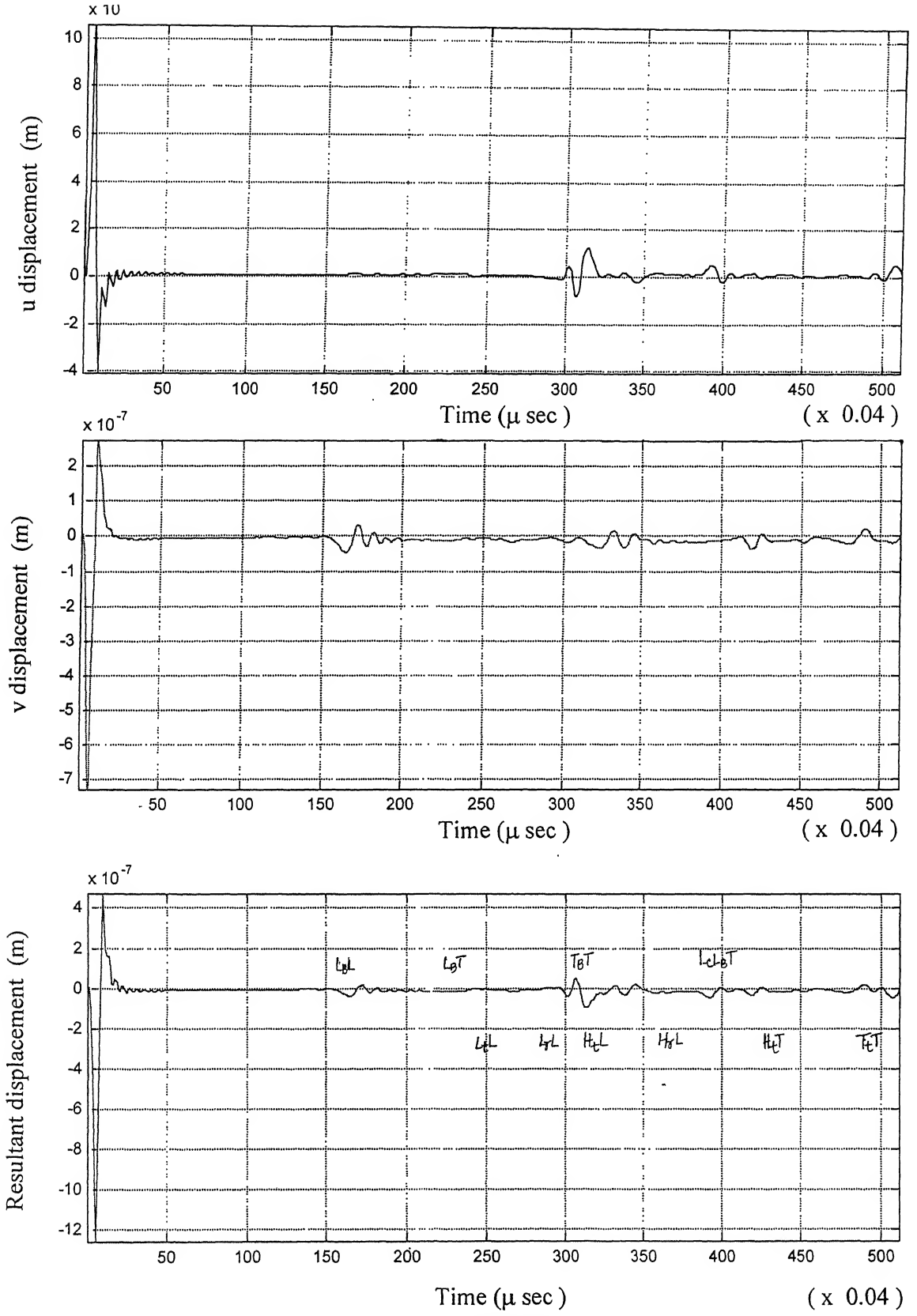

Fig 6.5 u, v and Resultant displacement at 45° for the source located at a (ref. to Fig. 6.1)

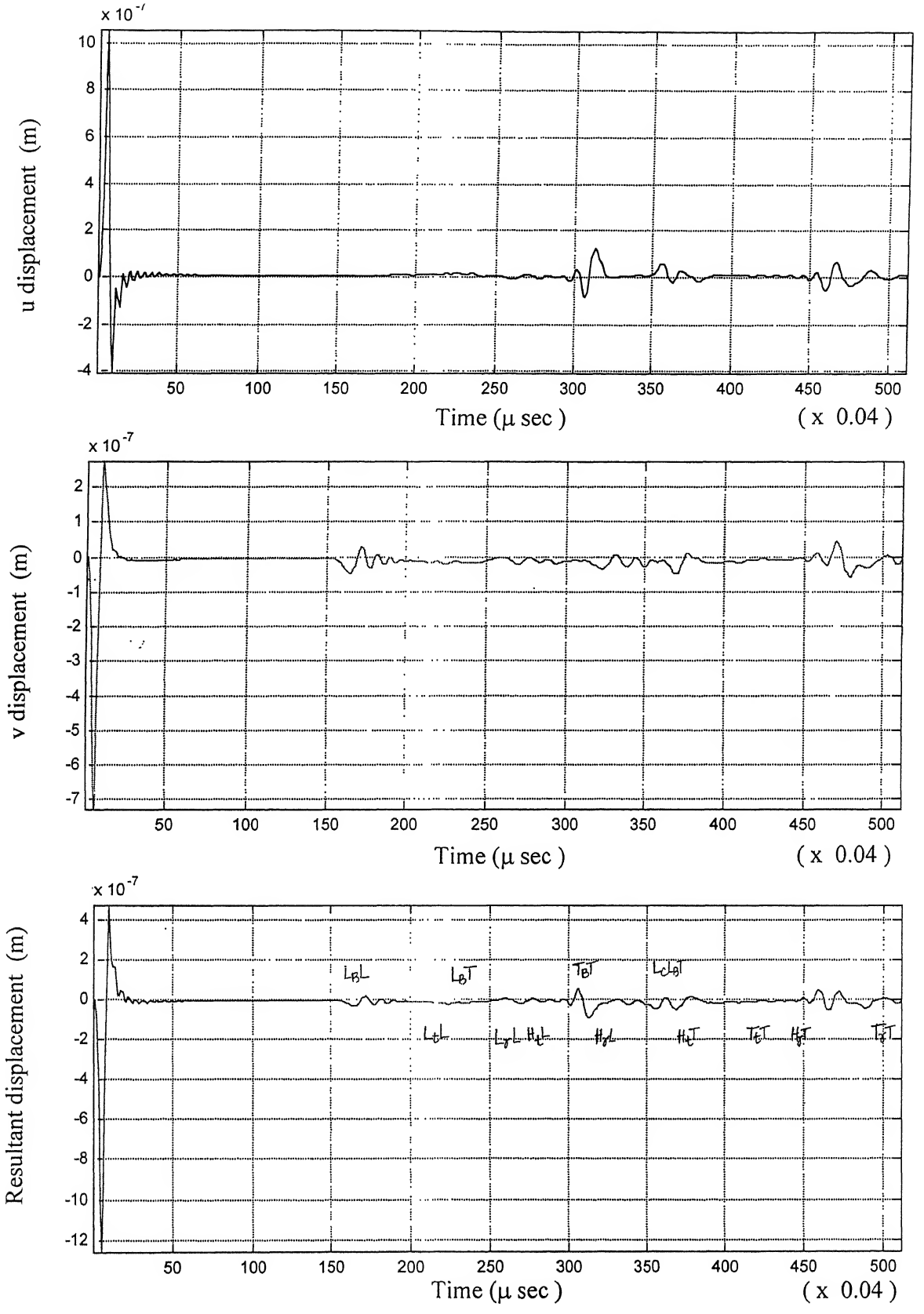

Fig 6.6 u, v and Resultant displacement at 45° for the source located at b (ref. to Fig. 6.1)

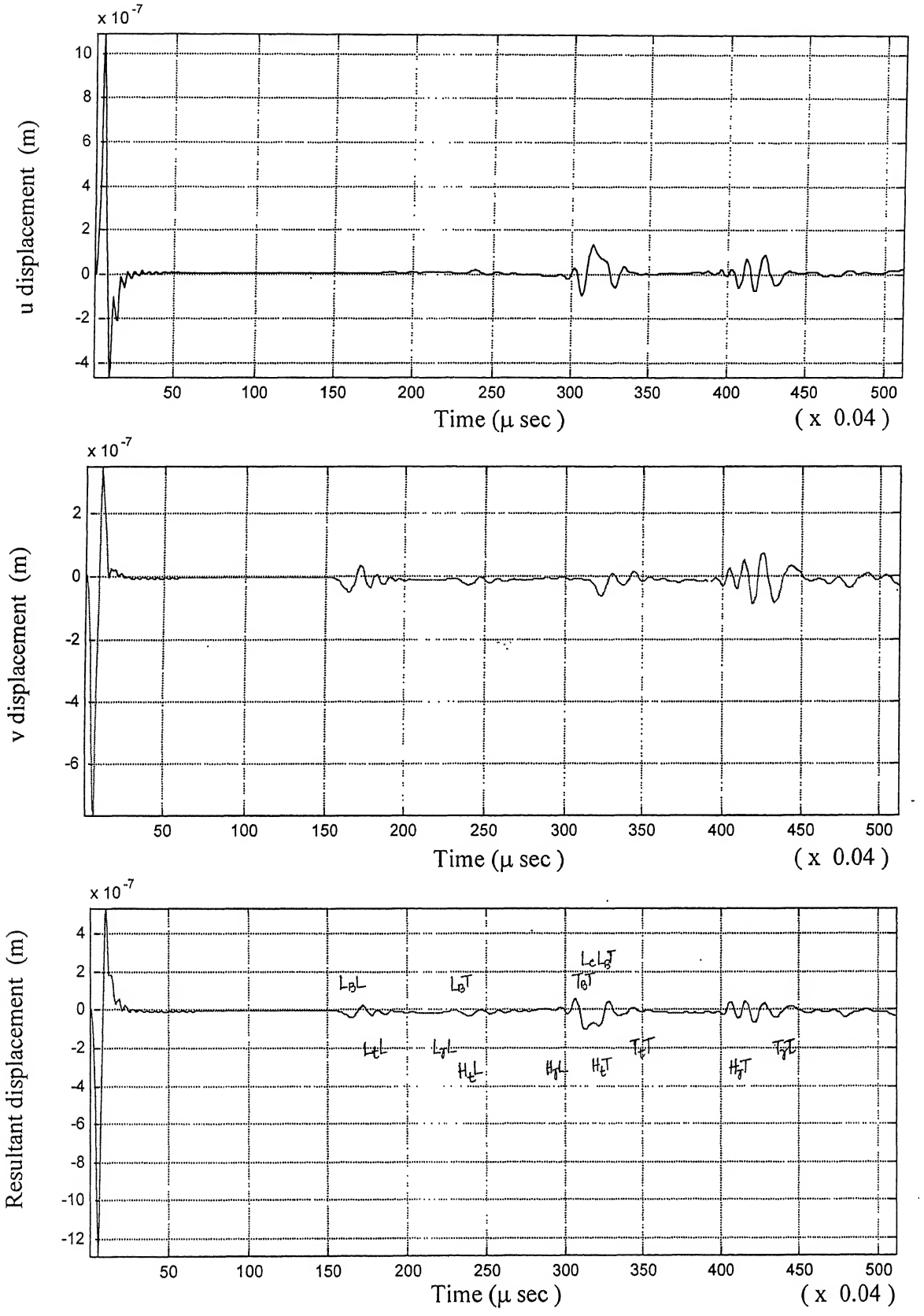

Fig 6.7 u, v and Resultant displacement at 45° for the source located at c (ref. to Fig. 6.1)

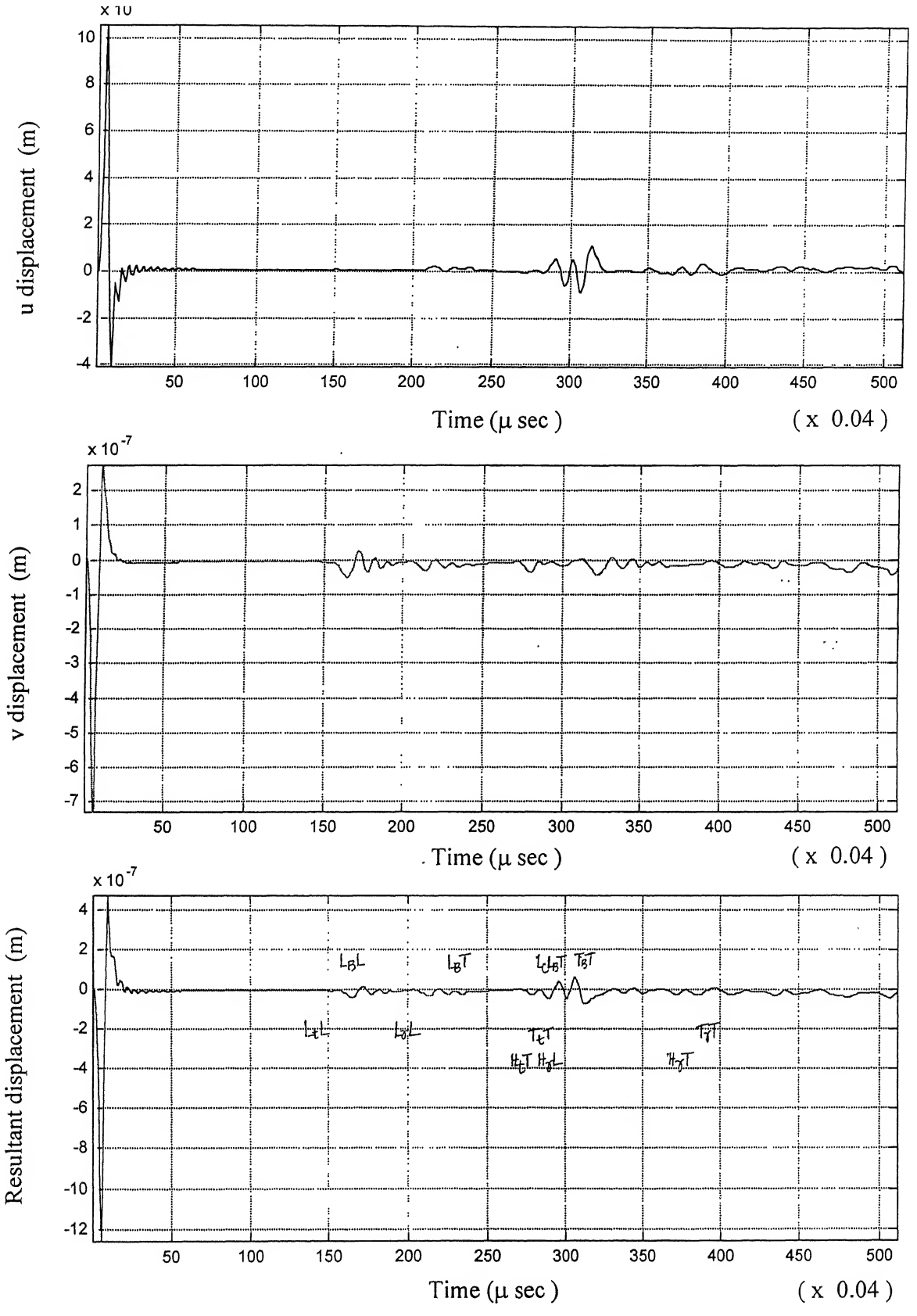

Fig 6.8 u, v and Resultant displacement at 45° for the source located at d (ref. to Fig. 6.1)

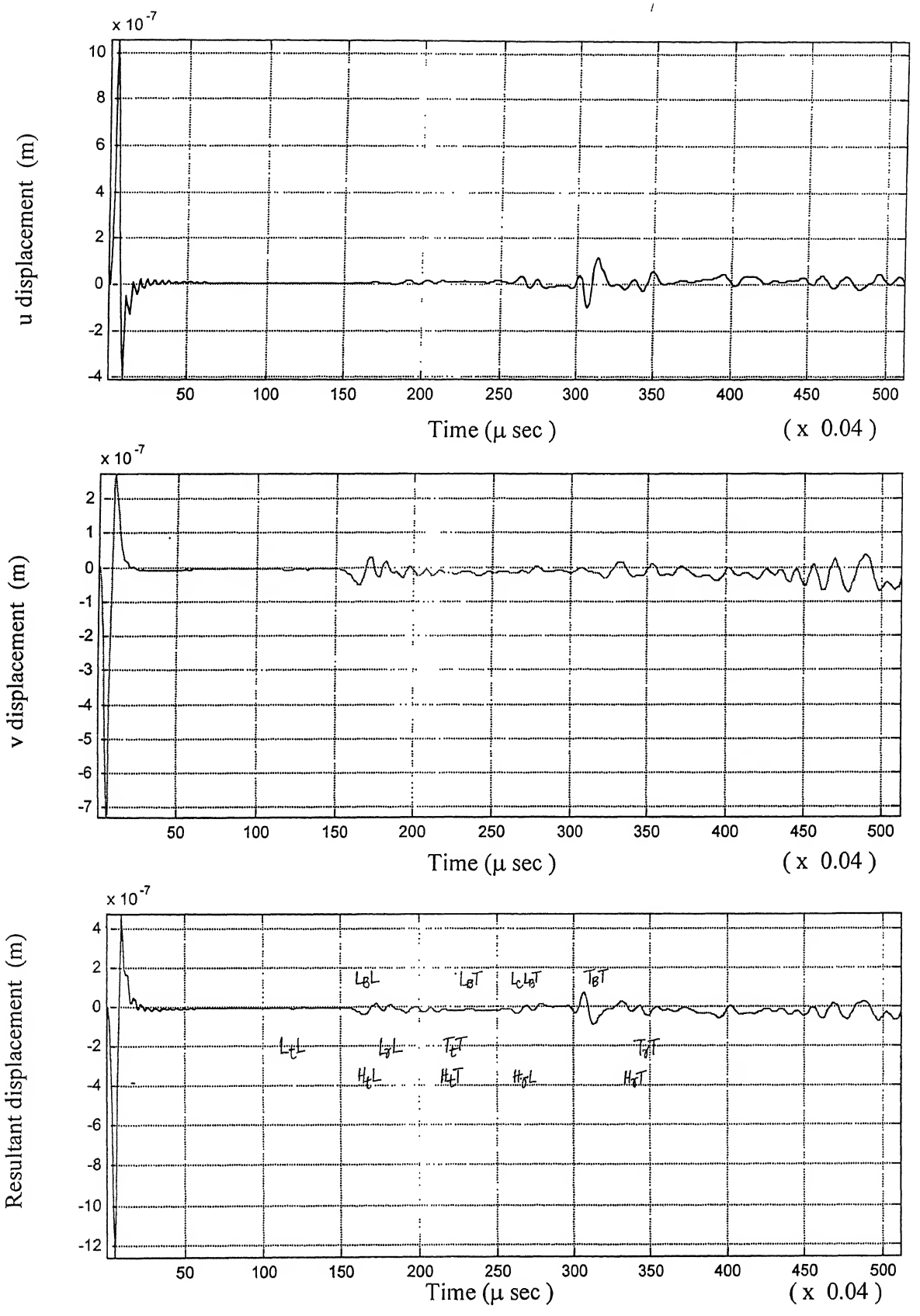

Fig 6.9 u, v and Resultant displacement at 45° for the source located at e (ref. to Fig. 6.1)

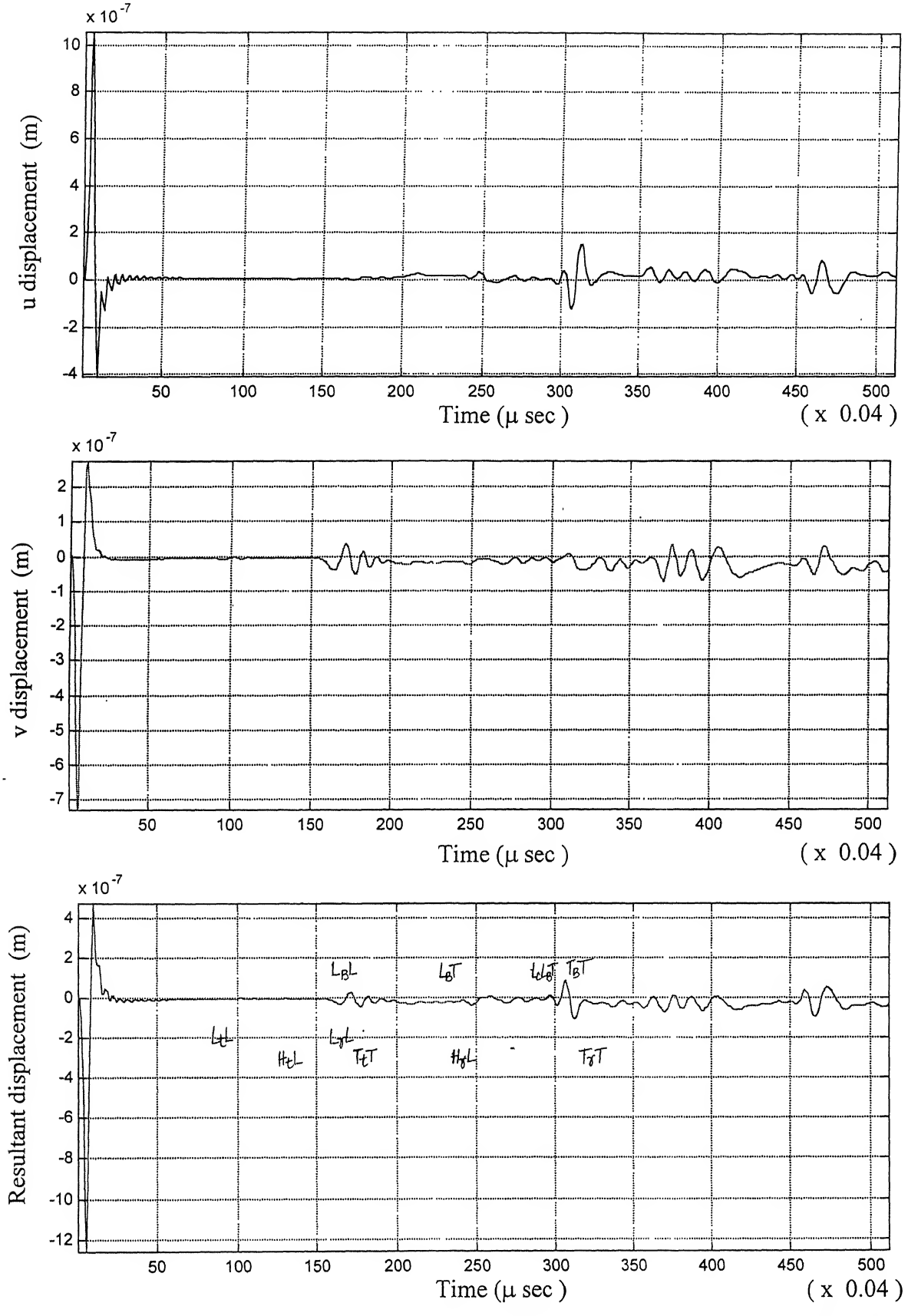

Fig. 6.10 u, v and Resultant displacement at 45° for the source located at f (ref. to Fig. 6.1)

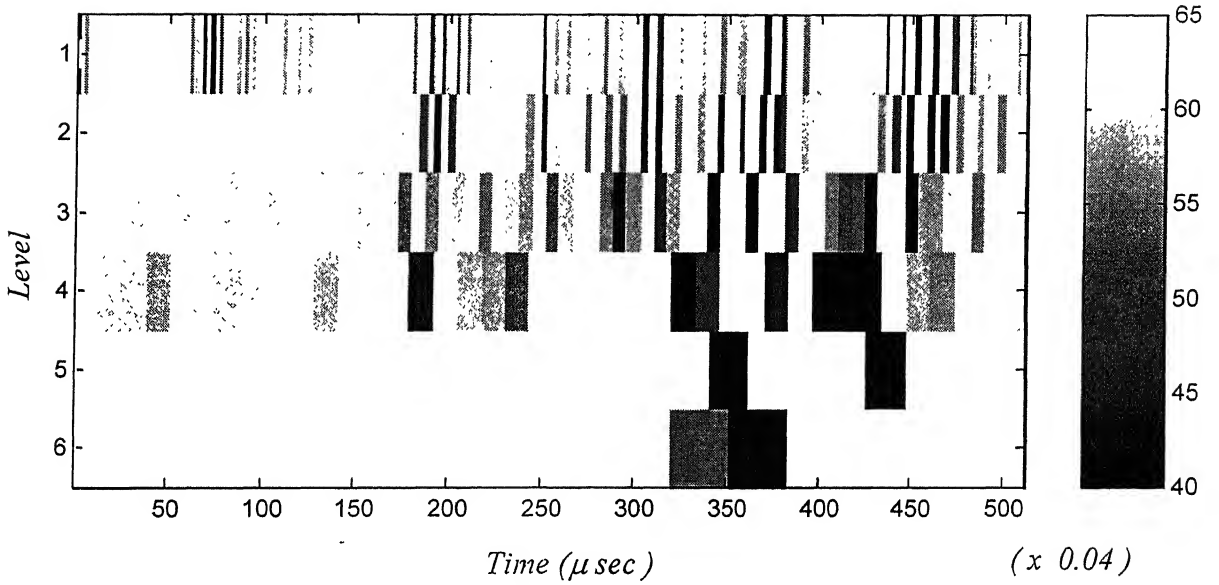

Fig 6.11 Wavelet decomposed levels of signal at location e (ref. to Fig 6.1) using db5 wavelet

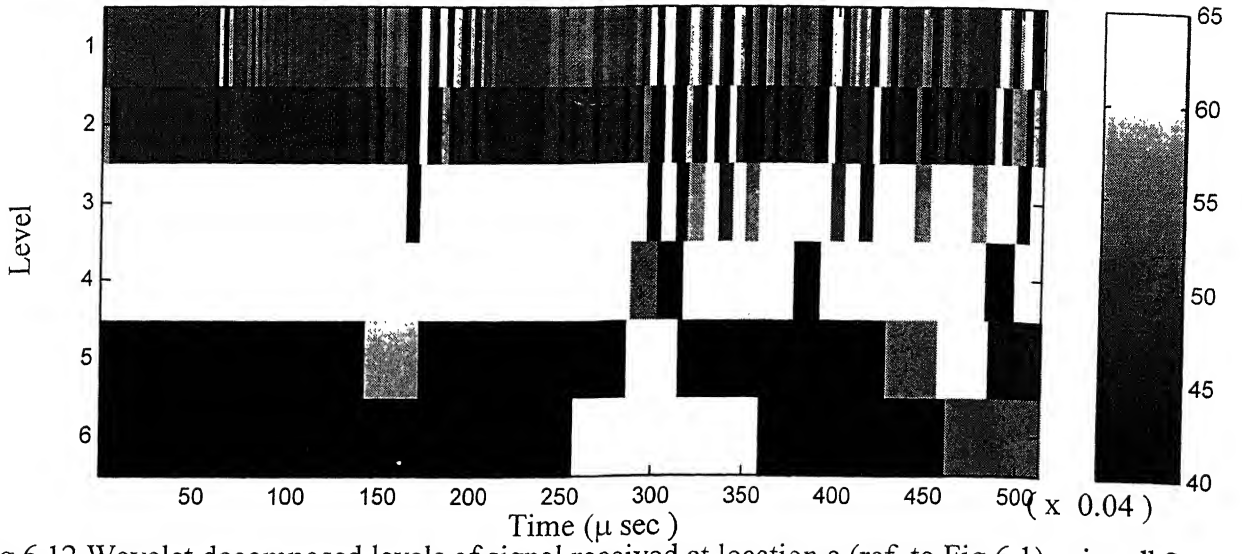

Fig 6.12 Wavelet decomposed levels of signal received at location a (ref. to Fig 6.1) using db2 wavelet

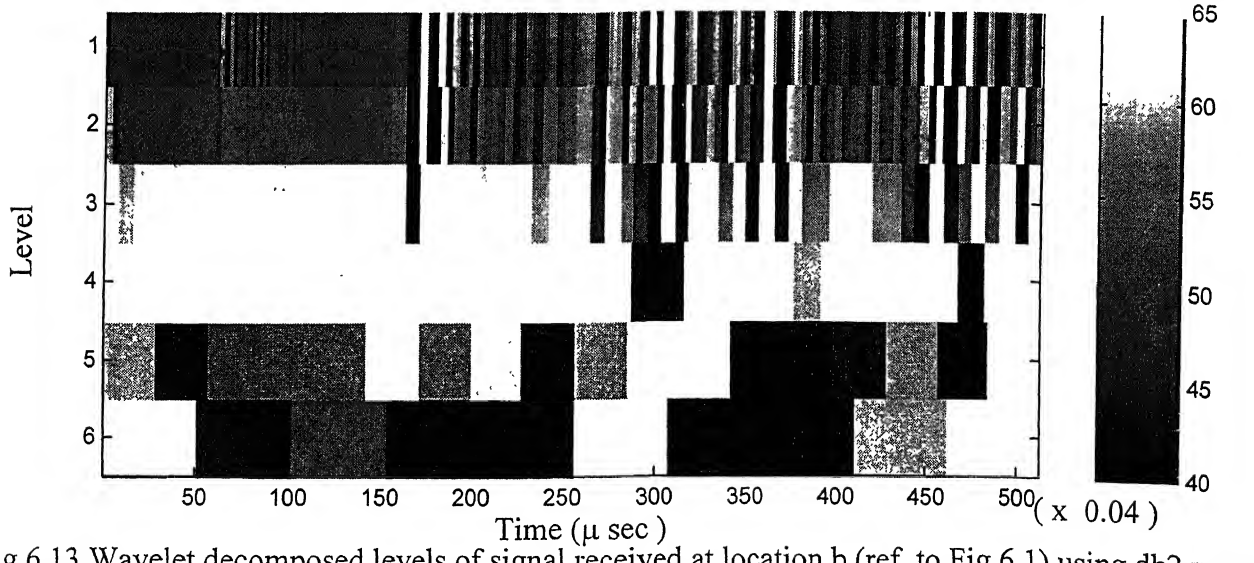

Fig 6.13 Wavelet decomposed levels of signal received at location b (ref. to Fig 6.1) using db2 wavelet

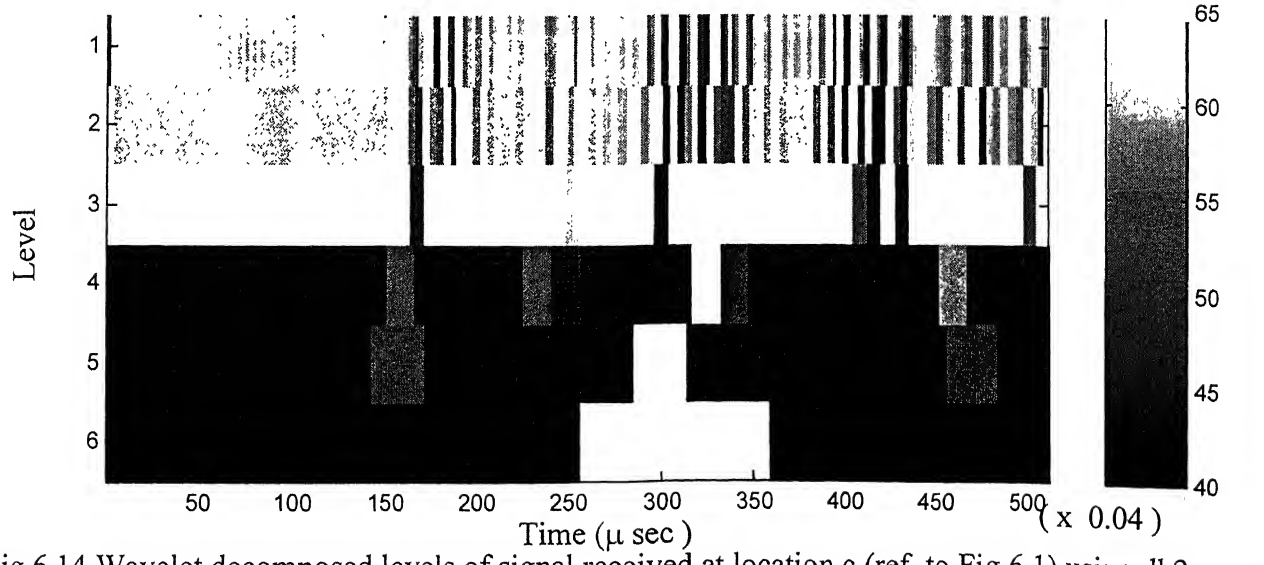

Fig 6.14 Wavelet decomposed levels of signal received at location c (ref. to Fig 6.1) using db2 wavelet

Each wavelet level of every signal is normalized between 1 and 128

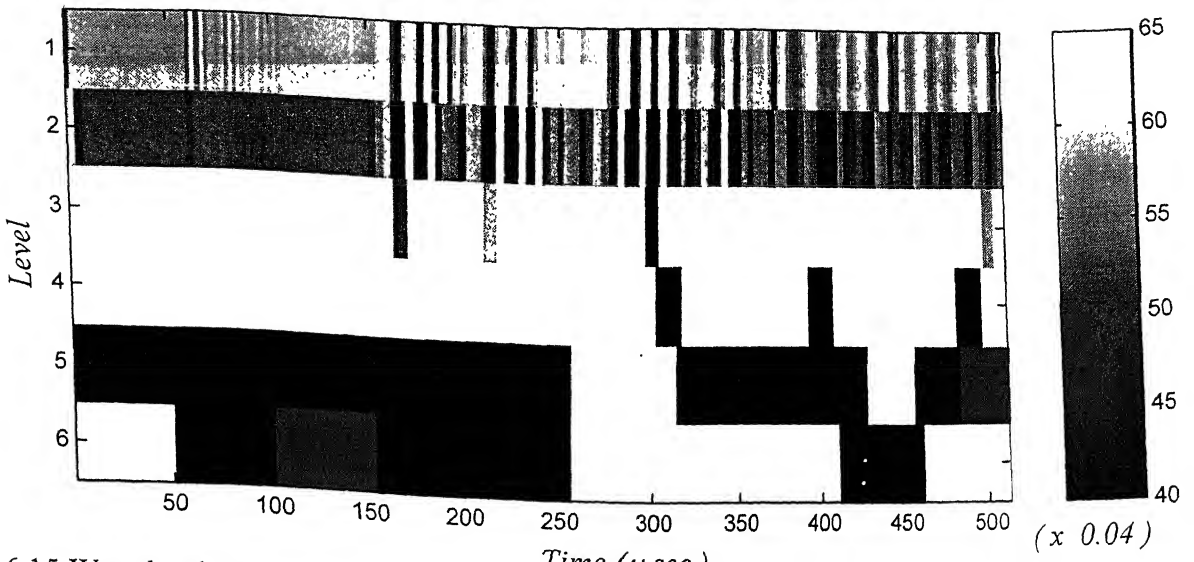

Fig 6.15 Wavelet decomposed levels of signal received at location d (ref. to Fig 6.1) using db2 wavelet

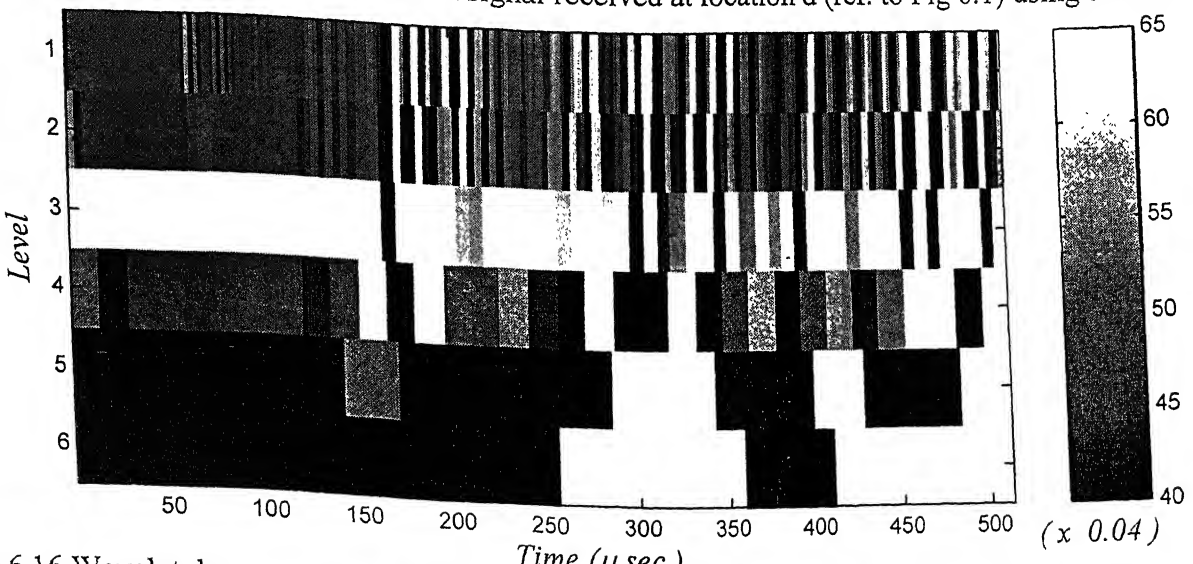

Fig 6.16 Wavelet decomposed levels of signal received at location e (ref. to Fig 6.1) using db2 wavelet

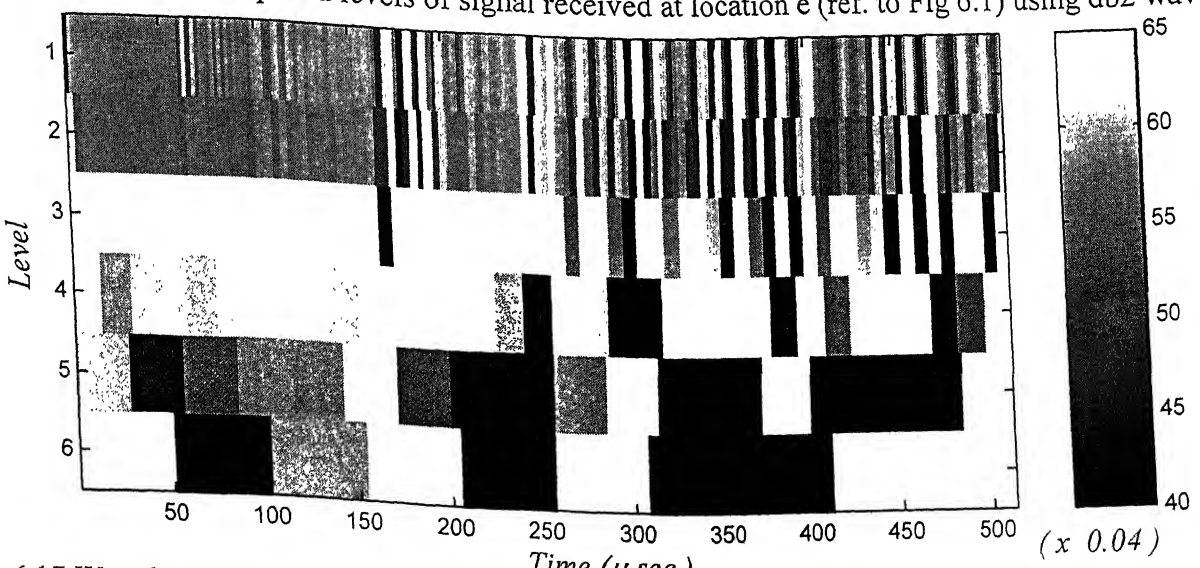

Fig 6.17 Wavelet decomposed levels of signal received at location f (ref. to Fig 6.1) using db2 wavelet

Each wavelet level of every signal is normalized between 1 and 128

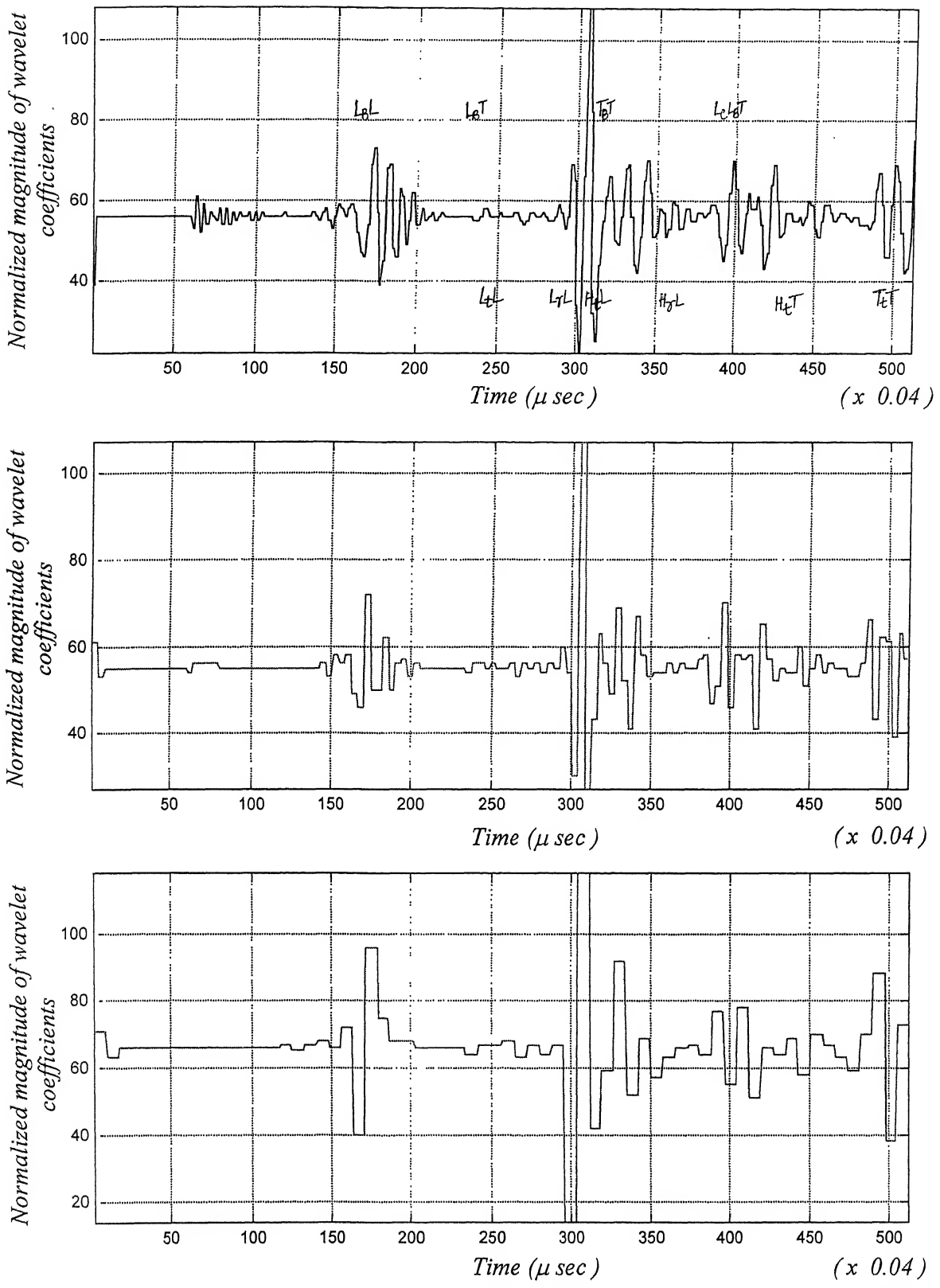

Fig 6.18 Wavelet decomposed levels 1, 2 and 3 of signal at location a (ref. to Fig 6.1) using db2 wavelet

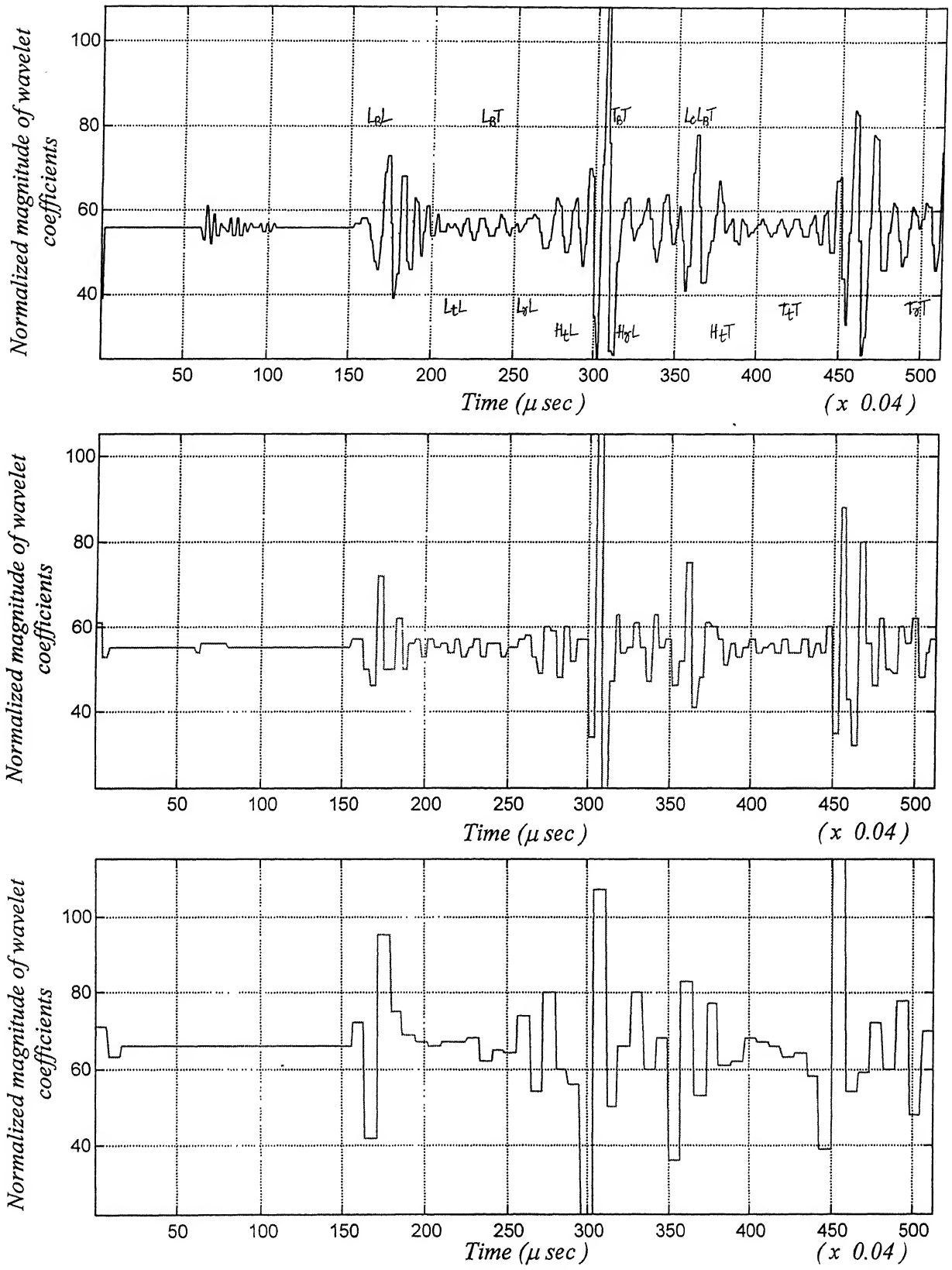

Fig 6.19 Wavelet decomposed levels 1, 2 and 3 of signal at location b (ref. to Fig 6.1) using db2 wavelet

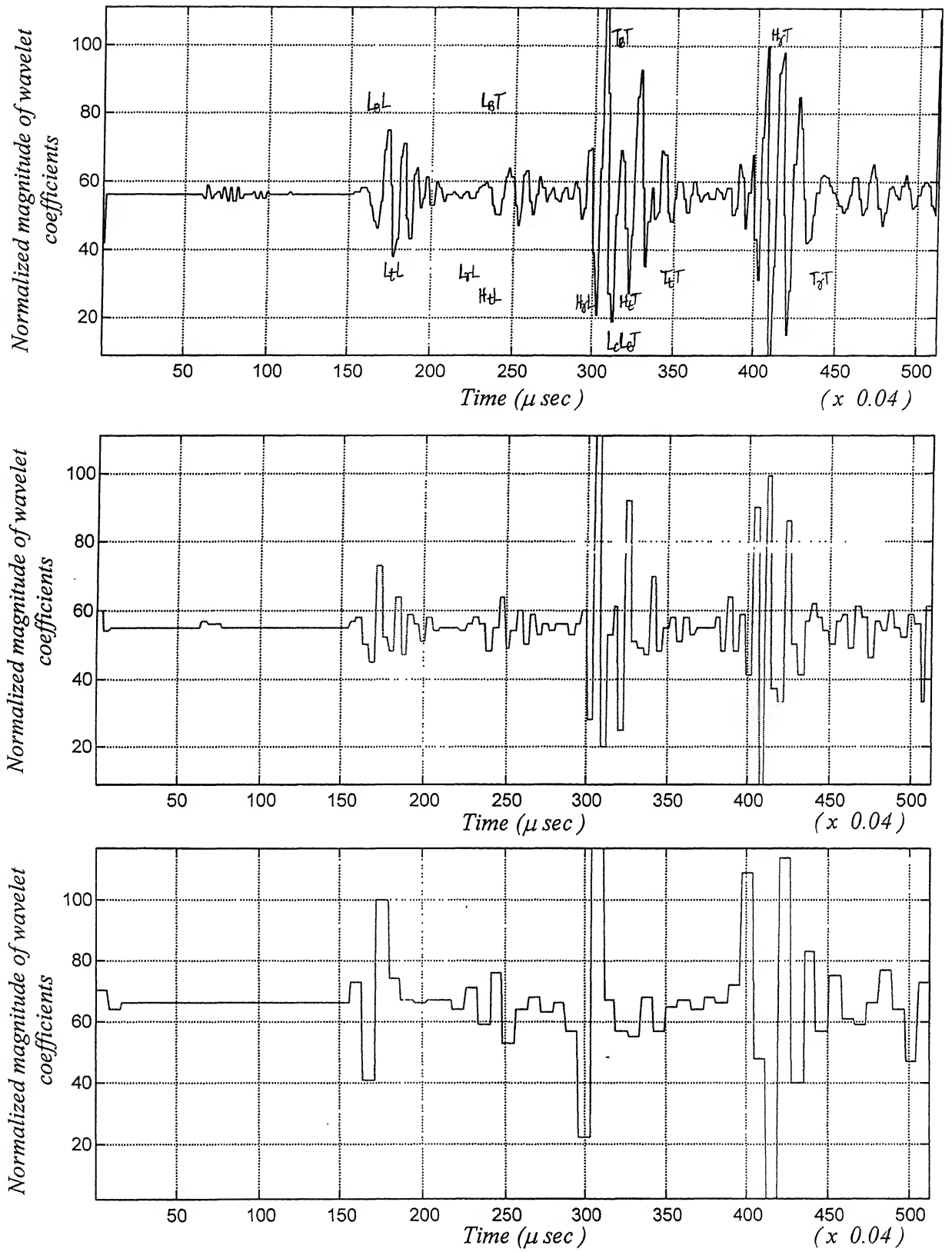

Fig 6.20 Wavelet decomposed levels 1, 2 and 3 of signal at location c (ref. to Fig 6.1) using db2 wavelet

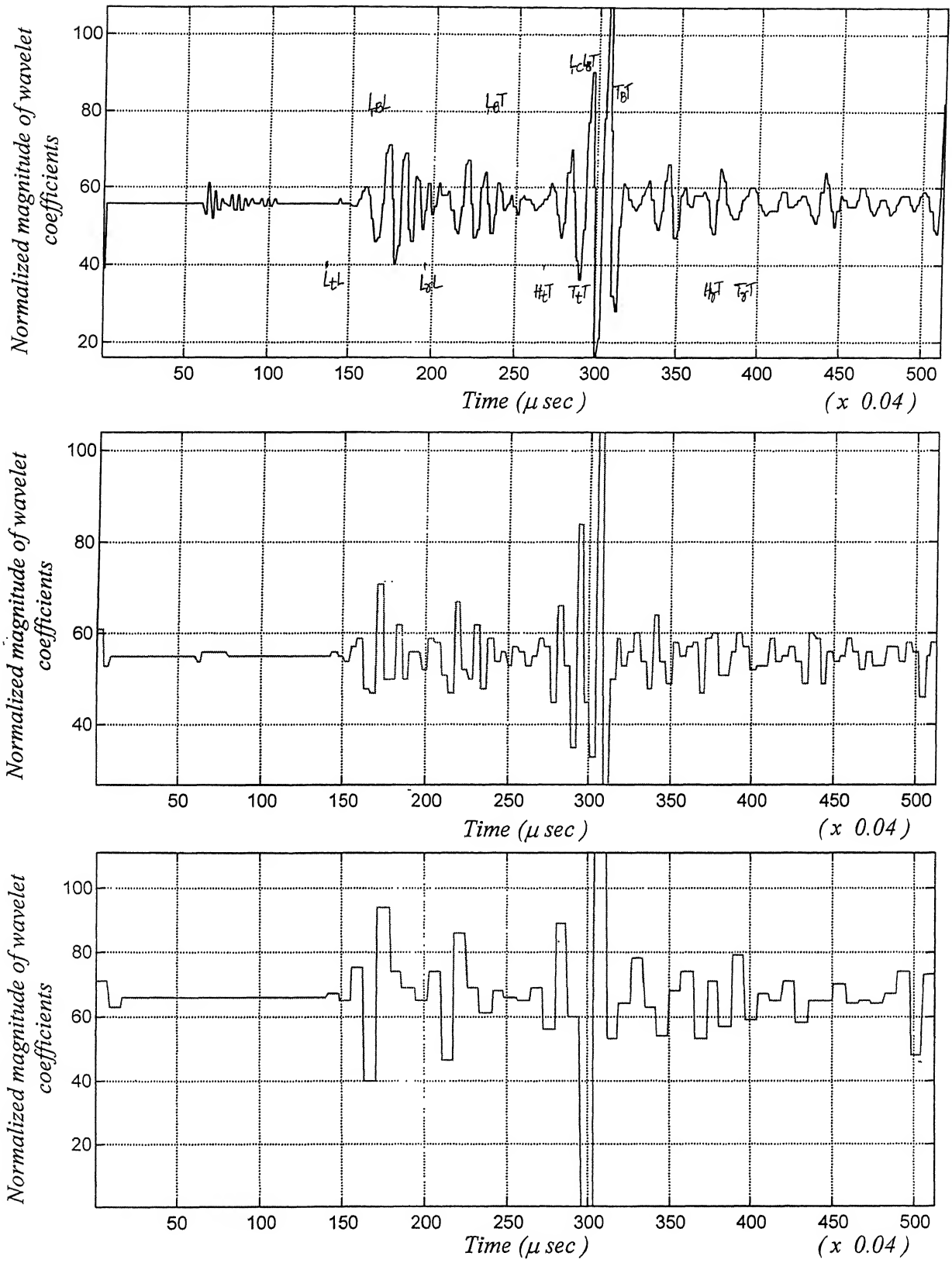

Fig 6.21 Wavelet decomposed levels 1, 2 and 3 of signal at location d (ref. to Fig 6.1) using db2 wavelet

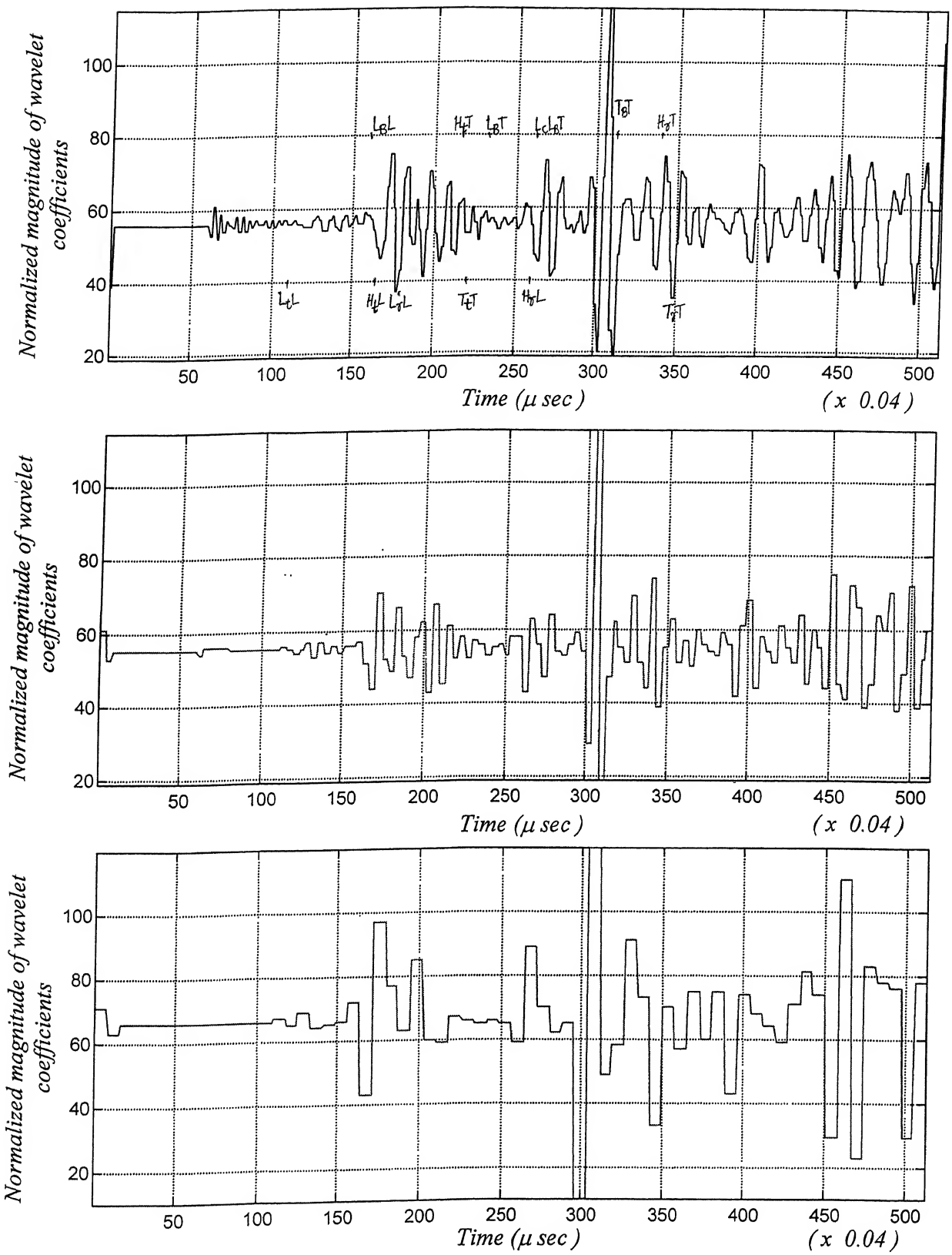

Fig 6.22 Wavelet decomposed levels 1, 2 and 3 of signal at location e (ref. to Fig 6.1) using db2 wavelet

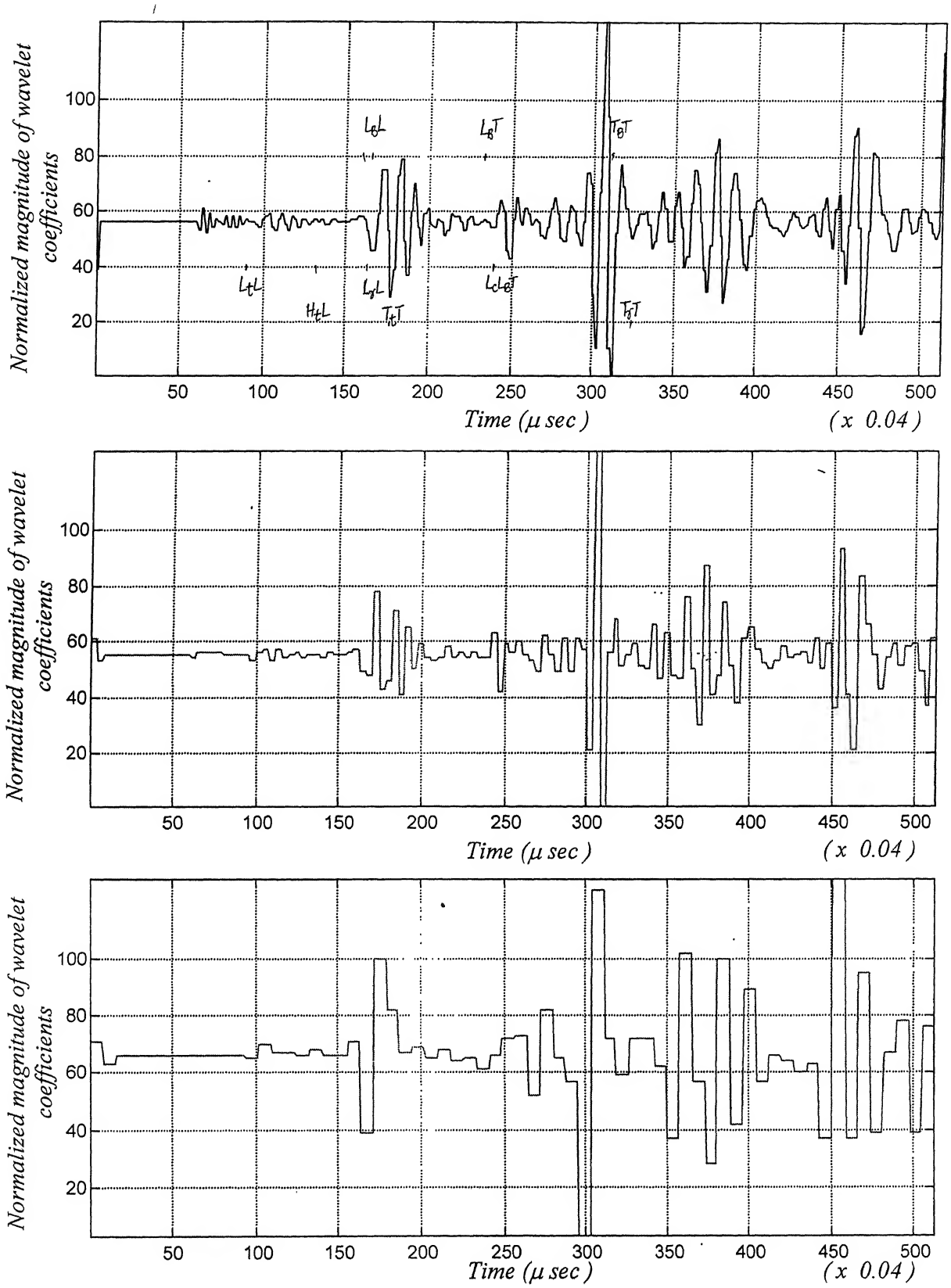

Fig 6.23 Wavelet decomposed levels 1, 2 and 3 of signal at location f (ref. to Fig 6.1) using db2 wavelet.

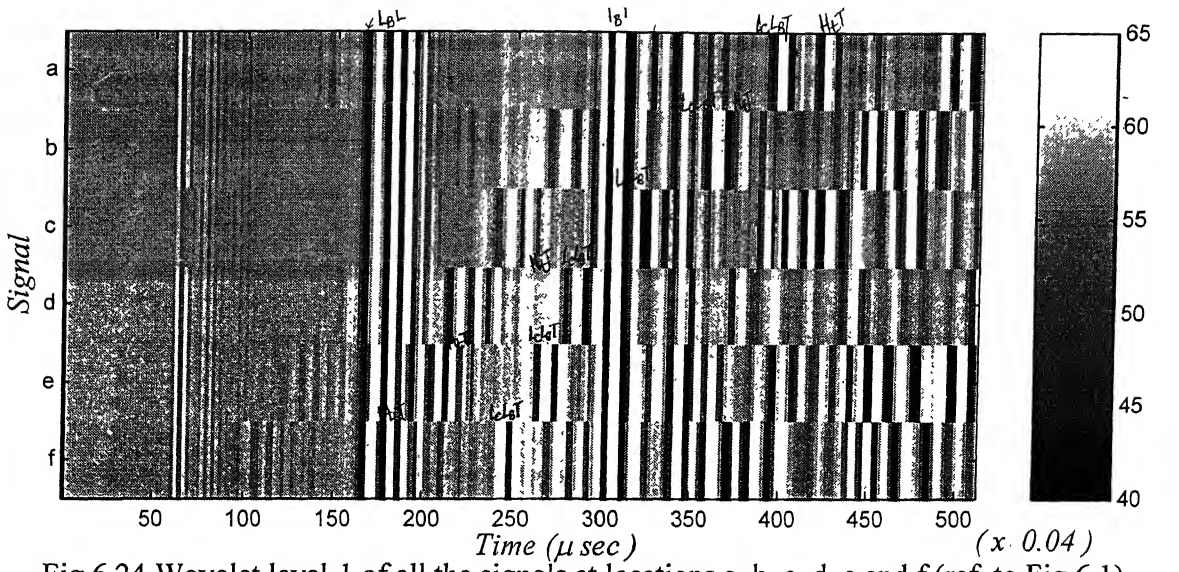

Fig 6.24 Wavelet level-1 of all the signals at locations a, b, c, d, e and f (ref. to Fig 6.1)

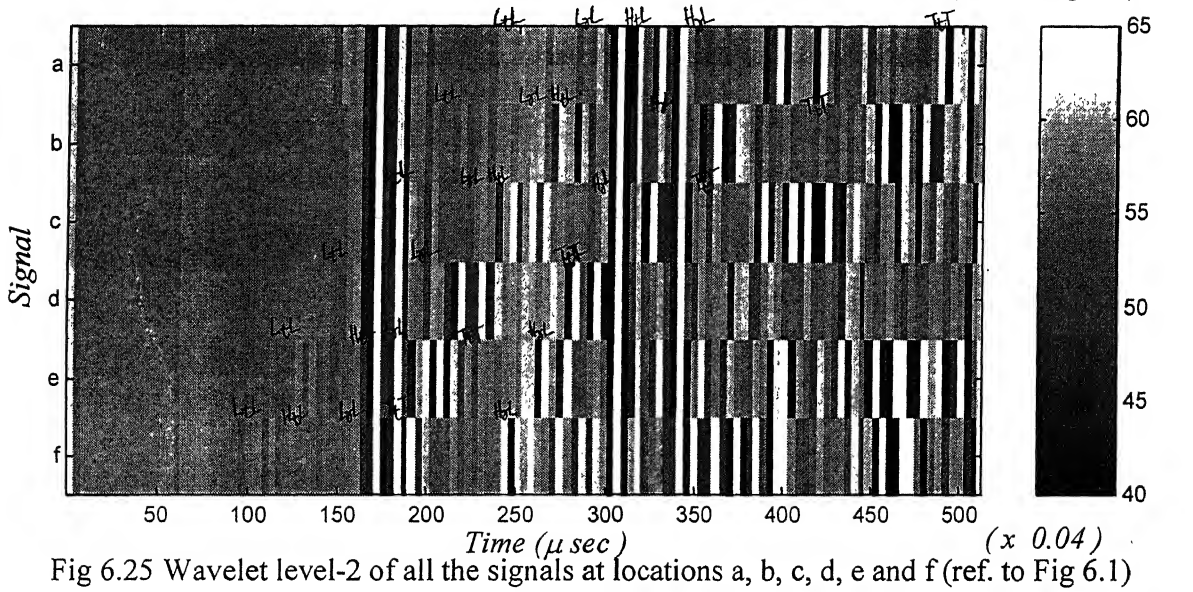

Fig 6.25 Wavelet level-2 of all the signals at locations a, b, c, d, e and f (ref. to Fig 6.1)

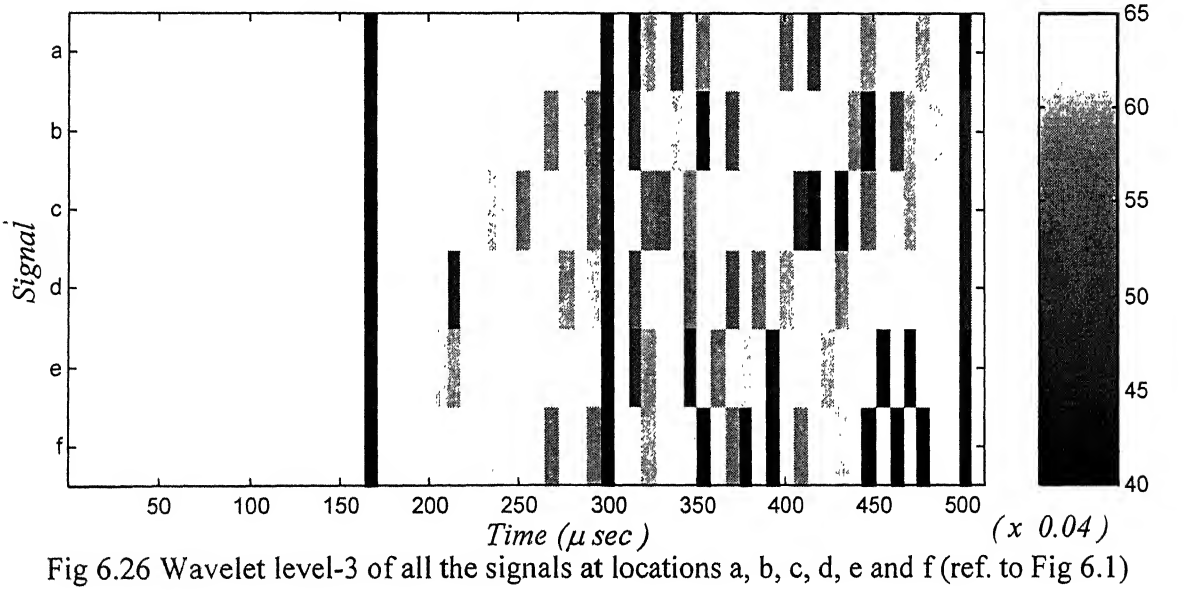

Fig 6.26 Wavelet level-3 of all the signals at locations a, b, c, d, e and f (ref. to Fig 6.1)

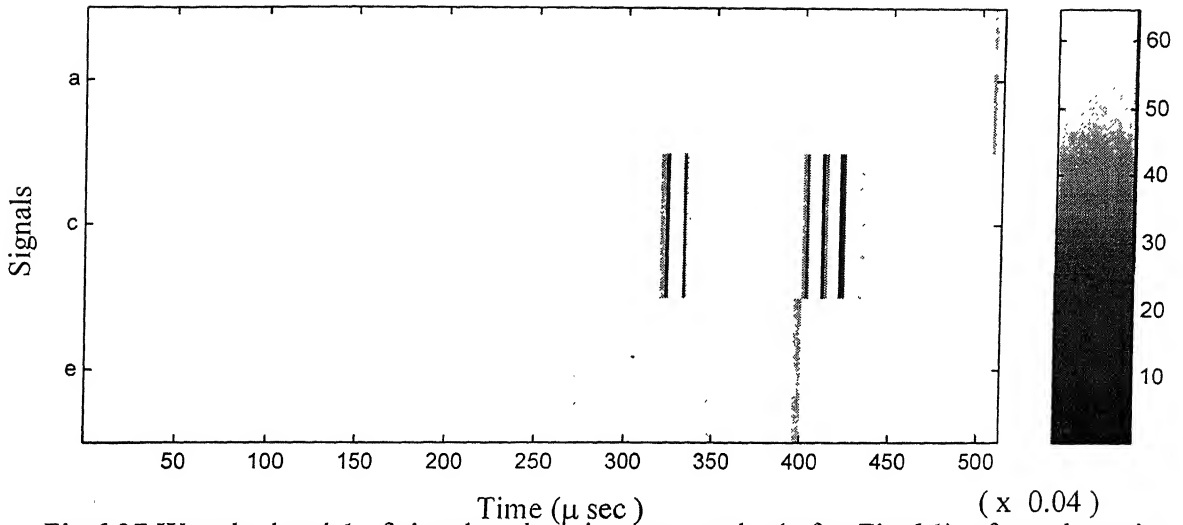

Fig 6.27 Wavelet level-1 of signals at locations a, c, and e (ref to Fig 6.1) after subtracting the respective crack free signal.

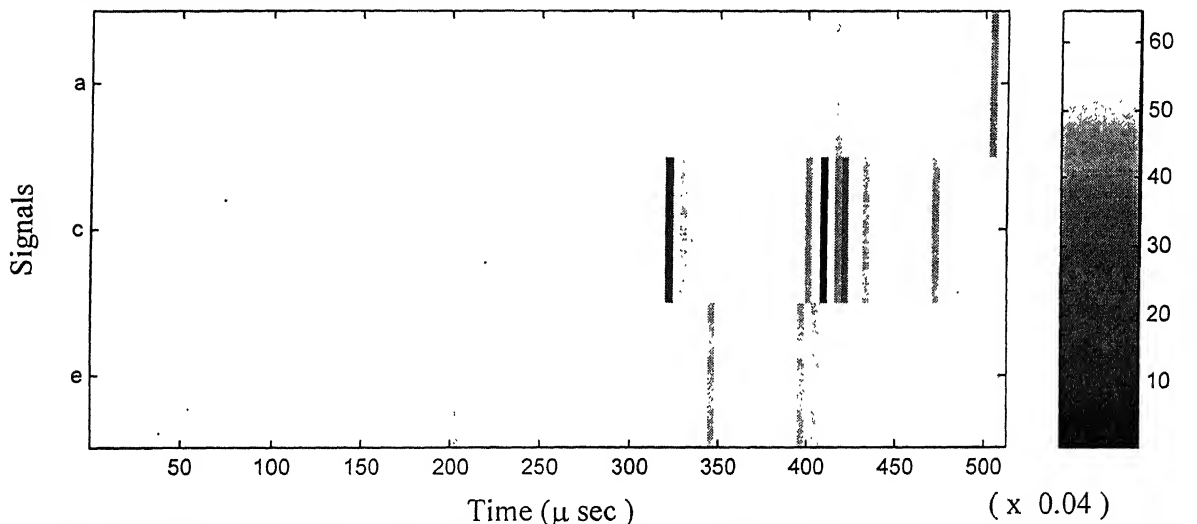

Fig 6.28 Wavelet level-2 of signals at locations a, c, and e (ref to Fig 6.1) after subtracting the crack free signal.

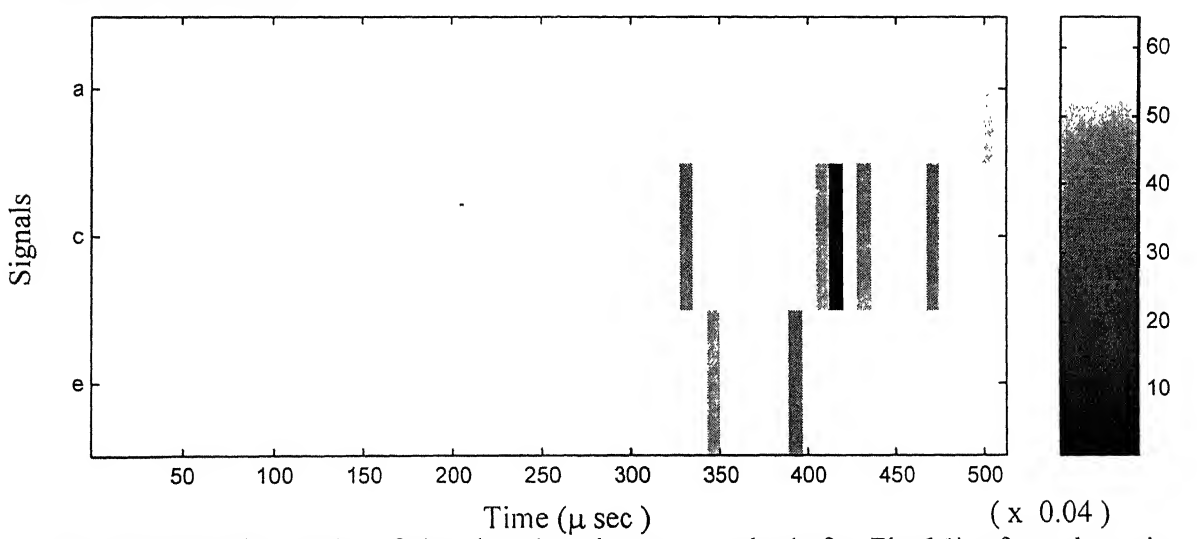

Fig 6.29 Wavelet level-3 of signals at locations a, c, and e (ref to Fig 6.1) after subtracting the crack free signal.

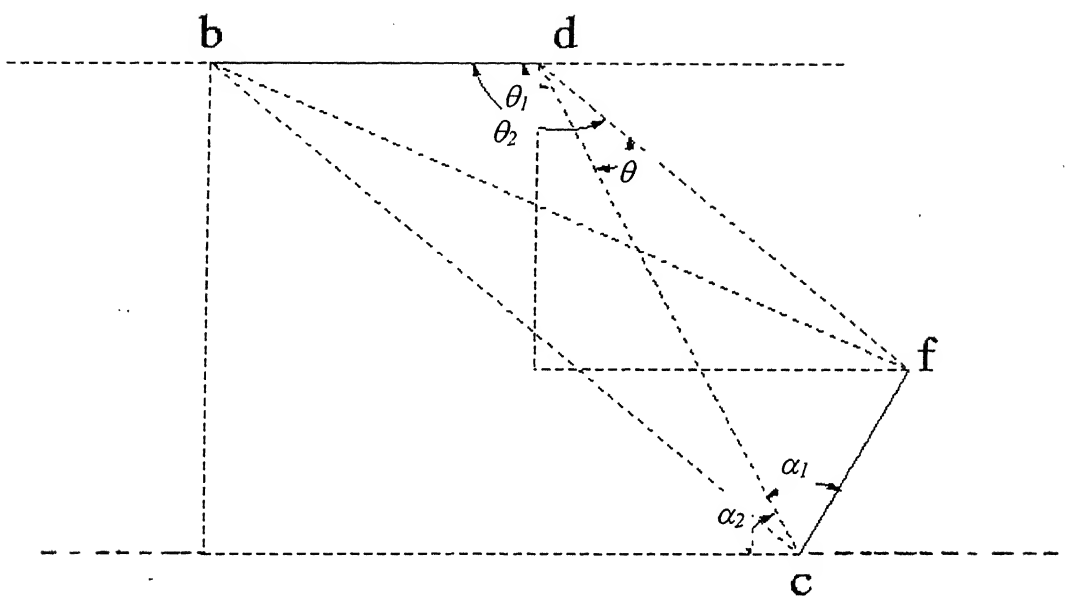

Fig. 6.30 Method used to evaluate crack angle, crack length, inclination

Chapter 7

Conclusions and Scope for Future work

7.1 Conclusions

In the present work, an attempt has been made to use Finite element method for the simulation of elastic wave propagation and wavelet analysis for crack detection. Based on the present work and results obtained, the following conclusions are drawn

- The wavelet transform technique on FEM simulated data can wavelet detect the surface cracks in thick plates reasonably well. This technique can separate the various artifacts from the signal data, where in separate reflections are not easily visible.
- The db2 wavelet gives best results for the present problem. And only first three wavelet levels contain the information about the crack reflections.
- Levels 1, 2 can be used to detect the cracks where as level 3 gives the approximate arrival times of the reflection.
- It is difficult to separate each and every reflection in to separate wavelet coefficients.
- Sine pulse as input during simulation gives relatively good results and it is also easy to apply.
- Using image plot for each wavelet level of all the signals at a time gives good visualization of the crack reflections rather than directly viewing the wavelet coefficients of each level.

7.2 Scope for the future work

- To detect the cracks, the damping boundary condition on the sides may be improved further to eliminate unwanted reflections.
- To improve the analysis, a wavelet can be designed, which looks similar to the input pulse.

- A 2-dimensional wavelet transform can be applied to the B-scan data to detect cracks and its inclination directly from the plot of wavelet coefficients. B-scan data can be obtained similar to the A-scan data in post-processing stage of computation.

References

[1] Thompson R.B. "Quantitative ultrasonic non-destructive evaluation methods", Journal of Applied Mechanics, Vol.50, 1983, pp 1191-1201.

[2] Temple J.A.G. "A survey of models predicting the ultrasonic response of multiple flaws", Harwell laboratory Report No. AERE M3771, Oct 1989.

[3] Bond L.J. "Numerical techniques and their use to study wave propagation and Scattering- A review", in Elastic waves and ultrasonic NDE, Datta S.K., Achenbach J. D. and Rajapakse Y.S. (Eds.), North-Holland, 1990, pp 17-27.

[4] Jaleel A. "Finite element modelling of wave interactions with cracks in composite materials", M.Tech Thesis, March 1992, IIT Kanpur.

[5] Kishore N.N., Sridhar.I., Iyengar N.G.R. "Finite element modelling of scattering of ultrasonic waves by isolated flaws", NDT & E International, Oct 1999.

[6] Hoff C., Paul P.J. "Development of an implicit method with numerical dissipation from a generalized single step algorithm for structural dynamics", Computer methods applied to Mechanical Engineering Vol.67, 1986, pp 367-385.

[7] Moubarik S.E., Vadder D.D., Benoist P. "Wavelets and Nondestructive Evaluation", Review of progress in Quantitative Nondestructive Evaluation, Vol.12, 1993, pp 727-734.

[8] Abbate A., Koay J., Frankel J., Schroeder S.C., Das P. "Application of Wavelet Transform signal processing to ultrasounds", IEEE ultrasonic symposium, 1994, pp 1147-1152.

[9] Abbate A., Frankel J., Das P. "Wavelet Transform signal processing for dispersion analysis of ultrasonic signals", IEEE Ultrasonic symposium 1995, pp 751-755.

[10] Nevel A.V., Defacio B., Neal S.P. "An application of wavelet signal processing to ultrasonics", Review of progress in Quantitative Nondestructive Evaluation, Vol.15, 1996, pp 733-740.

[11] Abbate A., Frankel J., Das P. "Wavelet Transform signal processing applied in ultrasonics", Review of progress in Quantitative Nondestructive Evaluation, Vol.15 1996, pp 741-748.

[12] Roy O., Sallard J., Moubarik S.E. "Echo extraction from an ultrasonic signal using continuous wavelet transform", Review of progress in Quantitative Nondestructive

Evaluation, Vol.15, 1996, pp 749-755.

[13] Choa J., Udpa L., Udpa S.S. "Ultrasonic signal analysis using wavelet transform", Review of progress in Quantitative Nondestructive Evaluation, Vol.12, 1993, pp 735-742.

[14] Jun-Botham, Jian-chen chang, Tie-Hai Wang, Yves Berthelet "Mode analysis of laser generated transient ultrasonic Lamb wave forms in a composite plate by wavelet transform", Materials Evaluation, Aug 1999, pp 837-840.

[15] Daubechies I. "Compactly supported wavelets", Communications and pure Applied Mathematics, Vol 41, 1988, pp 909-996.

[16] Chui C.K. "An introduction to wavelets", Vol.1, Academic press, Boston, 1992.

[17] Achenbach D. "Wave propagation in solids", North-Holland, 1970.

[18] Bathe K.J. "Finite element procedures in engineering analysis", Prentice hall Inc., 1996.

[19] Smith W.D. "A non-reflecting plane boundary for wave propagation problems", Journal of computational physics, Vol.15, 1974, pp 492-503.

[20] Lysmer J., Kuhlemeyer R.L. "Finite dynamic model for infinite media", J. of Engg. Mechanics Division, ASCE, Vol.95, 1969, pp 859-877.

[21] Chow Y.K. "Accuracy of consistent and lumped viscous dampers in wave propagation problems", Int. J Nume Math Engg., Vol.21, 1985, pp 723-732.

[22] Seron F.J., Sanz F.J., Kindelan M., Badal J.I. "Finite element method for elastic wave propagation", comm. in applied Nume. Math., Vol.6, 1990, pp 359-368.

[23] Amara G. "An introduction to wavelets", IEEE computational science and engineering, Vol.2, 1995.

[24] Fliege N.J. "Multirate Digital Signal processing", John wiley and sons Ltd., 1994.

[25] Sudheer C. "Study of wavelet transforms and its application", B.Tech Project, K.S.R.M. College, Cuddapah, 1998.

[26] Newland D.E. "Introduction to Random Vibrations, spectral analysis and wavelet analysis", Longman scientific and technical, Harlow, 1993.

[27] Mallat S.G. 'A theory of Multi Resolution signal decomposition, the wavelet representation', IEEE transactions on pattern analysis and m/c intelligence, Vol.12 1989, pp 674-689.

Wavelet toolbox

Wavelet toolbox is a collection of functions on the MATLAB technical computing environment. It provides tools for analysis and synthesis of signals and images using wavelets.

It has command line as well as graphical user interface (GUI) tools. We can add our own wavelets to the toolbox. Many functions of the toolbox are written from the book *wavlets and filter banks* by *Gilbert strang and Truong Nguyen.*

Some important functions present in the toolbox are:

Wavemenu	*starts the GUI.*
Wfilters	gives the required wavelet filters.

Wavelet families present in the MATLAB are:

biorwavf	computes biorthogonal spline wavelet filters.
coifwave	computes coieflet wavelet filters.
dbaux	computes daubechies wavelet filters.
dbwavf	computes daubechies wavelet filters.
mexihat	computes mexican hat wavelet filters.
meyer	computes meyer wavelet.
morlet	computes morlet wavelet.
symwavf	computes symlet wavelet filters.
cwt	continuous wavelet transform one-dimensional.
appcoef	extracts 1-D approximates coefficients.
detcoef	extracts 1-D detail coefficients.
dwt	single-level discrete 1-D wavelet transform.
idwt	single-level inverse discrete 1-D wavelet transform.
upcoef	direct reconstruction from 1-D wavelet coefficients.
wrcoef	reconstruct single branch from 1-D wavelet coefficients.
wavedec	multi level wavelet decomposition of 1-D signal.
waverec	multi level wavelet reconstruction of 1-D signal.

Denoising and Compression functions

ddencmp	gives the default values for denoising and compression.
thselect	threshold selection for denoising.
wden	automatic 1-D denoising using wavelets.
wthcoef	wavelet coefficients thresholding 1-D.
wthresh	perform soft or hard thresholding.
wcodemat	converts the matrix into pseudocolor matrix scaling.

MATLAB and toolbox Functions used for the Present work

Function *wavedec* is used to decompose the signal into *n* levels. Where *n* is the number of decomposed levels required. For the present problem *n* is taken as 6. The number of coefficients obtained will be different for all levels. As each level should depict the entire signal, the number of coefficients present are zoomed to the required length by writing the required code in MATLAB. After zooming the coefficients they should be visualized in a manner to identify the cracks. MATLAB provides the function *wcodemat* to code the data into image gray scale data.

After coding into image data, it is plotted with the function *image* or *imagesc*. Imagesc is used to visualize some required range of the coded data. In the present problem the wavelet coefficients are coded between 1 and 128. Then to visualize the cracks, the data between the range 40 to 65 is plotted.

If each level is to be reconstructed, then wrcoef function is used with specification of detail or approximation.

Appendix B

Layout of the Thesis

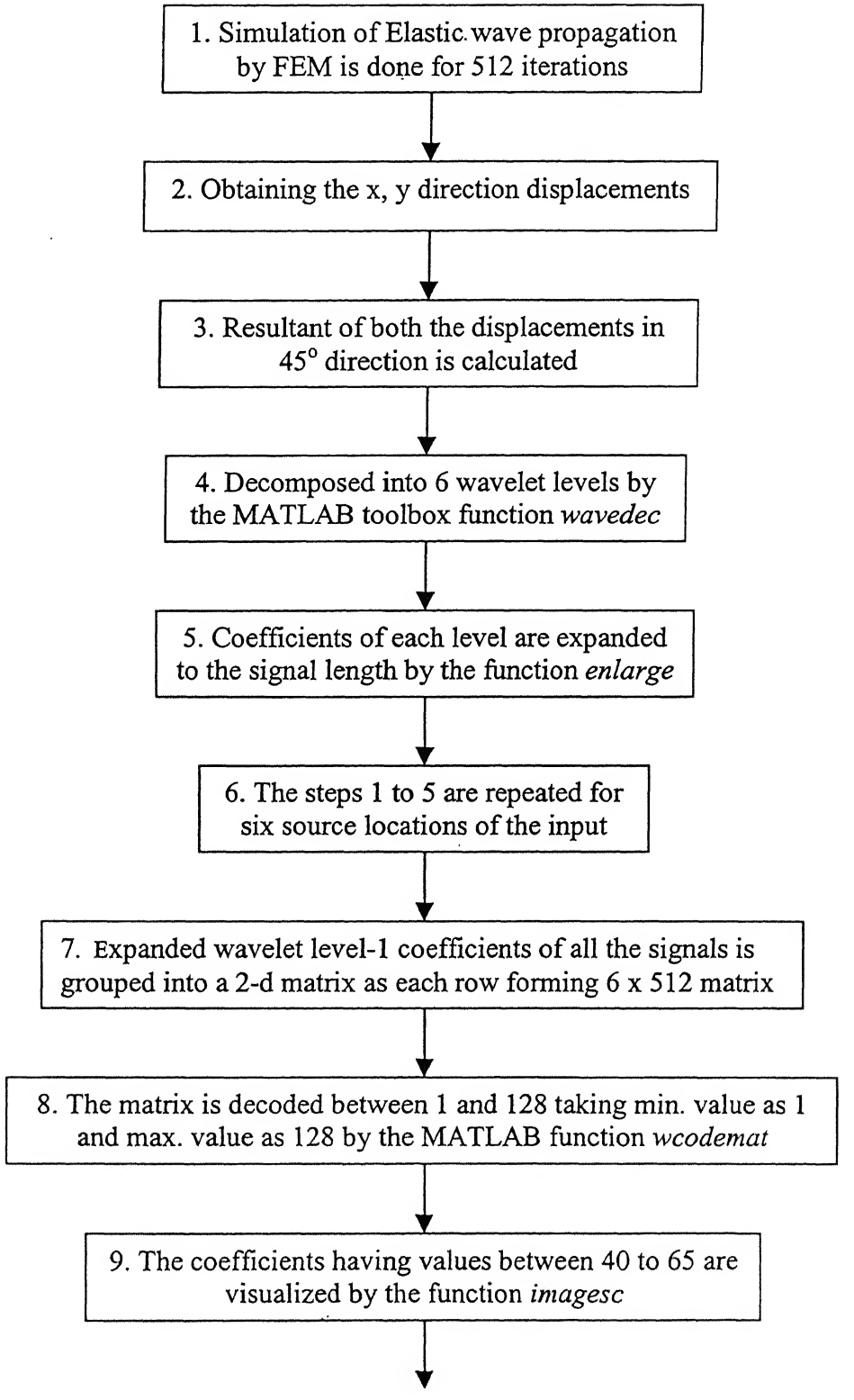

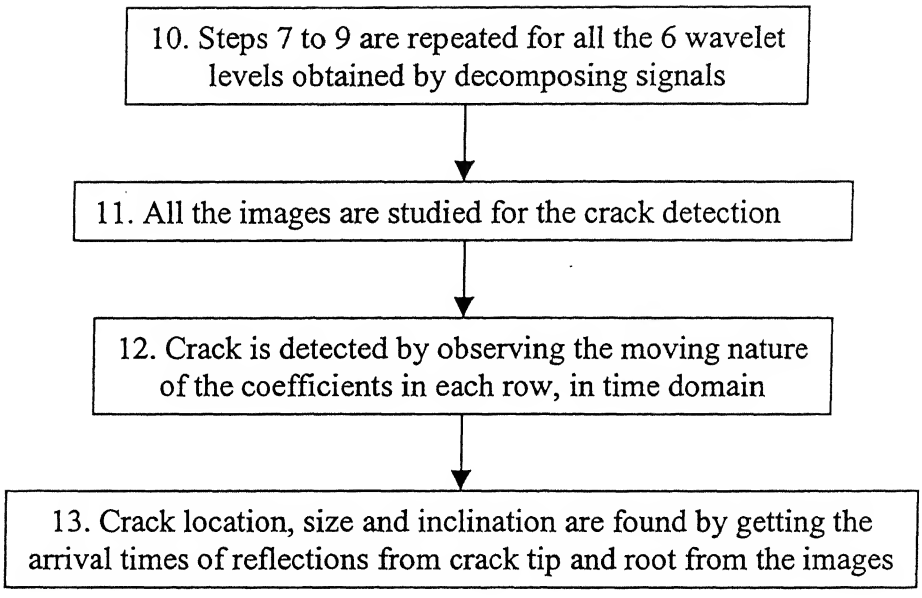

The different functions that are used in the present work other than MATLAB functions are given as follows

```
function dsimple(sigs,n,swname)
%sigs should contain no crack signal obtained at any one source as first row and with
%crack signals obtained at 6 locations in other six rows. n is the number of wavelet levels
%required and swname is the mother wavelet name with which you want to decompose

sig1=sigs(1,:)'; sig2=sigs(2,:)'; sig3=sigs(3,:)';
sig4=sigs(4,:)'; sig5=sigs(5,:)'; sig6=sigs(6,:)'; sig7=sigs(7,:)';
figure(9);zoom
while isstr(swname)
  [C1,L1]=wavedec(sig1,n,swname);
  [C2,L2]=wavedec(sig2,n,swname);
  [C3,L3]=wavedec(sig3,n,swname);
  [C4,L4]=wavedec(sig4,n,swname);
  [C5,L5]=wavedec(sig5,n,swname);
  [C6,L6]=wavedec(sig6,n,swname);
  [C7,L7]=wavedec(sig7,n,swname);
```

```
  % these are used if you want to subtract the no crack signal from the crack signal and
%visualize the data
  %C2=C2-C1 ;C3=C3-C1 ;C4=C4-C1 ;C7=C7-C1 ;
  %C5=C5-C1 ;C6=C6-C1 ;C1=C1-C1;

  C1=enlarge(C1,L1); C2=enlarge(C2,L2); C3=enlarge(C3,L3);
  C4=enlarge(C4,L4); C5=enlarge(C5,L5); C6=enlarge(C6,L6); C7=enlarge(C7,L7);

  for i=1:n
   img=wcodemat(img,128,'mat',0);
   %if i==6, save dauo6 img -ascii,end
   imagesc(img,[40 65]); colorbar
   %image(img);
   colormap gray
   setgcaaft; %function which sets the y-axis to location names
   title(['comparing ,all the signals. ',swname,' , level ',int2str(i)])
   end
 swname=input('enter the wavelet required :');
end

function recs=enlarge(sig,lens)
%sig and lens are the output arguments of the function wavedec these are two vectors in
%which sig contain the wavelet coefficients and lens contain the lengths of each wavelet
%level recs is a matrix which has the dimensions(no. of levels x signal length)
maxleng=lens(end);
n=size(lens,1)-2;
recs=[];
for i=n:-1:1
  leng=lens(i+1);
  k=maxleng/leng; kceil=ceil(k);
  lim1=sum(lens(1:i))+1;
  lim2=sum(lens(1:i+1));
```

```
  cutsig=sig(lim1:lim2);
  %errlow1=0; errup1=0;
  err=0;de=[];
  for j=1:leng
    check=kceil*j-ceil(k*j)-err;
    if check>0,err=err+1;end
    low=((j-1)*kceil+1)-err ;up=j*kceil-err ;
    de(low:up)=cutsig(j);
  end
    recs(n-i+1,:)=de;
end

function times=path_times()
%calculates the path lengths and arrival time periods of different reflections
E=210e9 ; nu=0.33 ; dens=7700 ; elen=0.25e-3;
%of the header wave towards tip and root .
L_vel = sqrt((E*(1-nu))/(dens*(1+nu)*(1-2*nu))) ; % Longitudinal Velocity
T_vel = sqrt(E/(2*(1+nu)*dens)) ;                 %Transverse Velocity
R_vel = ((0.87+1.12*nu)/(1+nu)) * T_vel ;
i=0;
% calculating the times simultaneously for all the six source locations
for node_no=41:20:141
  X1=(161-node_no)*elen ;                         %horizontal length from crack
  theta_1=acos(T_vel/L_vel) ;theta_2=atan(X1/0.01);
  theta_3=acos(X1/0.02) ;
  theta_tip = theta_1 + theta_2 -pi/2 ;
  theta_root= theta_1 + theta_3 -pi/2 ;
  %propagation angle
  i=i+1;
  cra_len=160*elen ;node_dist=(node_no-1)*elen ;
    lengs(1) = sqrt(X1^2+0.01^2);
  lengs(2) = sqrt(X1^2+0.02^2);
```

```
  time(1) = 2*lengs(1)/L_vel ;                    %1.LL tip
  time(2) = 2*lengs(2)/L_vel ;                    %2.LL root
  lengs(3) = 0.02 ; time(3) = 2*lengs(3)/L_vel ;  %3.LL backwall
  time(7) = 2*lengs(1)/T_vel;                     %7.TT tip
  time(8) = 2*lengs(2)/T_vel ;                    %8.TT root
  time(9) = 2*lengs(3)/T_vel ;                    %9.TT back
  time(4) = (time(1) + time(7))/2 ;               %4.LT tip
  time(5) = (time(2) + time(8))/2 ;               %5.LT root
  time(6) = (time(3) + time(9))/2 ;               %6.LT backwall
  H_tip_vel = T_vel/cos(theta_tip) ;
  H_root_vel = T_vel/cos(theta_root) ;
  H_to_L_tip_time = lengs(1)/H_tip_vel + time(1)/2 ;
  H_to_T_tip_time = lengs(1)/H_tip_vel + time(7)/2 ;
    H_to_L_root_time = lengs(2)/H_tip_vel + time(2)/2 ;
  H_to_T_root_time = lengs(2)/H_tip_vel + time(8)/2 ;
  time(10) = H_to_L_tip_time;                     %10.HL tip
  time(11) = H_to_T_tip_time;                     %11.HT tip
  time(12) = H_to_L_root_time;                    %12.HL root
  time(13) = H_to_T_root_time;                    %13.HT root
  time(14) = 2*node_dist/L_vel ;                  %14.LL sidewall
  time(16) = 2*node_dist/T_vel ;                  %15.TT sidewall
  time(15) = (time(14) + time(16))/2 ;            %16.LT sidewall
    time(17) = node_dist/R_vel + node_dist/L_vel ;%17.RL sidewall
  time(18) = node_dist/R_vel + node_dist/T_vel ;%18.RT sidewall
    dtime(i,:) = round(time/4e-8);
end
pna=pnames;
dtime=dtime';
load other    %other containes the times of complicated reflections
dtime=[dtime;other];
times=dtime;
```